Radiation Stability of EUV Multilayer Mirrors

Dissertation

zur Erlangung des akademischen Grades
doctor rerum naturalium (Dr. rer. nat.)

vorgelegt dem Rat der
Physikalisch-Astronomischen Fakultät
der Friedrich-Schiller-Universität Jena

von

Dipl.-Phys. Nicolas Benoit
geboren am 21. Januar 1979 in Paris

Gutachter
1. Prof. Dr. rer. nat. habil. Andreas Tünnermann, Friedrich-Schiller-Universität Jena
2. Prof. Dr. rer. nat. habil. Eckhart Förster, Friedrich-Schiller-Universität Jena
3. Prof. Dr. rer. nat. habil. Ute Kaiser, Universität Ulm

Tag der letzten Rigorosumsprüfung: 12.06.2007
Tag der öffentlichen Verteidigung: 28.06.2007

Abstract

This thesis describes the development and characterization of high thermal and radiation stable Si-based multilayer mirrors for their application in extreme ultraviolet lithographic steppers. Although EUV Lithography (EUVL) is an optical lithography, the reduced wavelength introduces new challenges because all materials are absorbing at 13.5 nm: The application of multilayer mirrors in EUVL requires not only the highest possible normal-incidence reflectivity but also a long-term thermal and radiation stability at operating temperatures. This requirement is most important in the case of the collector mirror of the illumination system close to the EUV source where a short-time decrease in reflectivity is most likely.

Stability of Mo/Si multilayer mirrors and optics lifetime under heavy radiation loads remains one of the big challenges for EUVL for both collector and imaging optics. The formation of an EUV-induced contamination layer (carbon growth and oxidation of the top layers) is a known process that induces a degradation of the optical properties. Si-capped Mo/Si multilayer mirrors, designed for high normal reflectivity at the wavelength of 13.5 nm and deposited by dc-magnetron sputtering, were directly exposed to EUV radiation as collector mirrors (without mitigation system). They presented a loss of reflectivity of more than 18 % after irradiation by a Xe-discharge source with an EUV-dose of 40 mJ/mm^2. It was found that the degradation of the optical properties was due to the oxidation of the silicon and molybdenum top layers. The introduction of a Zr-filter, that mitigates the impact of the out-of-band radiation and partially protects the optics from the debris coming from the source, reduced that loss of reflectivity to -1 % after irradiation with an EUV-dose D = 40 mJ/mm^2 for classical Si-capped Mo/Si multilayer mirrors used as imaging optics. In order to enhance the radiation stability of Si-based multilayer mirrors, new perspective capping layer materials as TiO_2 and RuO_2 have been investigated and compared under similar irradiation conditions. The RuO_2-capped multilayer mirrors presented a drop of reflectivity of -0.8 % after similar irradiation conditions, because of the oxidation of the silicon sub-layer. TiO_2-capped multilayer mirrors showed no degradation of their optical properties after irradiation.

Another problem of Mo/Si multilayers is the instability of the reflectivity and peak wavelength under high heat load. It becomes especially critical at temperatures above 200°C, where interdiffusion between the molybdenum and the silicon layers is observed. The development of high-temperature multilayers was focused on two alternative Si-based systems: $MoSi_2$/Si and interface engineered Mo/C/Si/C multilayer mirrors. The multilayer designs as well as the deposition parameters of all systems were optimized in

terms of high peak reflectivity at a wavelength close to 13.5 nm and high thermal stability. Annealing was carried out under vacuum (10^{-3} Pa) at temperatures up to 650°C. The optimization of $MoSi_2$/Si multilayer mirrors resulted in a peak reflectivity R = 41.2 % at the wavelength $\lambda = 13.6$ nm. They consisted of amorphous Si- and $MoSi_2$-layers. Crystallization of the $MoSi_2$-layers at temperatures above 400°C induced small changes of the $MoSi_2$/Si multilayer optical properties but they were independent of the annealing time at temperatures below 600°C. A wavelength shift of -1.7 % and a reflectivity drop of -1.0 % have been found after annealing at 500°C for 100 hours. The total degradation of optical properties above 650°C is explained by a recrystallization process of $MoSi_2$-layers. Optimized as-deposited Mo/C/Si/C multilayers presented a peak reflectivity R = 59.6 % at the wavelength $\lambda = 13.5$ nm. Thermally induced changes of the optical and structural properties were dependent on both annealing times and temperatures. The interdiffusion coefficients in Mo/C/Si/C systems have been calculated from the decay rate of the peak reflectivity during isothermal annealings at different temperatures (250, 400 and 500°C). The interdiffusion coefficient at 400°C was found to be around 10^{-26} m^2/s. The degradation of the optical properties of Mo/C/Si/C multilayer mirrors was due to the the formation of a SiC-layer at the interfaces and a development of an interface roughness in the multilayer structure.

The combination of high reflective properties and enhanced thermal and radiation stability of Mo/Si multilayer mirrors provides good prospects for their use as coating for EUVL mirrors.

Zusammenfassung

Obwohl die EUV-Lithografie (EUVL) ein optisches Verfahren ist, führt die reduzierte Wellenlänge neue Herausforderungen ein, da alle Materialien bei 13,5 nm absorbieren. Die Anwendung von Multilayeroptiken für die EUVL erfordert nicht nur eine höchstmögliche Reflexion, sondern auch eine anhaltende Strahlungs- und thermische Stabilität. Dies gilt besonders für den Kollektorspiegel, da wegen seiner unmittelbaren Nähe zur EUV-Quelle ein vorzeitiger Reflexionsverlust erfolgen kann. Im Rahmen dieser Arbeit wurde die Strahlungs- und thermische Stabilität von EUV-Spiegeln untersucht. Neue Schichtsysteme mit einer höheren Stabilität wurden entwickelt.

Die Lebensdauer Mo/Si- beschichteter Optiken stellt eine der größten Herausforderungen für die Produktionseinführung der EUVL dar. Problematisch bei der Verwendung von Mo/Si-Multilayeroptiken ist die Verringerung der Reflexion auf Grund von Kohlenstoffkontaminationen und Oxidation der Silizium-Deckschicht bei intensiver EUV-Bestrahlung. Klassische, für 13,5 nm optimierte, Mo/Si-Multilayerspiegel wurden als Kollektorspiegel mit einer EUV-Lampe, die auf einer Xe-Plasma-Entladung basiert ist, bestrahlt. Sie zeigen einen Reflexionsverlust von 18 % nach einer Strahlungsdosis von 40 J/mm^2. Der Reflexionsverlust kann durch die Oxidation der obersten Si-Schicht und die partielle Oxidation der darunter liegenden Mo-Schicht erklärt werden. Der Einsatz eines Zr-Filters, der den Einfluss der "Out-of-Band" Strahlung reduziert und die Optiken vor den Debris aus der Quelle schützt, verringert den EUV-induzierten Reflexionsverlust. Er beträgt 1 % nach einer Strahlungsdosis von 40 J/mm^2 für Mo/Si-Abbildungsoptiken. Um die Strahlungsstabilität solcher Spiegel zu erhöhen wurden neue Deckschichtmaterialien für EUVL-Optiken wie TiO_2 und RuO_2 untersucht. Mo/Si Multilayeroptiken mit optimierter RuO_2-Deckschicht zeigen einen Reflexionsverlust von 0,8 % nach einer Strahlungsdosis von 40 J/mm^2. Als Ursache dieses Reflexionsverlusts konnte partielle Oxidation der Si-Unterschicht nachgewiesen werden. Dahingegen wurde bei Mo/Si-Multilayerspiegeln mit optimierter TiO_2-Deckschicht kein Reflexionsverlust nach Bestrahlung festgestellt.

Klassische Mo/Si-Schichtsysteme zeigen bei thermischer Beanspruchung (T > 200°C) eine Instabilität der Schichtstruktur durch Diffusionsprozesse zwischen den Si- und Mo-Schichten. Daraus resultiert ein Verlust der Reflektion sowie eine Verschiebung der Peak-Wellenlänge. Mit dem Ziel einer deutlichen Verbesserung der thermischen Stabilität wurden zwei alternative Schichtsysteme auf Si-Basis entwickelt: $MoSi_2$/Si und Mo/C/Si/C. Die Schichtdesigns sowie die Beschichtungsparameter wurden für eine Maximalreflexion bei einer Wellenlänge um 13,5 nm sowie einer hohen Arbeitstemperatur optimiert. Zur

Untersuchung der thermischen Stabilität wurden die Spiegel unter Hochvakuumbedingungen (10^{-3} Pa) bis 650°C erhitzt. Die untersuchten $MoSi_2$/Si-Systeme zeigen eine Reflexion R = 41,2 % bei λ = 13,6 nm. Sie bestehen aus amorphen Si- und $MoSi_2$-Schichten. Die hauptsächlich auf Kristallisationsprozesse ab 400°C zurückzuführenden Strukturveränderungen der $MoSi_2$-Schichten sind im untersuchten Temperaturbereich bis 600°C zeitlich invariant. Während sich nach einer hundertstündigen Temperatureinwirkung von 500°C die Peak-Wellenlänge um ca. 1,7 % verringert, konnte ein Reflexionsverlust von lediglich 1,0 % nachgewiesen werden. Die Rekristallisation der $MoSi_2$-Schichten nach einer Temperatureinwirkung von 650°C ergabt eine völlige Zerstörung der optischen Eigenschaften. Eine Reflexion R = 59,6 % bei λ = 13,5 nm wurde für die optimierten Mo/C/Si/C-Schichtsystemen gemessen. Für Temperaturen $T \geq 400$°C sind die thermisch induzierten Veränderungen der optischen und strukturellen Eigenschaften zeitabhängig. Die Berechnung der effektiven Diffusionskoeffizienten bei 250°C, 400°C und 500°C in Mo/C/Si/C-Schichtsystemen erfolgte durch die Bestimmung der Rate der Reflexionsabnahme unter isothermische Heizung. Bei 400°C beträgt der Interdiffusionskoeffizient 10^{-26} m^2/s. Die Entstehung einer SiC-Schicht an den Grenzflächen, sowie die Erhöhung der Grenzflächenrauheit führen zu einer Zerstörung der optischen Eigenschaften von Mo/C/Si/C-Schichtsystemen.

Die Kombination von thermischer und Strahlungsstabilität sowie optischen Eigenschaften von Mo/Si Schichtsystemen unterstreicht ihre potenzielle Nutzung als Beschichtung von EUVL Spiegeln.

Contents

List of Figures

List of Tables

List of acronyms

AC	Alternative Current
AES	Auger Electron Spectroscopy
AFM	Atomic Force Microscopy
BIB	Broad Ion Beam
DC	Direct Current
DWBA	Distorted-Wave Born Approximation
ETS	Engineering Test Stand
EUV	Extreme UltraViolet
EUVL	Extreme UltraViolet Lithography
FWHM	Full Width at Half Maximum
HRTEM	High-Resolution Transmission Electron Microscopy
LAXD	Large Angle X-ray Diffraction
LPP	Laser Produced Plasma
NA	Numerical Aperture
PSD	Power Spectral Density
RF	Radio-Frequency
RMS	Root-Mean-Square
SAXR	Small Angle X-ray Reflectivity
TBD	To Be Determined
TEM	Transmission Electron Microscopy
UHV	Ultra High Vacuum
XPS	X-ray Photoelectron Spectroscopy

List of symbols

Res	Resolution
λ	Wavelength
$\tilde{n}$	Complex refractive index
n	Refractive index
β	Extinction coefficient
δ	Complement to the unity
r_0	Classical radius of an electron ($r_0 = 2.818\times10^{-15}$ m)
N_{at}	Number of atoms per unit volume
f_1, f_2	Atomic scattering factors
λ_L	Si-L absorption edge
P_w	Power delivered to the wafer
P_s	Spectral power of the source
R	Reflectivity
H	Multilayer period
t	Layer thickness
θ	Grazing angle
Θ	Grazing angle with refraction correction
θ_c	Critical angle
$\tilde{\delta}$	Weighted average index
Γ	Thickness ratio
N	Number of periods
σ	RMS-roughness
ρ	Material density
D	EUV-dose
χ	Molar fraction
D_e	Effective interdiffusion coefficient
τ	Annealing time
E_a	Activation energy
k_B	Boltzmann constant ($k_B = 8.617\times10^{-5}$ eV/K)
α	Incidence angle
a	Lattice spacing
I	Light intensity
A	Relative atomic mass
L	Coherence length

f	Spatial frequency
r	Radius of the AFM tip
V	Molar volume

1 Introduction

The work presented in this thesis is based on the development of thermal and radiation stable multilayer mirrors for Extreme Ultraviolet Lithography (EUVL). The Extreme Ultraviolet (EUV) spectral range can be defined as the part of the electromagnetic spectrum placed between the ultraviolet and the X-ray spectral ranges. According to the conventions used in the research on physics of plasma and synchrotron radiation [1], it corresponds to the photon energies between 30 eV and 250 eV (wavelength range between 5 nm and 40 nm). The development of lithographic processes, supplied by the semiconductor industry, leads to a permanent decrease of the lithographic wavelength in order to satisfy the Moore's law [2] , that induces a doubling of the components fabricated on a chip every 18 months. In the last years, it has even decreased from 248 to 13.5 nm with the introduction of the EUVL as next generation lithography. It should be introduced in volume production at the 32 nm microprocessor node in 2009 [3].

The success of the EUVL is greatly dependent on the optical performances of the Mo/Si multilayer mirros, used as high-reflective optics for in the EUVL steppers [4], since EUV radiation cannot be transmitted because of the strong absorption of all materials at this wavelength. It requires not only the highest possible normal-incidence reflectivity but also a long-term thermal and radiation stability at operating temperatures. This requirement is most important in the case of the collector mirror of the illumination system close to the EUV source where a short-time decrease in reflectivity is most likely. A serious problem of Mo/Si multilayers capped by silicon is the considerable reflectivity degradation due to carbonization and oxidation of the silicon surface layer under high intensive exposure by EUV radiation. The instability of Mo/Si multilayers becomes especially critical at elevated pressures of water vapor and hydrocarbons, thus noticeably limiting the application time of Si-capped Mo/Si multilayers mirrors for EUVL. Another problem of Mo/Si multilayer mirrors is the instability of reflectivity and peak wavelength under high heat load. It becomes especially critical at temperatures above 200°C, where interdiffusion between the molybdenum and the silicon layers is observed.

The chapter 2 provides an introduction of the requirements induced by the application of EUV lithography and of the theoretical optical and structural properties of Mo/Si multilayer mirrors. The both thermal and radiation stability of Mo/Si multilayers are discussed and the state of the art of the different solutions already existing for the improvement of these stabilities is then introduced. All investigation and characterization methods used in this work are presented in the chapter 3.

The chapter 4 introduces the results obtained during the investigation of the stability of Mo/Si multilayer mirrors. The growth, structure and optical properties of such mirrors are first presented (part 4.1) as the basis for all comparisons of stability enhancements. The radiation stability of collector and imaging optics is then investigated (part 4.2) under EUV radiation produced with a Xe-gas discharge source. The application of different capping layer materials (TiO_2 and RuO_2) on top of the mirrors demonstrates an enhancement of stability under EUV radiation. The enhanced thermal stability of two Si-based multilayer mirrors ($MoSi_2$/Si and Mo/C/Si/C) is finally demonstrated, as potential solution for high thermal applications of multilayer mirrors (part 4.3).

Finally, the chapter 5 concludes the results of the presented work and provides a detailed enumeration of the stability enhancement of Mo/Si multilayer mirrors for both thermal and radiation stability.

2 Literature

2.1 EUVL as candidate for the next generation of lithography

The lithography can be defined as the process that creates features on a silicon wafer. For optical lithography, the wavelength has decreased from 365 nm to 248 nm and to 193 nm in order to improve the resolution and to satisfy the Moore's law [2], which states that the number of components fabricated on a chip will double every 18 months. In the last years, it has even migrated to 157 nm with the introduction of the immersion processes to reach the 65 nm half-pitch node [5]. EUVL, with a wavelength of 13.5 nm, must be introduced in volume production at the 32 nm microprocessor node in 2009 (the 22 nm half-pitch node is also hoped) with a throughput of about 40 to 120 wafers per hour (depending for instance on the source power or the resist sensitivity) [3]. The success of the EUVL is also greatly dependent on the stability (temporal, thermal and radiation stabilities) of Mo/Si multilayer coatings, either for high-reflective optics [4] or for defect free mask blanks [6].

Although EUVL is an optical lithography, the reduced wavelength introduces new challenges because all materials are absorbing at 13.5 nm. EUVL systems need therefore vacuum operations (because of the air absorption). Decreasing the operated wavelength for lithography scanners means obtaining a better resolution. The resolution resulting of a lithographic process can be described as the smallest feature size that a system can print (the minimal distance between two points or two lines on the wafer). It is defined by [7]:

$$Res = \frac{k_1 \lambda}{NA} \tag{2.1}$$

where Res is the resolution, k_1 a constant (that depends on the photo-resist, specific system irradiation characteristics, mask geometries and manufacturing processes), λ the wavelength of the radiation used and NA the numerical aperture of the system. Best amount for the k_1 constant is about 0.5 and typical values of the numerical aperture NA are in range from 0.1 to 0.3 [8]. So, as reducing the wavelength as possible, the best resolution may be achieved.

2.1.1 The EUV spectral range

The EUV spectral range can be defined as the part of the electromagnetic spectrum [1] which contains the wavelengths between 5 and 40 nm, corresponding to photon energies from 30 to 250 eV, as shown in Fig. 2.1 [1].

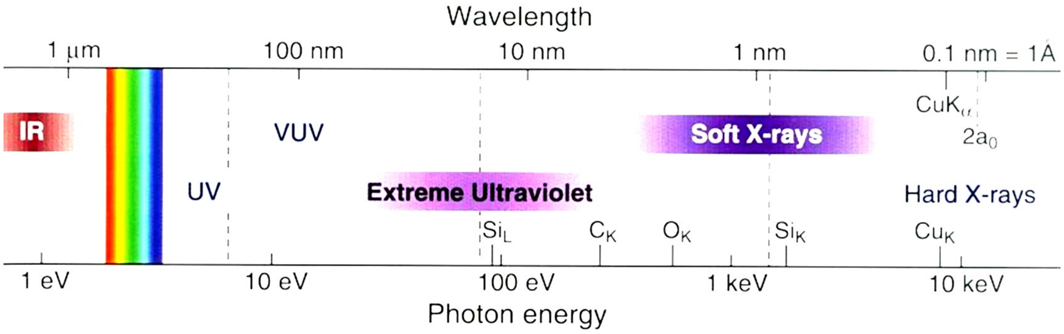

Figure 2.1: Electromagnetic spectrum from the infra-red to the hard X-ray range [1]

This spectral region is characterized by a strong absorption of the light by all materials and by refractive indexes close to the unity. Those indexes are commonly described in terms of the complex refractive index, which is a function of the wavelength [9]:

$$\tilde{n} = n + i\beta = 1 - \delta + i\beta \tag{2.2}$$

where n is the refractive index (that is linked to the refractive properties of a medium), β the extinction coefficient (that describes the absorption of a medium) and δ the complement to the unity (n = 1 - δ). In the EUV region, β and δ are in the range from 10^{-2} to 10^{-4} for wavelengths from 5.0 to 0.5 nm respectively. In order to obtain the relation between the atomic scattering factors (used for X-rays) and the refractive index (used in visible light), the model of a free electron gas can be applied and gives [10].

$$\tilde{n} = n + i\beta = 1 - \delta + i\beta = 1 - \frac{r_0\lambda^2}{2\pi}N_{at}(f_1 - if_2) \tag{2.3}$$

where r_0 is the classical radius of an electron ($r_0 = 2.818\times10^{-15}$ m), λ the wavelength and N_{at} the number of atoms per unit volume. For high photon energies (short wavelengths), the atomic factor f_1 approaches the number of free electrons per atom (electrons whose bond energies are lower than the photon energy). For higher energies, it remains constant and close to the total number of electrons contained in the atom. The atomic scattering factors f_1 and f_2 of all materials have been tabulated for wavelengths from 0.04 to 41 nm [11]. Optical constants δ and β can be therefore calculated with the Eq. 2.3. Silicon and molybdenum ones are introduced in Fig. 2.2.

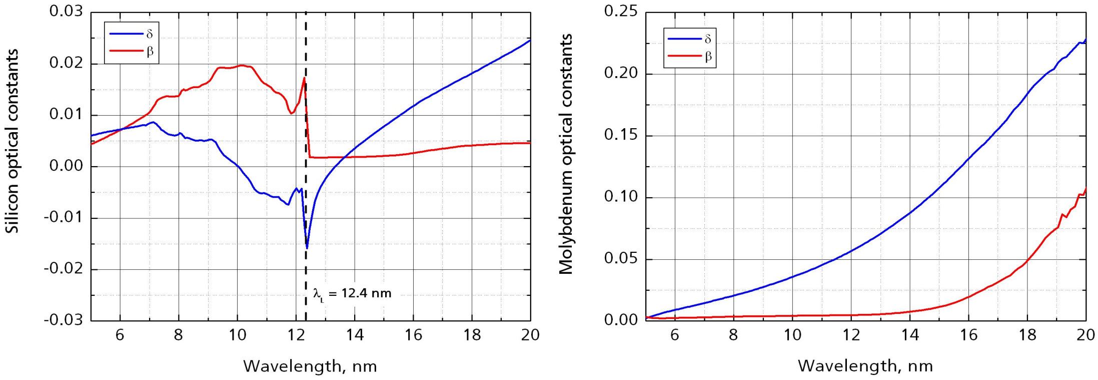

Figure 2.2: Optical constants δ and β for silicon and molybdenum

At the Si-L absorption edge ($\lambda_L = 12.4$ nm), δ reaches a minimum while β strongly increases. The behavior of the ratio δ/β describes the transparency of a material. For wavelengths greater than λ_L, silicon has a very low absorption: Mirrors designed for 13.5 nm have thereby a Si-based design.

2.1.2 Critical issues in EUVL

The shift of optical lithography to EUVL introduces new requirements depending on the interaction between the EUV radiation and the matter in this spectral range (as EUV radiation is absorbed in all materials, the process must be under a high-vacuum atmosphere). The first suggestions that EUVL could viably extend Moore's law came in 1988 [12, 13]. Since that time, many technological challenges have been met and still has to be overcome [14]. The general set-up of the EUVL is presented in Fig. 2.3 [15].

In such a system, EUV radiation is produced by a thermal excitation of target materials (xenon, lithium or tin) made either by laser heating (Laser Produced Plasma) or by electromagnetic pinch (Discharge Produced Plasma) [16]. The light is then collected by condenser optics and driven to a mask stage through beam shaping optics. At the end, it is directed onto a wafer stage by projection optics. For each stage of this set-up, a technology road map has been introduced (alpha-tool in 2005, beta-tool in 2007 and production in 2009) with specific requirements in order to reach a high wafer throughput for the high volume manufacturing production. The last main requirements are presented in Tab. 2.1 [17, 18].

Since the actual reported values do not stick to the requirements, efforts have to be made to improve the performances of each part contributing to the lithographic process as optics, masks, resists, or sources. Contrary to others optical lithographic processes, EUVL is not based on transmissive lenses but on reflective mirrors (all known lens materials absorb the EUV wavelengths). The collector and projection optics consist of

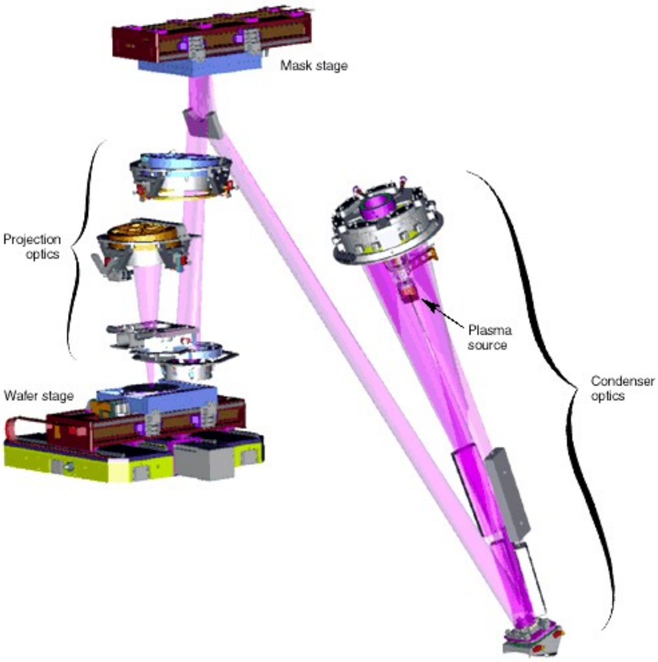

Figure 2.3: General EUV lithography set-up [15]

Table 2.1: Main requirements for EUVL [17, 18]

Specifications	**Requirements**			**Best reported**
	Alpha	Beta	Production	
Central wavelength, nm	13.5	13.5	13.5	13.5
Throughput, WPH	20	60	100	–
EUV power (in-band), W	10	30	115	50 (Sn target)
Repetition frequency, kHz	2	5	7–10	6.5
Source cleanliness, h	TBD	TBD	30,000	–
Resist sensitivity, mJ/cm^2	5	4	3	–

EUV-reflective Mo/Si multilayer mirrors [19]. Properties (optical and structural ones) and requirements (high EUV-reflectivity, thermal and radiation stability) of such optics are reported later (see parts 2.1.3 and 2.2).

EUV sources are another critical factor for the success of EUVL. Sources have to be evaluated using criteria such as in-band power (at the wavelength of 13.5 ± 0.2 nm) wafer throughput, cost of ownership, debris contamination issues and dose repeatability [20]. As EUVL was proposed, all known concepts of EUV sources (based on electron impact [21], synchrotron radiation [22] or hot plasmas [23]) were lacking power, stability and lifetime. Commercial efforts have been made in source development and new concepts to improve existing ones, like pinch plasma [24], laser produced plasma [25] and synchrotron

[26] have been developed over the last ten years. Even they are absolutely clean sources, synchrotrons are not enough compact and require expensive facilities. Therefore, gas discharge and laser produced plasma sources are the only real candidates for EUVL [27].

All gas discharge plasma sources are based on a common principle: A current, running between a cathode and an anode, induces a magnetic field that compresses and heats a ionized gas (electron density in the range of 10^{18} cm^{-3}). It leads to the formation of a plasma hot enough (temperature of several 10 eV) to emit EUV radiation [28]. In the case of a laser produced plasma source, a pulsed laser light is focused to high intensities onto a target to produce EUV radiation [29]. That emission and the resulted EUV power strongly depend on the material and the nature of the target and on the temporal development of the plasma [30]. The choice of the target material is mostly based on the spectral output of the material but also on the contamination characteristics of the substance. Three materials (lithium [31], xenon [32] and tin [33]) are mainly known to be potential targets for the production of EUV sources and achieve the in-band EUV power of 115 W. Another major factor that determines whether a source is suitable for EUVL is its cleanliness. Optical components and especially the collector mirror of the EUVL set-up should not be changed because of contamination coming from the source. Actual EUV sources produce atoms, ions and particles which have to be mitigated to avoid a source-generated contamination of the optics. It can be made with the use of a background buffer gas [34], foils [35] or magnetic-field shield [36].

A similar challenge exists in producing EUV masks, which are also based on a Mo/Si technology, able to deliver a high definition patterning. Masks are reflective and require a very high coating quality with less than 0.003 defect/cm^2 [37]: multilayers are deposited by ion beam sputtering [38, 39], which must generate the lowest defect density. The mask is effectively imaged onto the wafer, so any defects in the structure will be transferred to the resist, producing defects in the final product. Masks requirements for the beta-tool (2007) and the high volume manufacturing production (2009) are introduced in Tab. 2.2 [40]. Another challenge concerning the production of mask blank is the development of characterization methods, which are able to detect such small defects [41]. In the case of non defect-free masks are produced, new defect repair methods have also been developed as scooping out a few Mo/Si layers or covering defects with an absorber pattern [42]. But masks control and reparation as well must be made without introducing any additional contamination.

Table 2.2: EUV mask blank road map requirements [40]

Specifications	**Beta-tool**	**Production**
Defect density, def/cm^2	0.01	0.003
Defect size, nm	40	25
Peak reflectivity, %	66	67

Finally resists developed for EUVL must be surface imaging resists because of the short penetration length of EUV radiation [43]. However, they absorb easily the EUV light so that they have to be quite thin (typical layer thickness around 100–130 nm). For commercial viability, EUVL requires a resist material with a good resolution, a high contrast for printing, a good etch resistance, a sensitivity better than 5 mJ/cm^2 and a low outgassing to prevent optics contamination [44].

2.1.3 Critical issues for optical elements in EUVL

Due to the strong absorption of EUV radiation by all materials, the optical components of a EUVL set-up are reflective. Therefore usual optical systems such as refractive optics cannot be used with EUV and advances in multilayer coatings becomes a solution for the development of EUVL by providing mirrors that have to fulfill three main requirements: a maximal reflectivity at the wavelength of 13.5 nm, a good stability (temporal, thermal and radiation stability) and low mechanical stresses [45]. A high reflectivity is very important: Considering a EUVL system with nine mirrors (projection optics, illuminator and masks), the difference between two sets of multilayer mirrors with respectively 70 % and 68 % reflectivity results in a 30 % difference in integral light intensity at the wafer plane. However the peak reflectivity is not the only key factor. The power on the wafer is given by the integral of the spectral power of the source and the multiplied reflectivities of the N (N $\geq$ 9) mirrors of the EUVL stepper [46]:

$$P_w = \int P_s(\lambda) \prod_{k=1}^{n} R_k(\lambda) d\lambda \tag{2.4}$$

where P_w is the power delivered to the wafer, P_s the spectral power of the source and R_k the reflectivity of the kth mirror. Thus the bandwidth, the peak-wavelength match of the different mirrors and the spectrum of the source are also important factors to achieve a high power at the wafer plane.

As EUVL steppers are required to produce wafers over more than three years (30,000 hours) non-stop operating, optical elements of the system have also to keep reflecting for that time. The lifetime of EUV mirrors can be defined as when a transmission loss of about 10 % in the overall system is reached (that corresponds to an irreversible reflectivity loss of more than 1 % per mirror) [47]. The application of mirrors for EUVL requires not only the highest possible normal-incidence reflectivity at the wavelength of 13.5 nm but also a long-term temporal, thermal (under high heat) and radiation (under EUV radiation loads) stability. This requirement is most important in the case of the collector mirror (first mirror of the illumination system nearest to the EUV source) where a reflectivity decrease is most likely [48]. The role of the collector mirror is to capture as much light as possible of the radiation emitted by the source. A long term thermal stability around 400–500°C can be therefore a main asset in order to protect the mirrors against the contamination coming from the source [49]. Methods that can be used to enhance the thermal stability of such optics are described in the part 4.3. Two main issues of contamination under EUV radiation are known: oxidation and carbon growth on the mirror surfaces, which emit secondary electrons under EUV exposures responsible for the dissociation of hydrocarbons and water molecules [50]. A detailed investigation of that phenomenon and methods developed to reduce it are presented in the part 2.3.

Due to the stringent surface figure requirements for the optics in EUVL system, deformations due to the structure stress have to be minimized [51]. However, stresses must be reduced or compensated without reducing the EUV reflectivity (deposition of buffer sub-layers), since it has a strong impact on the throughput of the EUVL stepper.

2.2 Mo/Si multilayer mirrors as high-reflective elements for EUVL

EUVL steppers requires high-reflective optics designed for a wavelength of 13.5 nm. Considering a single boundary between two materials with refractive indexes $\tilde{n}_1$ and $\tilde{n}_2$ (one layer mirror), the reflectivity at normal incidence can be calculated by the Fresnel equations [52]:

$$R = \left| \frac{\tilde{n_1} - \tilde{n_2}}{\tilde{n_1} + \tilde{n_2}} \right|^2 \tag{2.5}$$

The reflectivity of a boundary between vacuum ($\tilde{n}_1 = 1$) and another material ($\tilde{n}_2 = 1 - \delta + i\beta$) becomes with the Eq. 2.5:

$$R = \frac{\delta^2 + \beta^2}{(2-\delta)^2 + \beta^2} \approx \frac{\delta^2 + \beta^2}{4}, \delta << 1, \beta << 1 \tag{2.6}$$

Since the deviation δ decreases quadratically with decreasing wavelength ($\delta \propto \lambda^2$), the reflectivity at normal incidence drops proportionally to λ^4 in regions where the effective number of free electrons stays constant [53]. Grazing incidence mirrors are a first way to overcome that problem. They are mainly used in X-ray telescopes [54] and for synchrotron applications [55]. In 1972 it was demonstrated that multilayer coating techniques, as employed in visible optics to construct dielectric, anti or high reflection interference coatings, could be extended to the EUV and soft X-ray spectral range to get high-reflective mirrors [56].

2.2.1 Main parameters of multilayer mirrors

Such multilayer coatings consist of alternating layers of two materials with different refractive indexes [57]. The two materials usually have a large difference in atomic number Z to maximize the difference in electron density (Eq. 2.3) and enhance the normal incidence reflectivity at one boundary (Eq. 2.5) [58]. So multilayer mirrors may be described as a stack of at least two materials (an absorber and a spacer with respectively high and low electron densities) deposited on a substrate. The period of such a structure is defined as following [59]:

$$H = t_A + t_S \tag{2.7}$$

where t_A is the thickness of the absorber layer and t_S of the spacer layer. The required period of the multilayer system can be simply evaluated by using the classical Bragg equation:

$$2H \sin\theta \cong m\lambda \tag{2.8}$$

where θ is the grazing angle, m the order of reflection and the λ wavelength. In the case of a normal incidence reflectivity ($\theta = 90$ deg) at the wavelength $\lambda = 13.5$ nm, the Eq. 2.8 gives for the first order of reflection H = 6.75 nm.

The principle of such reflector is based on a constructive adding up of reflectivities from many boundaries as shown in Fig. 2.4 [56]. In an ideal Bragg crystal, atomic planes, spaced of $\lambda/2$, reflect the incident wave. That design gives a high reflectivity for a large number of layers, even if they are absorbing (assuming that the space between the atomic planes is non-absorbing) [60]. The basic design of a multilayer structure is based on positioning a high-absorbing material close to the nodes of the standing wave established in the periodic structure and by filling the space in between with a low absorbing material.

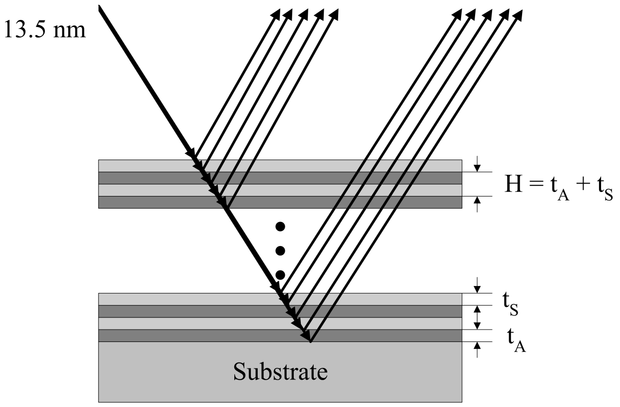

Figure 2.4: Principle of a multilayer design [56]

The theory of X-ray diffraction on crystal planes [61] can be well described by both the recursive method [62] (successfully applied to each interface) and the matrix formalism

[63] (each interface is represented by a matrix). The calculation of the final integral reflectivity of a multilayer mirror by the recursive method shows that the maximal reflectivity is reached under the Bragg condition (Eq. 2.8 without the approximation $\delta = \beta = 0$) [64]:

$$m\lambda = 2H \sin\Theta_m \sqrt{1 - \frac{2\tilde{\delta}}{\sin^2\Theta_m}} \tag{2.9}$$

where Θ_m is the grazing angle with refraction correction [65] and $\tilde{\delta}$ the weighted average index of the two materials in the coating:

$$\tilde{\delta} = \frac{\delta_A d_A + \delta_S d_S}{d_A + d_S} \tag{2.10}$$

and is directly linked to the thickness ratio Γ:

$$\Gamma = \frac{d_A}{d_A + d_S} = \frac{d_A}{H} \tag{2.11}$$

that is typically between 0.3 and 0.5. In order to select the most suitable couple of materials for the design of high-reflective multilayer mirrors, the spacer material should have the lowest extinction coefficient β_S for the desired wavelength and the absorber material has also to provide a high reflectivity at the boundary with the spacer material with an extinction coefficient as low as possible [66]. Finally both materials should have the ability to be deposited with smooth and sharp boundaries. Several couple of materials have been investigated for the EUV and soft X-ray spectral region (like Mo/Be [67] or Mo/Si [68]). For wavelengths greater than 12.4 nm (that corresponds to the Si-L absorption edge), silicon has a very low absorption and becomes the best spacer material. It has been demonstrated that the couple Mo/Si is the most suitable for high-reflective optics at the wavelength of 13.5 nm [69]. Such a multilayer system is commonly described by four parameters: its couple of materials (a spacer and an absorber), its number of periods N (each period consists of a spacer layer and an absorber layer), its period H (thickness of one period) and its thickness ratio Γ (Eq. 2.11). The optimization of these parameters leads to a theoretical reflectivity of about 75 % at the wavelength of 13.5 nm [70] with the following parameters: N = 60, H = 6.92 nm, $\Gamma = 0.4$.

2.2.2 Imperfections of Mo/Si multilayer mirrors

Although the theoretical calculations predict that high normal incidence reflectivities can be achieved through multilayer mirrors for the EUV spectral range [71], actual values significantly differ from the theory. So far the best achieved normal incidence reflectivity for Mo/Si systems is about 70 % with N = 60 periods [72]. Imperfections of the multilayer structure, like interface roughness and diffuse intermixing [73], (Fig. 2.5 [58]) are mainly responsible for that drop of reflectivity. An interface roughness of a few Angstroms can reduce the reflectivity because of non-specular scattering [74]. The reduction of reflectivity R of a real multilayer mirror because of the roughness σ can be described with a model analog to the Debye-Waller factor [75, 76]. The drop of reflectivity induced by the development of roughness becomes [77, 78]:

$$R = R_0 \exp\left[-\left(2\pi m \frac{\sigma}{H}\right)^2\right] \tag{2.12}$$

where R_0 is the reflectivity of an ideal structure ($\sigma = 0$), H the period of the multilayer and m is the order of reflection. One reason for that columnar growth (development of the roughness through the multilayer structure) is the low surface mobility of the adatoms and the correlated low surface energy of the growing layers during the deposition of mirrors [79].

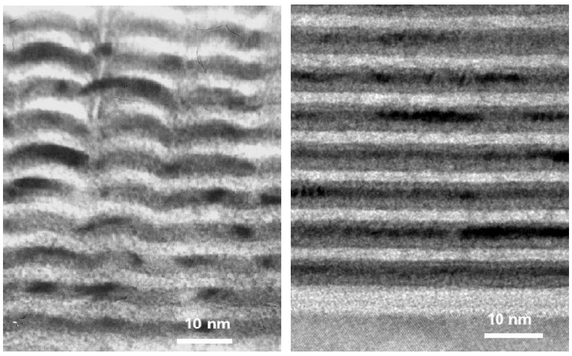

Figure 2.5: Cross-section TEM images of imperfections in a multilayer structure: Interface roughness (left) and diffuse intermixing (right) [58]

The diffuse intermixing between the layers in the multilayer structure is another cause of a drop of reflectivity. Although the deposition process of the layers is optimized and the interfaces are smooth, the silicon and molybdenum layers are separated by a $\mathrm{Mo}_x\mathrm{Si}_y$ silicide layer [80]. The thickness of such intermixing layers has been demonstrated to be asymmetric and depends on the degree of perfection of the crystalline structure of the molybdenum layer: At the Mo-on-Si interface $t_{Mo_xSi_y} \approx 1.2$ nm and at the Si-on-Mo interface $t_{Mo_xSi_y} \approx 0.6$ nm [81]. That phenomenon can be minimized but not totally suppressed [82], that shows that the formation of intermixing layers is an intrinsic property of the Mo/Si multilayers and could be a barrier to reach the theoretical maximal reflectivity.

A great number of layers has to be deposited in order to achieve high reflective optics. But it is impossible to obtain homogenous thicknesses through the whole structure and it has been shown that random errors in period thicknesses, as stochastic errors (the periods have different values, $H_1 \neq H_2 \neq H_n$) or linear errors (the value of the period linearly increases or decreases in the structure, $H_1 < H_2 < H_n$) introduce a decrease in reflectivity and an increase in the bandwidth of the multilayer mirror reflectivity [83]. Therefore new systems of in-situ monitoring has been developed in order to control the layer thickness during the deposition process [84]. Defects on the substrate and impurities in the multilayer stack due to the deposition process (as argon atoms if the mirror is deposited under argon atmosphere) are two other reasons for a decrease in reflectivity of the Mo/Si multilayer optics.

Finally an another reason for a drop of reflectivity of EUV mirrors is the oxidation of the top-layer. It has been demonstrated that a silicon top-layer naturally oxidizes and effectively forms an about 2 nm thick capping layer of native oxide [85]. As the oxidation of the silicon top-layer is accompanied by an increase in the absorption (the attenuation length becomes shorter) and a change of the top thickness, the optimization of the top-layer is an important step in the design of Mo/Si multilayer mirrors with high reflective properties.

2.2.3 Interface-engineered multilayer mirrors

In order to enhance the reflectivity of Mo/Si multilayer mirrors, interdiffusion processes at the interfaces have to be suppressed or at least reduced. That could be done by the introduction of super-thin diffusion barriers between the molybdenum and silicon layers. Therefore the design of the multilayer is no more a traditional binary Mo/Si system but an interface-engineered Mo/X/Si/X one, where X is one material used as barrier against the intermixing. Successful attempts by application of the interface-engineered design Mo/B_4C/Si/B_4C was performed and a normal incidence reflectivity of about 70 % was achieved [86]. Other materials like carbon C and silicon carbide SiC can be used to improve both the reflective properties of the mirror and its thermal stability [87].

2.3 Radiation stability

It was shown that Mo/Si multilayer mirrors have a good temporal stability [88]: The temporal stability of the reflectivity of a Mo/Si multilayer mirror stored in air has been demonstrated over a period of 25 months. A decrease of 0.4 % of the normal incidence reflectivity appeared over a period of 400 days. Therefore one of the main issues for Mo/Si multilayer mirrors stability is no more the temporal stability but the stability of the optics under EUV radiation. Then Mo/Si multilayer mirrors become contaminated, which results in a reduced reflectivity, a shorter lifetime and thus a reduced wafer throughput [89]. Two different processes are responsible for the contamination of Mo/Si multilayer mirrors under EUV radiation. There is a contamination because mainly of the hydrocarbons and water molecules present in the vacuum system, which results in an oxidation and a carbon growth on the top-layer of the mirror, but also a contamination coming from the source (debris, high-energy ions), which can remove a few layers of the multilayer stack or erode it.

2.3.1 Degradation of the condenser optics

Contrary to the imaging optics, the condenser optics are directly exposed to the source and therefore to all particles coming from the source. Those so-called debris induce a degradation of the optical properties of the multilayer mirrors but also a modification of their structure upon erosion because of both debris and high-energy ions bombardment.

The measurement of erosion rates of different materials (gold, molybdenum and silicon) deposited on quartz crystal thickness monitors gives an equivalent condenser erosion rate of about 1.4 bilayers per million source pulses under irradiation with a LPP source (liquid-xenon-jet target) [90]. Samples are positioned 110 mm from the source with an angle of 51° from the laser illumination axis and the fast ion flux (with kinetic energies of tens of keV in the case of xenon) is sufficient to be a strongly erosive agent.

Such a phenomenon leads to a reduction of the number of layers in a Mo/Si multilayer mirror designed for EUVL. A collector optic used in the Engineering Test Stand (ETS) [91] and exposed facing the plasma of a Xe-LPP source [92] to half a billion shots presents a relative reflection loss $\Delta R/R \approx -20$ %, which corresponds to a lost of about 15 bilayers. Replacing the real mirror by a 10 periods sample and analyzing it by Auger Electron Spectroscopy (AES), it shows an erosion of 1 bilayer per 15 million pulses [93].

Neither macroscopic mechanical abrasion by micro-sized xenon crystallites, nor chemical reactions, nor thermal evaporation is responsible for the erosion of condenser optics [94]. Time-of-flight Faraday cup measurements show the emission of high energy Xe ions from the Xe-filament jet plasma. Thus a xenon-surface kinetic sputtering by fast ions is the predominant erosion mechanism that alters the condenser optics. The exposition of different materials facing the plasma of a LPP source (Xe-filament) with a distance of 127 mm causes the following erosion rates introduced in Tab. 2.3 [94].

Table 2.3: Erosion rates for different materials exposed to Xe-LPP source [94]

Material	**Erosion rate**
Gold	99 nm/10^6 shots
Molybdenum	26 nm/10^6 shots
Silicon	19 nm/10^6 shots
Carbon	6 nm/10^6 shots

2.3.2 Contamination of the imaging optics

Whereas only the condenser optics are affected by the erosion and re-sputtering effects, all optics present in the EUVL stepper are degraded by the classical contamination processes induced by the EUV light: The oxidation and the carbonization of the top-layers of the multilayer mirrors. The phenomenon of oxidation is mainly due to adsorbed water molecules present in the vacuum system on the silicon surface. Once multilayer mirrors become irradiated with photons but also with electrons or ions, a strong enhancement of the silicon oxidation appears. The water molecules dissociate under secondary electrons, produced by the interaction between the EUV radiation and the multilayer material, into oxygen and hydrogen atoms, which diffuse into the silicon top-layer in order to form silicon oxide SiO_2 [95]:

$$Si + H_2O \overset{EUV}{\to} SiO_2 + H_2 \tag{2.13}$$

Similar to the mechanism of oxidation, a carbon contamination occurs because of the photoelectrons emitted from the top surface. They induce the cracking of the hydrocarbon molecules adsorbed in the illuminated area and lead therefore to carbon growth on top of the multilayer structure [96]:

$$C_xH_y \overset{EUV}{\to} C(s) + H_2 + CH... \tag{2.14}$$

The exposition of gold samples to synchrotron radiation under a pressure of $2{\times}10^{-4}$ Pa shows an initial fast growth rate of carbon and then a significantly slower rate (at least ten times less): The hydrocarbons are first absorbed by the surface and then dissociated by the secondary electrons (or photoelectrons) that are generated by the structure under EUV radiation [97]. An oxidation rate of 0.015 nm/h and a carbon growth rate of 0.25 nm/h per mW/mm of radiation exist under EUV radiation from a synchrotron source following the conditions expected for a EUVL wafer high-throughput (hydrocarbon pressure of 10^{-7} Pa) [98].

Since photoelectrons are known to be responsible for the surface modification, contamination issues of Mo/Si multilayer mirrors can be studied under irradiation by an electron gun set-up. Mirrors irradiated with a power density of 5 mW/mm^2 present a carbon growth on top, which directly depends on the type of the hydrocarbon molecule and its partial pressure (10^{-3}–10^{-9} Pa). The growth kinetics reveals a strong dependence on the irradiation time (linked to the radiation dose) with a fast growth at the beginning and then a slower one. According to X-ray Photoelectron Spectroscopy (XPS) analysis, the structure of the contamination carbon layer consists of a nanocrystalline graphite-like material with a density lower than the standard graphite one (ρ = 2.2 g/cm^3). That layer is also independent of the original hydrocarbon molecule [99].

Finally the carbon contamination of EUV multilayer mirrors not only reduces the throughput of the EUVL stepper because of a loss of reflectivity, but also alters the phase structure of the reflected light that leads to a deformation of the figure of the optics (aberrations, apodisation of the pupil) and thus affects the imaging performances [100].

2.3.3 Preventive methods: Capping layers and cleaning

In order to increase the lifetime of EUV multilayer mirrors for both condenser and imaging optics, a capping layer can be deposited on top of the structure. That layer must consist of a material which is resistant against oxidation, which can be smoothly deposited, which is chemically inert with respect to the multilayer materials (no interdiffusion process) and whose optical constants in the EUV spectral range do not lead to a drop of the peak reflectivity at the wavelength of 13.5 nm [101].

One of the best material for capping layer applications appeared to be ruthenium, which is more effective than silicon against EUV radiation [102]. Under a water pressure greater than 10^{-5} Pa, a Ru-capping layer oxidizes into RuO_2 when a Ru-capped multilayer mirror is irradiated during four hours by synchrotron radiation (EUV power density of 16 mW/mm^2). Nevertheless, contrary to the Si-capped multilayers, the molybdenum layers of such samples are not oxidized even under a water pressure of 10^{-3} Pa [103]. The efficiency of a Ru-capping layer also strongly depends on the crystalline microstructure of the layer that plays a crucial role in the oxidation resistance. A capping layer with randomly oriented grains is less resistant than one with a textured structure [104]. Multilayer mirrors with a new capping layer system consisting of a Ru on B_4C layer and a reflectivity of about 69.6 % at the wavelength of 13.2 nm exhibit a lifetime forty times longer than classical Si-capped mirrors [105].

Another possibility is to deposit a carbon capping layer. Although the initial reflectivity is 0.3 % lower than the reflectivity of a Si-capped Mo/Si multilayer mirror, it remains constant and stable over fifteen hours of continuous exposure [106]. Nevertheless the carbon properties critically depend on the deposition and stabilization process and lead to the formation of a stable oxidation resistant C + SiO_2 layer under initial EUV radiation. A carbon layer can also be deposited under ethanol atmosphere. The gas-phase is used to mitigate the oxidation of the multilayer mirrors caused by the dissociation of adsorbed water molecules. The introduction of ethanol into a water environment (partial pressure of 2.7×10^{-3}–2.7×10^{-5} Pa) inhibits the oxidation process. The ethanol first decomposes onto the mirror surface providing carbon atoms that react with oxygen atoms before they can oxidize the top-layer. Then the carbon atoms form a 0.5 nm thin graphitic layer that prevents the water adsorption on the surface [107, 108].

The last and most perspective material that has been introduced as capping layer is titanium dioxide TiO_2 [109]. TiO_2-capped multilayer mirrors present a normal incidence reflectivity of about 67 % at the wavelength of 13.5 nm. After 42 hours of irradiation by synchrotron radiation (EUV power density of 5 mW/mm^2 under a water pressure of

3×10^{-5} Pa), they show a drop of reflectivity of only -0.6 %, explained by the oxidation of the silicon sub-layer in the design $[Si/Mo]^{60}+Si+TiO_2$ [110].

Contrary to the oxidation process that is irreversible, the carbon growth is reversible. The induced contamination layer can be therefore cleaned. The exposition of Si-capped Mo/Si multilayer mirrors with 10 nm of sputtered carbon on top to Radio-Frequency-O_2 and RF-H_2 plasma discharges at different power (100, 200 and 300 W) shows the possibility to remove the carbon layer [111]. RF-O_2 exposure removes carbon six times faster than RF-H_2 for a given discharge power. However both methods induce degradations of the optical properties of the multilayer mirrors. The exposition to RF-O_2 leads for instance to a surface oxidation [112].

Higher cleaning rates in comparison with RF-discharge cleaning can be achieved by the use of atomic hydrogen, produced by the thermal dissociation of molecular hydrogen using a hot filament. Si wafers with sputtered carbon on top present a removal rate of about 6 nm/h while Mo/Si multilayer mirrors with EUV-induced carbon exhibit a rate of 12 nm/h, which are sufficient for the use in EUVL steppers. Nevertheless that process is more compatible with Ru-capped mirrors, which have an absolute reflectivity drop of -0.6 % after 20 hours of exposition (-1.2 % for Si-capped multilayers) due to the oxidation of the top-layer [113].

The use of molecular oxygen under EUV irradiation is another way to remove the EUV-induced carbon contamination layer. Multilayer mirrors, first contaminated by carbon, can be cleaned under molecular oxygen atmosphere (6.7×10^{-2} Pa) and EUV radiation (power density of 1–3 mW/mm^2) with a maximal removal rate of 6 nm/h. Such a method can also prevent carbon deposition even in presence of a hydrocarbon source and depends stronger on the oxygen pressure than on the EUV power. Nevertheless an oxide layer, with a thickness increasing with the exposure time, the oxygen pressure and the EUV power density, exists on top but the degree of oxidation does not lead to a large drop of reflectivity [114].

2.4 Thermal stability

2.4.1 Thermal stability of Mo/Si multilayer mirrors

Classical Mo/Si multilayer mirrors designed for the wavelength of 13.5 nm are not stable (decrease in period and reflectivity) at temperatures above 200°C. They are thermodynamic non-equilibrium systems that tend to degrade. The thermal degradation of that system is directly linked to the formation of molybdenum silicide compounds at its interfaces, which is due to the diffusion between the molybdenum and silicon layers [115]. Such modifications in the internal structure are shown in Fig. 2.6 [58]. Depending on the annealing temperature, three different kinds of silicides can be observed inside the Mo/Si structure. For temperatures below 400°C, only pure Mo crystallites are evident.

For a temperature range from 400 to 600°C, three phases of silicides are found: Mo_5Si_3, hexagonal $MoSi_2$ and tetragonal $MoSi_2$. The high temperature phase of Mo/Si multilayer mirrors is only tetragonal $MoSi_2$ [116, 117].

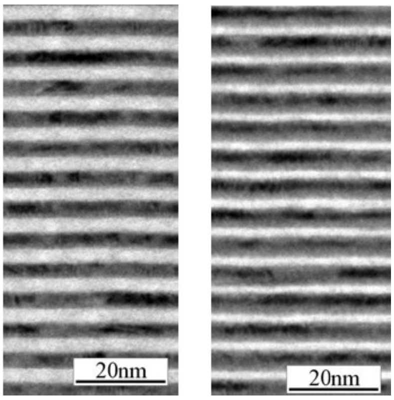

Figure 2.6: Cross-section TEM images of a Mo/Si multilayer as-deposited (left) and after 2 hours annealing at 400°C (right) [58]

That diffusion process can be characterized by the calculation of the interdiffusion coefficients based on the measure of the decay rate of the peak reflectivity of the multilayer mirror during isothermal annealing [118]. For two materials A and B, the interdiffusion coeffcient is defined as a weighted average of the two intrinsic diffusion coefficients D_A and D_B [119]:

$$D_e = \chi_B \; D_A + \chi_A \; D_B \tag{2.15}$$

where χ_A and χ_B are the molar fractions of A and B respectively. The decay of the reflectivity is then related to the effective interdiffusion coefficient D_e by [120]:

$$D_e = \frac{-H^2}{8\pi^2} \frac{d}{d\tau} \left[ln \frac{R(\tau)}{R(0)} \right] \tag{2.16}$$

where H is the multilayer period thickness, τ the annealing time, R(0) the reflectivity of the as-deposited state and R(τ) the reflectivity after annealing. Another main attribute of that phenomenon is the activation energy E_a of the interdiffusion process that is linked to the effective interdiffusion coefficient by [121]:

$$D_e = D_0 \exp \frac{-E_a}{k_B T} \tag{2.17}$$

where D_0 is a preexponential coefficient which is temperature independent and k_B the Boltzmann constant ($k_B = 8.617 \times 10^{-5}$ eV/K). Values of interdiffusion coefficients and activation energies calculated in different studies for Mo/Si multilayer mirrors after annealing at 400°C are reported in Tab. 2.4. It has to be noticed that the as-deposited structure of the interlayer varies from an amorphous mixture to a β-$MoSi_2$ structure, while the molybdenum and silicon structures are either amorphous or crystalline. Such differences may influence both values of the interdiffusion coefficients and activation energies [122].

Table 2.4: Interdiffusion coefficients and activation energies of the interdiffusion process in Mo/Si multilayer mirrors at 400°C

Reference	**Study**	$\mathbf{D_e}$**, m^2/s**	$\mathbf{E_a}$**, eV**
Cheng et al. [123]	TEM	1×10^{-20}	2.3
Holloway et al. [124]	SAXS	7×10^{-19}	2.0
Nakajima et al. [125]	SAXS	1.9×10^{-24}	1.1
Sloof et al. [126]	SAXS	1.7×10^{-25}	0.8
Stearns et al. [122]	EUV	3×10^{-22}	-

2.4.2 Multilayer mirrors with enhanced thermal stability

Two different methods have been developed in order to enhance the thermal stability of Mo/Si multilayer mirrors. The first one is based on a phase and structure equilibrium of the layers, a minimal specific energy of interfaces, high melting temperatures and a similar thermal expandability of the multilayer materials at all investigated temperatures [127]. The thermodynamic equilibrium of two phases at their interfaces can be only achieved if they are neighbors divided by a region of their own eutectic in the phase diagram of a binary alloy system [128]. According to the phase diagram of the binary system Mo/Si (Fig. 2.7) [129], a phase equilibrium between Mo and Si compounds is only possible if they are neighbors in the following sequence [130]:

$$Mo - Mo_3Si - Mo_5Si_3 - MoSi_2 - Si \tag{2.18}$$

The second method consists in a maximal increase of the activation energy of the diffusion process: The higher the activation energy is, the lower the interdiffusion is between the layers (Eq. 2.17). Therefore that phenomenon that happens in a non-equilibrium system is shift to an higher temperature range. Multilayer mirrors with enhanced thermal stability can be obtained by the selection of materials forming eutectics with high melting temperatures [131], by doping impurities in the layers in order to stabilize the amorphous structure [132] or by the insertion of very thin diffusion barriers between the molybdenum and the silicon layers [133].

Different applications for the enhancement of the thermal stability of Mo/Si multilayer mirrors thanks to the use of one of those two methods are presented in Tab. 2.5.

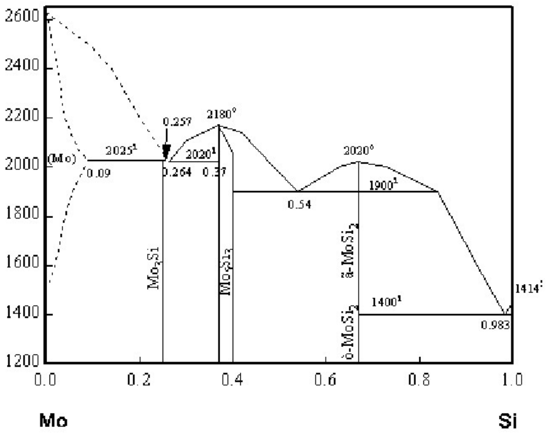

Figure 2.7: Mo/Si binary phase diagram [129]

Table 2.5: Comparison of different multilayer systems in terms of thermal stability

Reference	**System**	**Temperature range**
Feigl et al. [134]	Mo_2C/Si	≤ 300°C
Kondratenko et al. [130]	$MoSi_2/Si$	≤ 600°C
Takenaka et al. [135]	Mo/C/Si/C	≤ 500°C
Wang et al. [136]	Mo/SiO_2	≤ 400°C

It has to be noticed that the degradation processes of the $MoSi_2/Si$ and Mo/C/Si/C multilayer mirrors were only characterized by X-ray reflectivity (λ = 0.154 nm) making difficult the prediction of the degradation of their optical properties in the EUV spectral region.

3 Samples deposition and characterization methods

During all this work, samples were deposited, characterized and investigated by several methods. Here is presented an overview of the main tools used in this aim.

3.1 Magnetron sputtering deposition

All samples were deposited by dc-magnetron sputtering (direct current), using an industrial sputtering system MRC 903M from the firma Kenotec. A picture of this system is introduced in Fig. 3.1.

Figure 3.1: MRC 903M sputter deposition system

During the sputtering process, gas ions out of a plasma are accelerated towards a target consisting of the material that has to be deposited [137]. Each cathode can work under two different regimes: dc-sputtering and rf-sputtering. In the dc-sputtering [138], a negative potential up to some hundreds Volts is applied to the target. Argon ions are consequently accelerated towards the target and set material free. A bias voltage can also be applied to the substrate. It has the effect of accelerating ions towards the substrate [139]. During the deposition, the substrate holder moves beyond the target and the deposited film thickness scales to the inverse velocity of the movement. Magnetron sputtering technology ensures a good reproducibility of processes thanks to a high accuracy deposition speed control. The main deposition parameters for the MRC 903M sputtering system are presented in Tab. 3.1.

Table 3.1: Main deposition parameters

Magnetron size	120×360 mm^2
Distance target-substrate	50 mm
Base pressure	10^{-5} Pa
Working pressure	10^{-1} Pa
Working gas	Argon
Power on Mo	150 W
Power on Si	200 W
Bias	0–300 V

The principle of such a machine is based on a lateral translation of the substrate holder under three rectangular magnetrons with a size of 120 mm × 360 mm, corresponding to a sputter down process (the material is sputtered from the target down to the substrate). The base pressure of the system is around 10^{-5} Pa and is achieved by a cryopump. The deposition is performed under an argon atmosphere of 0.1 Pa.

3.2 X-ray reflectivity

Measurement of the X-ray reflectivity is the conventional method used for the characterization of EUV multilayer mirrors. All samples were measured by an X-ray diffractometer D 5005 from the firma Bruker AXS (Fig. 3.2) at the wavelength $\lambda = 0.154$ nm (Cu-Kα radiation) with a θ–2θ geometry. The X-ray tube FLCu-4KE was operated at a power of 1.6 kW (40 kV/40 mA) for Small Angle X-ray Reflectivity (SAXR) measurements with small grazing angles ($\theta \leq 20$ deg) and for Large Angle X-ray Diffraction (LAXD) measurements (20 deg $\leq \theta \leq$ 60 deg). The X-ray reflection of multilayer mirrors provides information about the layer thickness, the layer density and the layer roughness (interdiffusion and top-roughness) in the structure [140].

A wave can be totally reflected at the boundary between vacuum and another material for grazing angles θ (θ = 90 - α, if α is the incidence angle) smaller than a critical angle θ_c (grazing incidence angle at which a well-collimated beam of X-rays is no longer totally reflected off the free surface, but starts penetrating into the sample). From the Fresnel equations and the Snell´s law ($\tilde{n}_1\sin\alpha_1 = \tilde{n}_2\sin\alpha_2$), the critical angle for total external reflection can be approximated by ($\beta = 0$ and $\delta \ll 1$) [141]:

$$\sin\theta_c = \sqrt{2\delta} \tag{3.1}$$

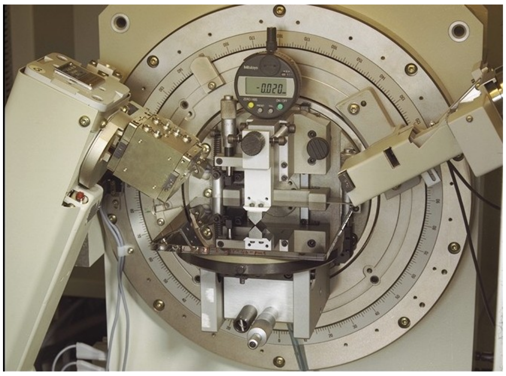

Figure 3.2: X-ray diffractometer D 5005

In the case of multilayer systems, Bragg peaks are obtained from the interference of the waves reflected at each interface. The period thickness of the multilayer can be calculated from their frequencies with the Eq. 2.9 and 3.1 [142]:

$$2d\sqrt{sin^2\theta_m - sin^2\theta_c} = m\lambda \tag{3.2}$$

where θ_m is the grazing angle corresponding to the mth maximum and θ_c the critical angle for total external reflection. Using an X-ray tube, the relative wavelength separation ($\lambda_{K\alpha_1}$ - $\lambda_{K\alpha_2}$)/$\lambda_{K\alpha}$ is comparable to the relative angular resolution $\Delta\theta/\theta \approx 0.001$ of the reflectometer [143]. The relative uncertainty on the layer thickness can be determined:

$$\frac{\Delta d}{d} = \frac{\Delta\theta}{\theta} + \frac{\Delta\lambda}{\lambda} \approx 0.002 \tag{3.3}$$

From the critical angle for total external reflection θ_c, the thin film electron density can be determined and then the material density [144]. θ_c practically approximately equals to the grazing angle corresponding to a reflection of half of the total reflection. Since critical angles are in a range from 0.2 to 0.5 deg, the following approximation can be made: sin$\theta_c \approx \theta_c$. Neglecting the absorption and with the Eq. 2.3 and 3.1, the material density of a layer can be calculted from the critical angle θ_c:

$$\theta_c \approx \sqrt{2\delta} = \lambda\sqrt{\frac{N_{at}r_0f_1}{\pi}} = \lambda\sqrt{\frac{6.02\times10^{23}\rho r_0 f_1}{\pi A}} \tag{3.4}$$

where A is the relative atomic mass. From the Eq. 3.4 the relative uncertainty on the layer density can be calculated:

$$\frac{\Delta\rho}{\rho} = 2\left(\frac{\Delta\lambda}{\lambda} + \frac{\Delta\theta_c}{\theta_c}\right) \approx 0.02 \tag{3.5}$$

Roughness on top of the samples, at each interface and interdiffusion processes in the structure lead to a drop of reflectivity of the Bragg peaks, following the behavior described by the Eq. 2.12. All X-ray reflection measurements were fitted using the commercial software REFSIM [145].

3.3 EUV reflectivity

The measurements of the EUV reflectivity were performed at the PTB reflectometer [146] at BESSY II in Berlin. Reflectometry, especially the measurement of the reflectivity of Mo/Si multilayer mirrors for EUVL, is a major activity at the beamline [147]. Mirrors were measured in the wavelength range from 12.5 to 14.5 nm at the beamline SX700 (using a plane grating monochromator) [148] with a wavelength resolution of about 0.02 nm (0.15 eV). The incidence angle of the beam was fixed at 1.5 deg and the beam spot had a diameter of about 1.5 mm on the sample surface. The reflectivity was calculated as following:

$$R = \frac{2I_2}{I_1 + I_3} \tag{3.6}$$

where I_1 and I_3 are the direct intensities measured before and after the measurement of the reflected beam I_2. A relative uncertainty of 0.1 % is achieved for the peak spectral reflectivity of a mirror in the EUV spectral region. Different factors contribute to this uncertainty: the stability of the normalized intensity (0.02 %), the inhomogeneity of the detector (0.04 %), the higher diffraction orders (0.02 %) and the diffuse scattered light (0.08 %) [149].

3.4 Atomic force microscopy

The surface microtopography of all samples was determined using a commercial Atomic Force Microscope (AFM) from the firma Digital Instruments/Veeco (Dimension^{TM} 3100). The AFM was developed to exploit contact and non-contact forces for imaging surface topology on an atomic scale [150]. It is based on a surface screening with a very thin tip (radius of a few nanometers) linked to a cantilever. As the tip is repelled by or attracted to the surface, the cantilever beam deflects. The magnitude of the deflection is captured by a laser that reflects at an oblique angle from the very end of the cantilever to a photodiode detector. A plot of the laser deflection versus tip position on the sample surface provides the resolution of the hills and valleys that constitute the topography of the surface [151]. In order to overcome all sample degradations due to tip-sample related difficulties, all measurements were performed with the TappingMode^{TM} technique [152]. This method has indeed the main asset to achieve high resolution without inducing destructive frictional forces [153]. Its principle is shown in Fig. 3.3: The cantilever oscillates near its resonant frequency (around 300 kHz) and the oscillation amplitude (typically from 10 to 100 nm) is reduced as soon as the tip and the sample surface are in contact. The oscillation amplitude scales then proportionally to the average distance between the probe and the sample [154].

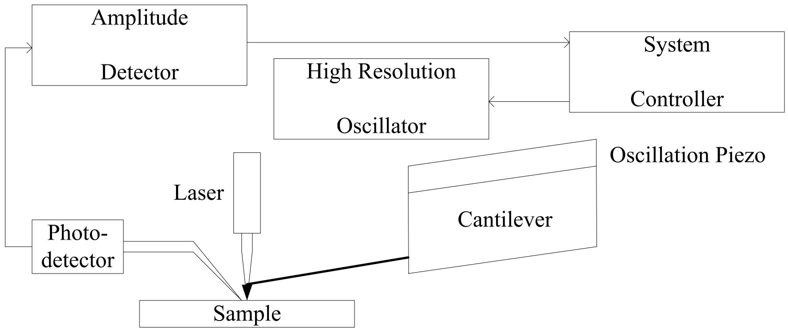

Figure 3.3: Principle of the atomic force microscopy

The spatial frequencies used during AFM investigations depend on the scan area L and the distance between two measured points ΔL. According to the sampling theorem, the range of the measurable spatial frequencies f is defined by:

$$\frac{1}{L} \leq f \leq \frac{1}{2\Delta L} \tag{3.7}$$

The quantative analysis of the surface roughness of investigated mirrors has been performed over a scan area of 1×1 μm^2 with a resolution of 512×512 data points. The corresponding spatial frequency range is then: 1 μm^{-1} $\leq$ f $\leq$ 250 μm^{-1}. The lateral resolution (maximal spatial frequency that can be measured) also depends on both the probe radius and the surface features. Assuming that the surface profile can be described by a simple sinusoidal wave (amplitude a), it is accurately represented by a tip with a radius r if [155]:

$$f_0 = \frac{1}{2\pi\sqrt{ar}} \tag{3.8}$$

For the investigation of EUV multilayer mirrors by AFM, typical surfaces have a maximal amplitude a $\approx$ 1 nm and an ultrasharp silicon probe of 10 nm radius is used [156]. The maximal spatial frequency that can be investigated is therefore $f_0 = 50$ μm^{-1}.

3.5 Transmission electron microscopy

Cross-sectional images of EUV multilayer mirrors have been obtained by Transmission electron microscopy (TEM). All samples were investigated with a microscope JEOL-JEM 3010 operated at 300 kV. The point-to-point resolution is about 0.2 nm for classical bright and dark field pictures. To observe smaller features High-Resolution Transmission Electron Microscopy (HRTEM) has been used (sub-angstrom resolution) [157]. TEM is an imaging technique whereby a beam of electrons is focused onto a specimen causing an enlarged version. Highly exited electrons, which are produced using a cathode ray tube or a filament in a vacuum, are accelerated towards the sample by creating a potential difference. Magnets and metal apertures are used in order to focus this steam of electrons into a monochromatic beam, which collides with the specimen and interacts depending on the density and the charge of the material [158]. TEM images provide structural information on the atomic scale from multilayer mirrors: The degree of crystallinity and the crystal orientation within the layers can be determined from the electron diffraction [159].

These interactions between the electrons and the matter are nevertheless greatly affected by the sample preparation. Any contamination (implantation of atoms, precipitation of particles) of the sample influences the observed image. For the investigation of EUV multilayer mirrors, samples were prepared by Broad Ion Beam (BIB) [160]. Cross-sectional discs of 2–3 mm in diameter are first mounted face-to-face, then mechanically polished down to a thickness of about 10 μm and finally thinned by low energy BIB milling. Typical BIBs use an argon beam with an accelerating voltage first of 8 kV to achieve a sample thickness of a few tens of nanometers (rough milling) and then of 3 kV to keep the thickness of the amorphous top-layer as thin as possible (fine milling). To avoid any degradation of the samples during the preparation, they are thinned under a small beam glancing angle [161].

3.6 X-ray Photoelectron Spectroscopy

X-ray Photoelectron Spectroscopy (XPS) investigations were performed at Jenoptik L.O.S. [162] in Jena with the following parameters (Tab.3.2):

Table 3.2: Main characteristics of XPS investigations

Detectable elements	$Z \geq 2$
Typical detection limit	5×10^{-1} at %
Typical information depth	5–10 nm
Lateral resolution	1 mm

XPS is based on the photoelectric effect outlined by Einstein in 1905 [163], where the concept of the photon was used to describe the ejection of electrons from a surface when photons impinge upon it. It has two major properties: The quantitative analysis and information on the chemical nature and the state of the detected elements (binding energy variations of photo-ionized atoms depend on their chemical environment). By absorbing a photon, an atom receives an energy equals to hν (photon energy). In order to come back to its original stable state, it then releases an electron containing all the energy of the striking photon, that escapes from the atom and even from the matter due to its kinetic energy. For XPS investigations, striking photons have an energy of 1486.6 eV (emitted from an aluminium source). The energy of the photoelectrons leaving the sample is determined using a concentric hemispherical analyzer, that consists of two metal hemispheres (one concave and one convex), arranged such that their centers of curvature are coincident. Different voltages are then placed on each hemisphere to create an electric field in between and the electrons, injected into the gap and running very fast, impinge on the outer hemisphere, while the slow ones are attracted to the inner hemisphere. Therefore only electrons in a narrow energy range succeed in getting all the way round the hemispheres to the detector, which results in a spectrum with a series of photoelectron peaks (the binding energies of the peaks are characteristic of each element) [164]. The peak areas can be used to determine the composition of the materials surface: The spectrum of photoelectron peaks is evaluated by integration of the photoelectron peaks and the chemical composition is extracted from the peak intensities (assuming an homogeneous mixing). For Mo/Si multilayer mirrors the Si2p- and Mo3d-peaks are fitted by gaussian distributions with variable full width at half maximum values and the binding energies of the chemical bonds are then extracted [165]. As the shape of each peak and the binding energy is slightly altered by the chemical state of the emitting atom, that also provides information about the chemical bonding. XPS analyses must be carried out in Ultra High Vacuum (UHV) conditions, otherwise molecules in the air land onto the surface and change its properties.

3.7 Annealing of multilayer mirrors

For the investigation of the thermal stability of different Si-based multilayer mirrors, the samples were annealed in an industrial high vacuum oven from the firma MUT (Oven HVO 400), evacuated to 10^{-3} Pa. The temperature was measured by a Pt-thermocouple directly on the sample holder (four additional places like the bottom or the top of the oven can also be monitored). The heating rate was fixed at 10 K/min and the whole process (heating, annealing and cooling) was performed under vacuum. The evolution of the temperature during the experiment was also monitored as introduced in Fig. 3.4 (100 hours annealing at 500°C). The zoom shows that the temperature homogeneity is +/- 5°C: The temperature measured on the sample plate corresponding to the yellow curve is ranged between 495 and 505°C while the target is 500°C. During the experiments, annealings in a temperature range from 250 to 650°C were performed.

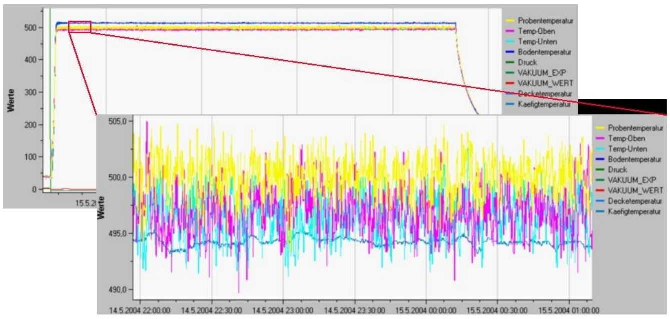

Figure 3.4: Temperature monitoring for 100 hours annealing at 500°C

3.8 Irradiation of multilayer mirrors

For the investigation of the radiation stability, the samples were irradiated with a Xe-gas discharge source (hollow-cathode Z-pinch plasma geometry, Fig. 3.5), pulsed at 50 Hz (pulse duration of about 100 ns) with a pulse energy of about 0.5 mJ/sr at the wavelength $\lambda = 13.5$ nm (± 2 %) [166]. The tests were carried out in an un-baked vacuum chamber at a working pressure of about 0.2 Pa (base pressure of 2×10^{-3} Pa). The typical Xenon EUV emission spectrum is also presented in Fig. 3.5 [167].

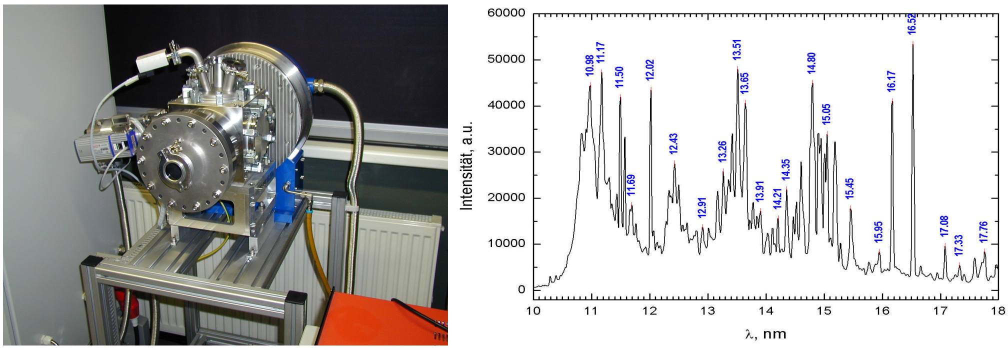

Figure 3.5: Xe-gas discharge source (left) and typical Xenon EUV emission spectrum (right)

Samples were placed 140 mm in front of the plasma and were exposed under a solid angle of about 0.03 sr. According to the source technical data, one hour of irradiation corresponds to 180,000 pulses and to a total EUV-dose of 2.9 J. In order to investigate the radiation stability of the collector mirror, samples were first irradiated without any mitigation system (and therefore exposed to all debris coming from the source). A Zr filter, that mitigates the impact of the out-of-band radiation in the UV, visible and IR spectral ranges, partially protects the optics from the debris coming from the radiation source and serves as a barrier for EUV absorbing gasses [168], was then introduced in the irradiation chamber between the plasma and the sample for the investigations on imaging optics. They consisted of 200 nm of zirconium mounted on nickel mesh and must have highest possible transmittance at 13.5 nm. The theoretical transmittance of such a filter is introduced in Fig. 3.6.

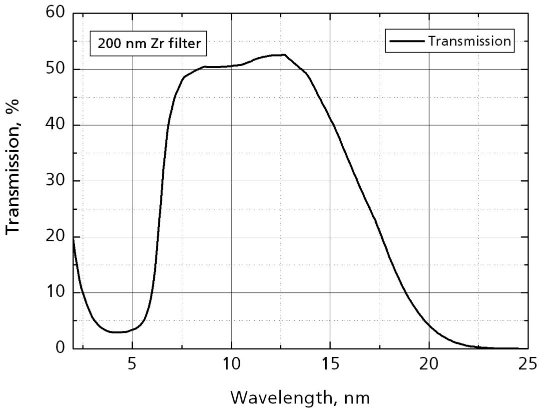

Figure 3.6: Theoretical transmittance of a 200 nm thick Zr filter

The introduction of such a filter leads of course to a reduction of the EUV-dose because of the absorption of one part of the light. Assuming an average transmission of 50 % for the different filters used during the experiments, the EUV-doses corresponding to the different investigated irradiation conditions are summarized in Tab.3.3:

Table 3.3: EUV-doses corresponding to the different irradiation conditions

Irradiation time	**EUV-dose without Zr-filter**	**EUV-dose with Zr-filter**
1 h	$\approx$ 5 mJ/mm^2	$\approx$ 2.5 mJ/mm^2
2 h	$\approx$ 10 mJ/mm^2	$\approx$ 5 mJ/mm^2
4 h	$\approx$ 20 mJ/mm^2	$\approx$ 10 mJ/mm^2
8 h	$\approx$ 40 mJ/mm^2	$\approx$ 20 mJ/mm^2
16 h	$\approx$ 80 mJ/mm^2	$\approx$ 40 mJ/mm^2

4 Results

4.1 Growth, structure and optical properties of Mo/Si multilayer mirrors

All investigations about the radiation and thermal stability of EUV multilayer mirrors (part 3.7 and 3.8) were performed on Si-based mirrors. Classical Mo/Si multilayer mirrors, designed for application in EUVL, were chosen as the reference for the comparison of both the radiation and the thermal stability performances. They consisted of 60 bilayers (one Si layer and one Mo layer) and were deposited by dc-magnetron sputtering onto monocrystalline (100) silicon substrates (part 3.1).

4.1.1 Calculated optical properties of Mo/Si multilayer mirrors

The maximal theoretical normal incidence reflectivity for Mo/Si multilayer mirrors designed for the wavelength $\lambda = 13.5$ nm and with a total number of periods N is introduced in Fig. 4.1. All calculations have been performed with the software FilmWizard [169] assuming ideal multilayer structures (no interface-roughness and no imperfection at the interfaces) and the layer thicknesses have been optimized for each number of period N. A top-layer of two nanometers of silicon oxide (SiO_2) has also been included into the multilayer design in order to represent the natural oxidation of the silicon top-layer in air. The optical constants of the materials used in the calculations are derived from the scattering factors of Henke [10, 11]. They have been calculated with the density of the bulk materials ($\rho_{Si} = 2.33$ g/cm^3, $\rho_{Mo} = 10.22$ g/cm^3 and $\rho_{SiO_2} = 2.55$ g/cm^3). Theoretical optical and design parameters of ideal Mo/Si multilayer mirrors with different number of periods N are summarized in Tab. 4.1.

Table 4.1: Optical and design parameters of Mo/Si mirrors designed for $\lambda = 13.5$ nm with different number of periods N

N	40	60	80
Reflectivity, %	72.7	73.6	73.7
FWHM, nm	0.63	0.57	0.56
Thickness ratio Γ	0.57	0.55	0.55

According to the previous theoretical calculations, there is no more increase in the reflectivity with increasing the number of bilayers from N = 60 to 80. Because of the

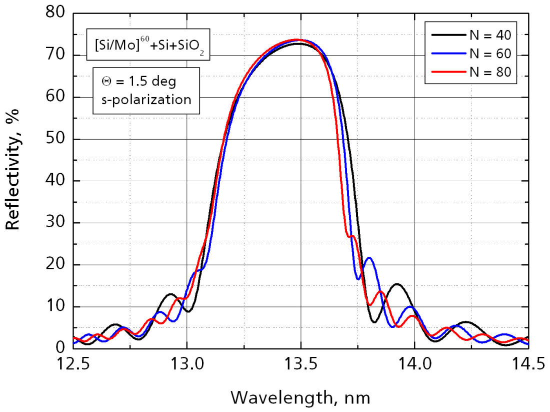

Figure 4.1: Theoretical optical performances of Mo/Si mirrors designed for $\lambda = 13.5$ nm

absorption of the materials, the penetration depth of the light is limited to a few hundreds of nanometers and a greater number of periods (N $\geq$ 60) does not induce a gain of reflectivity. The optimal Mo/Si multilayer mirrors have therefore the following design: [4.21 nm Si / 2.69 nm Mo]^{60} + 3.50 nm Si. Theoretical calculations performed by Singh et al. [69, 85] demonstrates the same level of reflectivity for Mo/Si multilayer mirrors designed for the wavelength $\lambda = 13.5$ nm.

4.1.2 Characterization of as-deposited Mo/Si multilayer mirrors

The main characteristics of Mo/Si multilayer mirrors (such as the period H, the layer ticknesses and the interface-roughnesses) can be extracted from the simulation of the X-ray reflectivity measurement curves with the commercial software REFSIM [145]. In order to achieve the best fit as possible of the measured curves, the choose of a correct design model is very important. As-deposited Mo/Si multilayer mirrors can be first described as a stack of 60 bilayers consisting of successive Mo- and Si-layers and a Si-top-layer oxidized in the air. That two-layer model only describes the theoretical structure of Mo/Si multilayer mirrors. To be closer to the real sructure, a four-layer model can also be applied, taking into account the formation of intermixing zones due to the interdiffusion between the Mo- and the Si-layers (part 2.2.2). The comparison between the fits achieved with both designs is presented in Fig. 4.2.

The large number of Bragg peaks (more than ten) is a piece of evidence of the good geometric quality of the multilayer stucture (sharp interfaces). The narrow and symmetrical peaks also indicate a constant thickness of the layers in depth in the multilayer structure. The disagreement in peak intensity between the measured and the fitting curves can be explained by a small thickness variation (less than 1%) inside the multilayer structure,

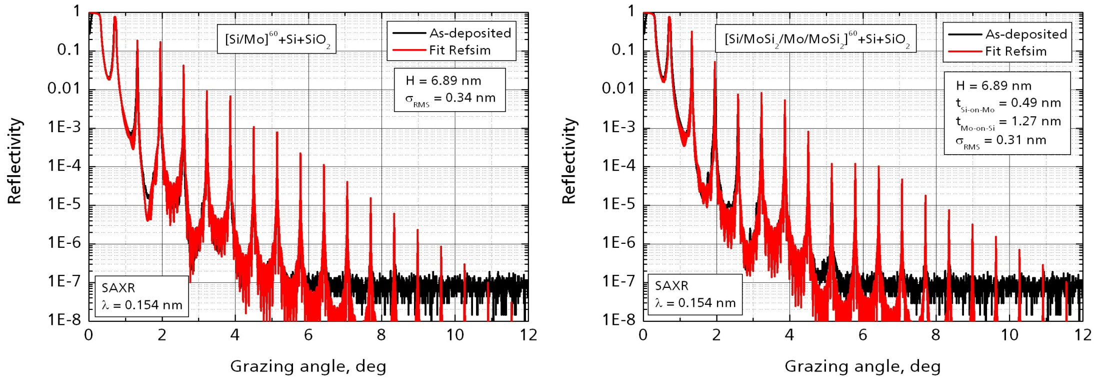

Figure 4.2: Measured and fitting SAXR curves of an as-deposited Mo/Si multilayer mirror achieved with a two-layer model (left) and with a four-layer model (right)

that cannot be included into the fitting model. Results achieved with the four-layer design exhibit a multilayer period H = 6.89 nm with a top-roughness of 0.30 nm. A silicon oxide layer (SiO$_2$) with a thickness of 1.90 nm has also been found on the top of the mirror, corresponding to the native oxidation of the silicon top-layer. Because of the presence of the intermixing zones, it is impossible to define and then to quantify the thickness ratio Γ of the multilayer structure. That could only be applied in the case of a two-layer model. Furthermore two different silicides depending on the interface resulted from that fitting process. At the Mo-on-Si interface, the Mo$_x$Si$_y$-layer has a thickness t = 1.27 nm and a density of 5.95 g/cm^3, while a thickness t = 0.49 nm and a density ρ = 5.81 g/cm^3 have been calculated at the Si-on-Mo interface. This asymmetry of the two different interfaces in Mo/Si multilayer mirrors was already demonstrated by many authors [81, 170]. According to the Mo/Si binary phase diagram (Fig. 2.7), three different silicides can be formed at a Mo-Si interface: Mo$_3$Si, Mo$_5Si_3$ and MoSi$_2$. The theoretical bulk densities of those silicides are respectively: ρ_{Mo_3Si} = 8.97 g/cm^3, $\rho_{Mo_5Si_3}$ = 8.24 g/cm^3 and ρ_{MoSi_2} = 6.24 g/cm^3. The intermixing zone have therefore a phase composition close to MoSi$_2$, as already shown in many works [124, 122].

According to the simulation results achieved with the two-layer model, the actual thickness ratio Γ (Γ = t$_{Mo}$/H) is 0.44 and the period H of this sample 6.89 nm. An additional interface-roughness in the range of 0.2–0.3 nm has been found between each layer and mirrors have a top-roughness σ = 0.34 nm. Although that two-layer model does not fit the measured curve as well as the four-layer model, the results extracted from these both methods are comparatively close for the main parameters of the multilayer mirrors: multilayer period, top-roughness, nature and thickness of the oxide top-layer. Finally, Si-layers have a density of 2.33 g/cm^3, that is equal to the density of the bulk material, and Mo-layers a density of 9.95 g/cm^3, whereas the molybdenum density is 10.22 g/cm^3. As-deposited Mo/Si multilayers consisted of amorphous Si- and polycrystalline Mo-layers as shown by the LAXD measurement in the Fig. 4.3. The broad peak at 20.35 deg (lattice spacing a = 0.222 nm) results of the reflection of the [110] plane of the body-centered cubic Mo modification (bcc-Mo). The quantative analysis of the surface roughness of Mo/Si multilayer mirrors, performed by AFM, exhibited a rms-roughness of $\sigma = 0.14$ nm (Fig. 4.3). This value is close to the one extracted from the SAXR simulation ($\sigma \approx 0.30$ nm) and to the one of the used Si subtrates ($\sigma = 0.20$ nm).

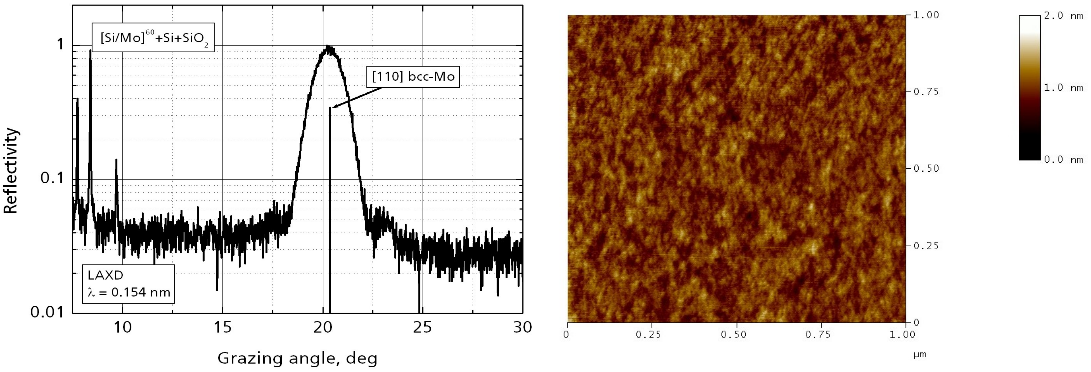

Figure 4.3: LAXD curve (left) and surface morphology ($\sigma = 0.14$ nm, right) of an as-deposited Mo/Si multilayer mirror

The optimization of the multilayer design and the deposition parameters results in a peak reflectivity of R = 68.2 % at the wavelength $\lambda = 13.44$ nm (FWHM = 0.50 nm). The fit achieved with the software IMD [171] shows a multilayer period H = 6.90 nm, a thickness ratio $\Gamma = 0.40$ and a natural 2 nm thick SiO_2-layer on top. The fit has been performed with the densities of the bulk materials. Both measured and fitting curves are introduced in Fig. 4.4. The fitting parameters shows a good agreement with the results of the SAXR simulation (Fig. 4.2). For this calculation, a two-layer model has been used and the intermixing zones have been incorporated in the quantification of the interface-roughness. The resulting top-roughness $\sigma = 0.30$ nm is in the range of the ones measured by AFM (Fig. 4.3) and SAXR (Fig. 4.2).

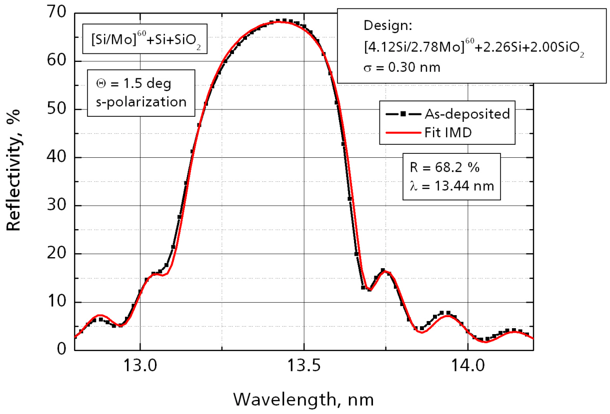

Figure 4.4: Measured and fitting EUV reflectivity curves of an as-deposited Mo/Si multilayer mirror (H = 6.90 nm)

4.2 Radiation stability of Mo/Si multilayer mirrors

The stability of Mo/Si-based multilayer mirrors under EUV radiation has been investigated with a Xe-gas discharge source for both collector mirrors (direct exposition to the source) and imaging optics (protection of the mirrors with a Zr-filter). Potential capping layer solutions for the improvement of the radiation stability of such optics have been developed.

4.2.1 Radiation stability of collector optics

The first tests on radiation stability of Mo/Si multilayer mirrors were performed in the case of optics used as collector mirrors for EUVL. The mirrors (Si-capped Mo/Si multilayers) were placed at 140 mm from the source and irradiated without any mitigation system (no Zr-filter) under normal incidence with the following EUV-doses: D = 5, 10, 20 and 40 mJ/mm^2 (part 3.8). The evolution of the EUV properties of such mirrors is introduced in Fig. 4.5. Optimized as-deposited Mo/Si multilayers present a peak reflectivity R = 68.4 % at the wavelength $\lambda = 13.44$ nm. The irradiation with an EUV-dose D = 40 mJ/mm^2 induces a drop of reflectivity of -18.4 % (R = 50.0 % at $\lambda = 13.44$ nm). As there is no modification of the shape of the peak reflectivity (the FWHM remains stable after irradiation), the degradation processes only happen on the top of the multilayer mirrors.

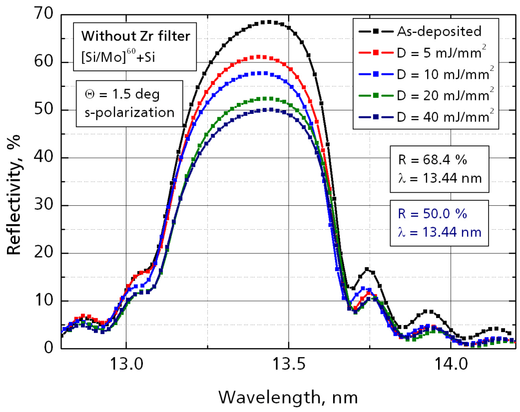

Figure 4.5: Evolution of the EUV properties of Si-capped Mo/Si multilayer mirrors after irradiations with doses up to 40 mJ/mm^2

The comparison of the SAXR curves (Fig. 4.6) for Si-capped Mo/Si multilayer mirrors measured in as-deposited state and after each irradiation shows no modification in the position of the Bragg peaks, but only changes in the valleys between the peaks. There is therefore no change of the multilayer period thickness and all changes occur in the first top-layers (modification of the top structure) as already demonstrated with the analysis of the EUV reflectivity curves. That phenomena of surface modification of Mo/Si multilayer mirrors under different EUV irradiation conditions has been already found by many authors [95, 97, 93]. The simulation of the first Bragg peaks (up to a grazing angle of two degrees) is also presented in Fig. 4.6. It corresponds to the part of the curve, that is the most dependent on the surface effects, and therefore provides information about the modification of the top-layers. The results of the simulation achieved after an irradiation EUV-dose D $=$ 40 mJ/mm^2 shows a full oxidation of the first silicon layers and a partial oxidation of the molybdenum sub-layer. A development of roughness on top of the mirrors has also been found from 0.3 to 0.6 nm with the formation of a SiO_2-layer on top of the multilayer structure.

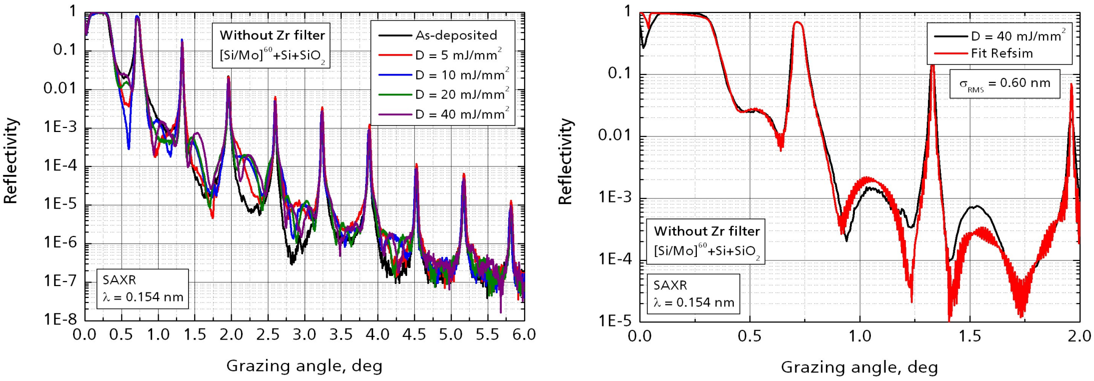

Figure 4.6: Comparison of the SAXR curves for Si-capped Mo/Si multilayer mirrors as-deposited and irradiated with doses up to 40 mJ/mm^2 (left) and simulation of the first Bragg peaks (right)

Such a development of the top-roughness has been also found with AFM investigations (Fig. 4.7) from 0.14 nm for the as-deposited state to 0.49 for the mirrors irradiated with an EUV-dose D $=$ 40 mJ/mm^2. That is close to the roughness determined by the simulation of the SAXR measurements, where $\sigma = 0.60$ nm with the maximal EUV-dose (Fig. 4.6).

In order to investigate that EUV-induced modification on top, XPS studies have been performed. The evolution of the XPS spectra of Mo/Si multilayer mirrors between the as-deposited state and after irradiation (D $=$ 40 mJ/mm^2) for the O1-, C1, Mo3d- and Si2p-peaks is introduced in Fig. 4.8. The variation of the peak intensity, found for the O1- and C1-peaks, corresponds to changes in the oxygen and carbon concentrations in the top-layers. The modifications of the peak shape (peak intensity, peak position) in the case of the Si2p- and Mo3d-peaks also demonstrate changes in the binding states of each compound, like those induce by the oxidation of a material.

The fit of those spectra shows a total oxidation of the Si-top-layer and a partial oxidation of the Mo-sub-layer after irradiation with an EUV-dose of 40 mJ/mm^2 (Tab. 4.2 and 4.3).

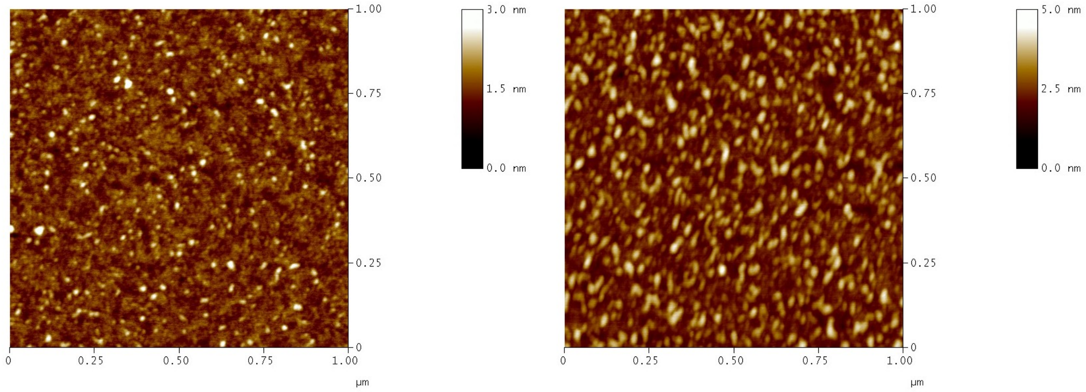

Figure 4.7: Evolution of the surface morphology of Mo/Si multilayer mirrors after irradiation: D = 10 mJ/mm^2 (σ = 0.24 nm, left), D = 40 mJ/mm^2 (σ = 0.49 nm, right)

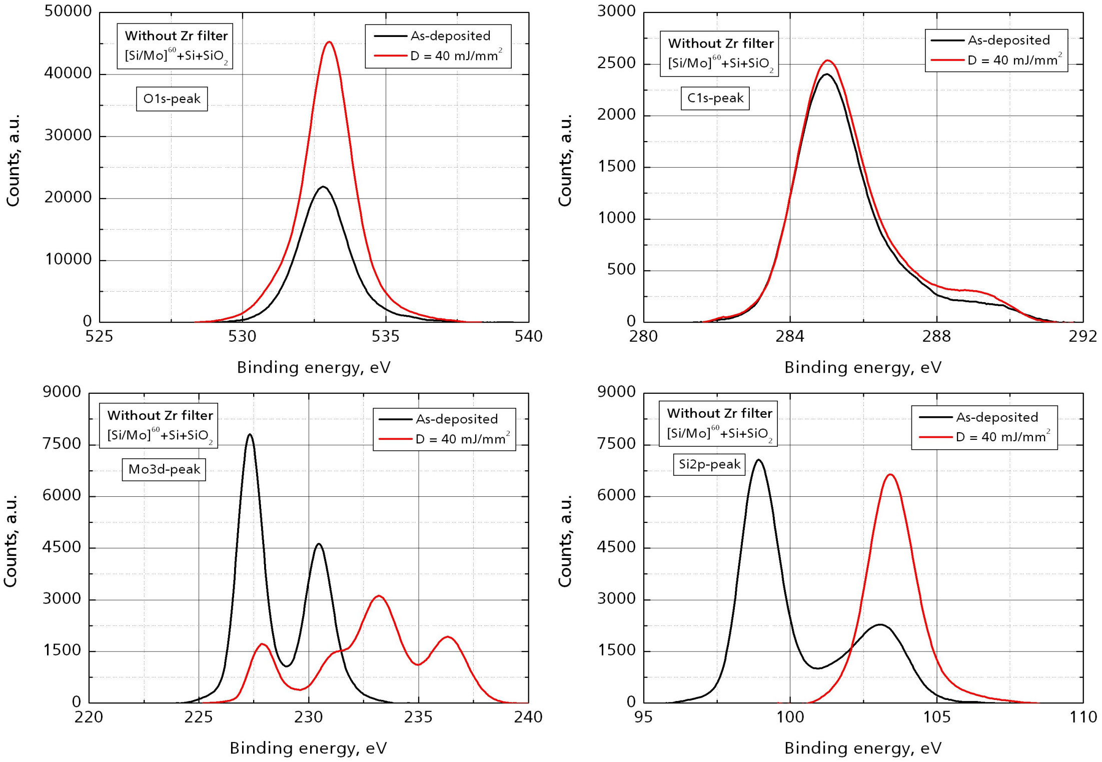

Figure 4.8: Evolution of the XPS spectra of Mo/Si multilayer mirrors after irradiation with D = 10 mJ/mm^2: O1s-peak (upper left), C1s-peak (upper right), Mo3d-peak (lower left) and Si2p-peak (lower right)

In the as-deposited state, only on third of the silicon is oxidized (SiO$_x$) and the whole molybdenum is in metal state. After irradiation, the whole silicon is oxidized and only one quarter of the molybdenum remains in metal state. That increase in the oxidation level of the top-layers has two main impacts on the reflectivity of the irradiated multilayer mirrors. The presence of more oxygen atoms firts leads to an increase of the absorption of the light by the oxidized layers. The oxidation of the Si and Mo top-layers also causes changes of the ticknesses of the top-layers (the oxidation process is accompanied by a variation of volume).

Table 4.2: Chemical composition of the sample surface, at %

State	**C**	**O**	**Si**	**Mo**	**Xe**	**Ar**
As-deposited	22.2	40.3	34.7	2.2	0.1	0.6
Irradiated	12.1	56.6	28.2	2.2	0.3	0.6

Table 4.3: Result of the fit of the Si2p- and Mo3d-Peaks, %

State	**Si**	**SiO$_x$**	**Mo**	**MoO$_x$**
As-deposited	63.6	36.4	100	0
Irradiated	0	100	22.8	77.2

Considering one-dimensional volume changes in the Mo/Si multilayer mirrors upon oxidation of the top-layers, the full oxidation of the Si-top-layer induces an increase in the thickness of the Si-based layer (the Mo-based layer as well becomes thicker through the oxidation of the Mo-sub-layer). Assuming that the molar volumes of Si and SiO_2 are respectively $V_{Si} = 12.1$ cm^3/mol and $V_{SiO_2} = 23.6$ cm^3/mol, the thickness of the SiO_2-layer obtained after the total oxidation of the Si-layer is:

$$t_{SiO_2} = \frac{V_{SiO_2}}{V_{Si}}\, t_{Si} \approx 1.95\, t_{Si} \tag{4.1}$$

The same calculation for the Mo-sub-layer ($V_{Mo} = 9.4$ cm^3/mol and $V_{MoO_2} = 19.7$ cm^3/mol) leads to the relationship:

$$t_{MoO_2} = \frac{V_{MoO_2}}{V_{Mo}}\, t_{Mo} \approx 2.1\, t_{Mo} \tag{4.2}$$

According to the previous result, a model for the degradation process of the Mo/Si multilayer mirrors under EUV radiation can be suggested (Fig. 4.9). As shown in the part 4.1, a natural oxidation of the silicon top-layer happens after the deposition of the mirrors. That layer has a thickness of about 2 nm. After irradiation of the mirrors with an EUV-dose of 40 mJ/mm^2, a full oxidation of the silicon top-layer and an oxidation of three quarters of the molybdenum sub-layer were found. Upon oxidation of the top-layers, the total thickness of the last two layers increases by a factor two (Eq. 4.1, 4.2). It has to be noted that Fig. 4.9 shows the application of that model for a maximal EUV-dose of 40 mJ/mm^2. A greater dose should induce a more important oxidation process, not only limited to the first two layers and leading to the oxidation of a few additional layers and therefore to a bigger drop of reflectivity.

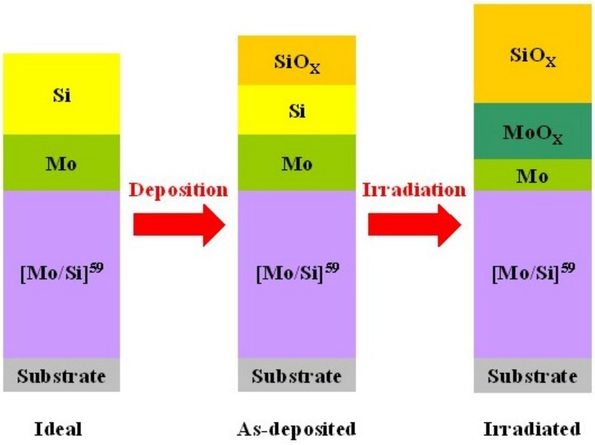

Figure 4.9: Model of degradation of the Mo/Si multilayer mirrors under EUV radiation

That model has been also used to fit the EUV reflectivity curve measured after the irradiation with D = 40 mJ/mm^2. It was obtained with the software IMD (Fig. 4.10). The fitting results show a good agreement with the model previously proposed, demonstrating an oxidation of the first two layers of the structure (total oxidation of the silicon layer and partial oxidation for the molybdenum layer). It also exhibits an increase in the top-roughness up to 0.50 nm, that has been found with the AFM investigations (Fig. 4.7) and the SAXR measurements as well (Fig. 4.6).

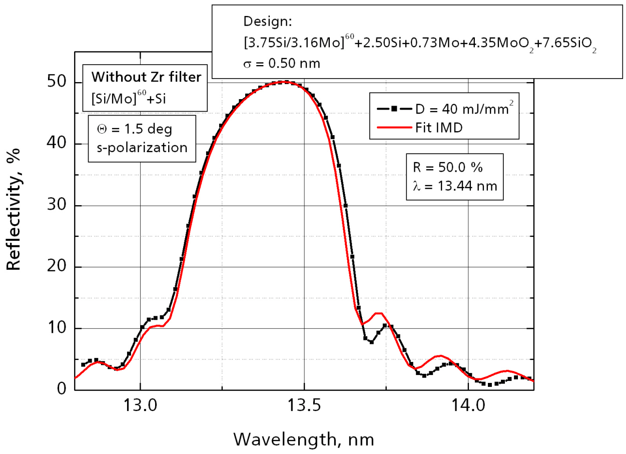

Figure 4.10: Measured and fitting EUV reflectivity curves of a Si-capped Mo/Si multilayer mirror irradiated with D = 40 mJ/mm^2

4.2.2 Radiation stability of imaging optics

Additional tests on radiation stability of Mo/Si multilayer mirrors were performed in the case of mirrors used as imaging optics for EUVL. The mirrors (Mo/Si multilayers with different capping layers) were placed at 140 mm from the source and irradiated with a Zr-filter between the source and the sample under normal incidence with the EUV-dose D $=$ 40 mJ/mm^2. The evolution of the EUV properties of Si-capped Mo/Si multilayer mirrors is introduced in Fig. 4.11. Optimized as-deposited Si-capped Mo/Si multilayers presents a peak reflectivity R $=$ 68.0 % at the wavelength $\lambda = 13.52$ nm. Irradiation with an EUV-dose D $=$ 40 mJ/mm^2 induces a drop of reflectivity of -1.0 % (R $=$ 67.0 % at $\lambda = 13.52$ nm). The introduction of the Zr-filter therefore considerably reduces the degradation of such mirrors under EUV radiation. According to the AFM investigations, no changes in the top-roughness were found after irradiation.

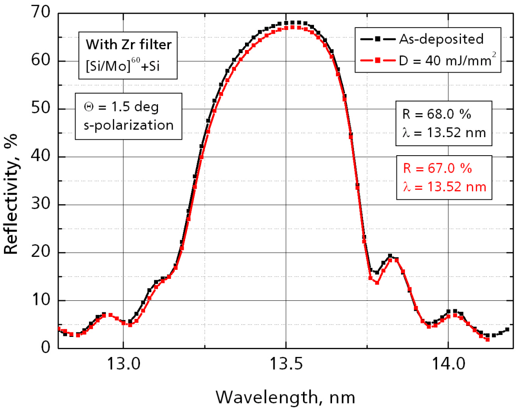

Figure 4.11: Evolution of the EUV properties of Si-capped Mo/Si multilayer mirrors irradiated with D $=$ 40 mJ/mm^2

The drop of reflectivity of -1 % after irradiation of Si-capped Mo/Si multilayer mirrors (D $=$ 40 mJ/mm^2) is due to the partial oxidation of the silicon top-layer, as shown by the XPS investigations. As no changes in the top-roughness were found with AFM investigations, it is possible to fit the EUV reflectivity curves before and after radiation with the sofware FilmWizard. Results of the simulation are presented in Fig. 4.12. They show an oxidation of the silicon top-layer and therefore an increase in the thickness of the SiO_2-top-layer from 2 nm (as-deposited state) to 3.5 nm (after irradiation). The corresponding reduction of the thickness of the Si-layer is in agreement with the ratio previously calculated (Eq. 4.1).

In order to enhance the radiation stability of Mo/Si multilayer mirrors designed for EUVL, different capping layer materials have been investigated as alternative to silicon. Such materials have to be resistant against oxidation, smoothly deposited and chemically

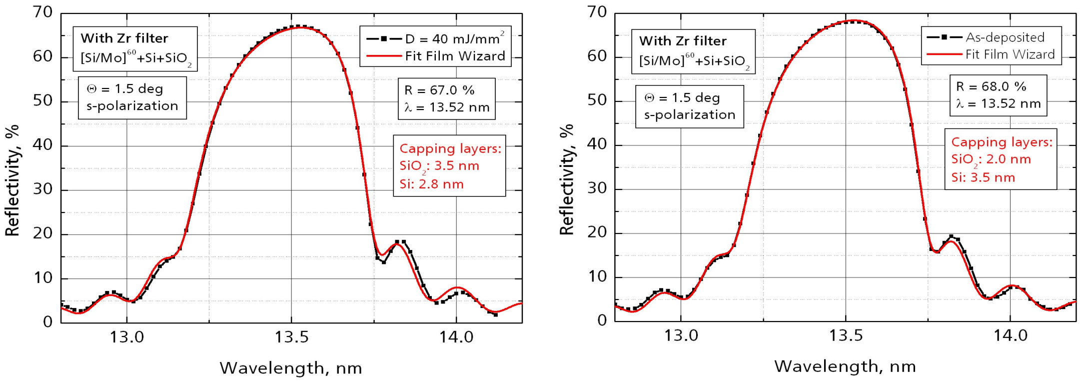

Figure 4.12: Measured and fitting EUV reflectivity curves of Si-capped Mo/Si multilayer mirrors in as-deposited state (left) and irradiated with D = 40 mJ/mm^2 (right)

inert with respect to the multilayer materials (no interdiffusion process). Furthermore their optical constants in the EUV spectral range should not lead to a drop of the peak reflectivity at the wavelength of 13.5 nm (part 2.3). The performances of Ru-, RuO_2- and TiO_2-capped multilayer mirrors have been compared in terms of reflectivity and stability against EUV radiation. The evolution of the EUV properties of Ru- and RuO_2-capped Mo/Si multilayer mirrors is shown in Fig. 4.13. Optimized as-deposited Ru-capped Mo/Si multilayers present a peak reflectivity R = 66.3 % at the wavelength $\lambda = 13.52$ nm. Irradiation with an EUV-dose D = 40 mJ/mm^2 induces a drop of reflectivity of -3.0 % (R = 63.3 % at $\lambda = 13.52$ nm). XPS investigations exhibit an oxidation of the silicon sub-layer in the capping layer system Si+Ru: 75 % of the silicon is oxidized (SiO_2) after irradiation with D = 40 mJ/mm^2. That process is responsible for the loss of reflectivity and was already found by Bajt et al. [101] to explain the degradation of the optical performances of Ru-capped multilayer mirrors exposed to EUV radiation. An additional oxidation of the Ru-cappping layer should be expected, but since the binding energy of the Ru3d-peak obtained after XPS investigations is typical for both Ru and RuO_2, it is impossible to determine the level of oxidation of the Ru-layer. The concentration of higher binding states as RuO_4 is less than 1 %. As-deposited RuO_2-capped Mo/Si multilayers present a peak reflectivity R = 66.7 % at the wavelength $\lambda = 13.32$ nm. Irradiation with an EUV-dose D = 40 mJ/mm^2 causes a drop of reflectivity of -0.8 % (R = 65.9 % at $\lambda = 13.32$ nm). Irradiations performed on such RuO_2-capped Mo/Si mirrors with synchrotron radiation [110] show no degradation at all with a dose of about 720 J/mm^2. According to XPS investigations, the loss of reflectivity found after irradiation is explained by the partial oxidation of the silicon sub-layer in the capping layer system Si+RuO_2.

According to the previous results, a model for the degradation process of the RuO_2-capped Mo/Si multilayer mirrors under EUV radiation can be developed (Fig. 4.14). The unstability of such mirrors is due to the oxidation of the silicon sub-layer. It first

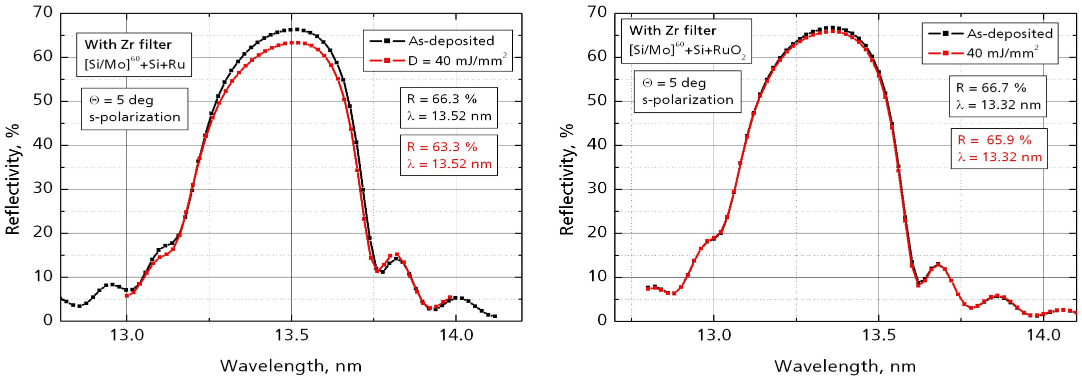

Figure 4.13: Evolution of the EUV properties of Ru-capped (left) and RuO$_2$-capped (right) Mo/Si multilayer mirrors irradiated with D = 40 mJ/mm^2

occurs during the deposition process, where the silicon layer little oxidizes to form a SiO$_2$-layer between the Si- and RuO$_2$-layers. During the irradiation of the mirrors with an EUV-dose of 40 mJ/mm^2, that SiO$_2$-layer gets thicker through the further oxidation of the silicon sub-layer. It has to be noted that Fig. 4.14 illustrates the application of that model for a maximal EUV-dose of 40 mJ/mm^2. A greater dose should induce a more important oxidation process, not only limited to the silicon sub-layer and leading to the oxidation of the next layers in the multilayer structure.

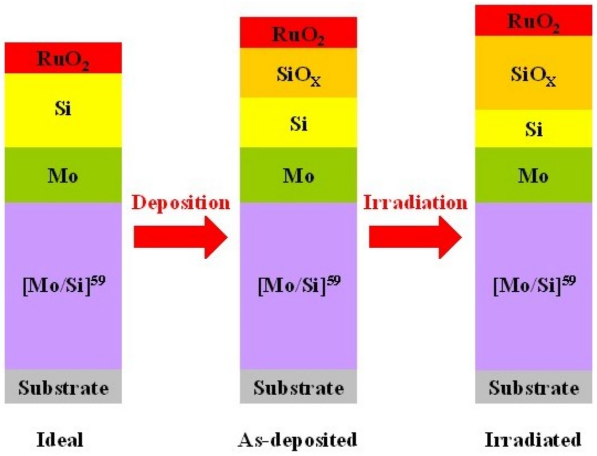

Figure 4.14: Model of degradation of the RuO$_2$-capped Mo/Si multilayer mirrors under EUV radiation

As no changes in the top-roughness were found with AFM investigations, it is possible to fit the EUV reflectivity curves before and after radiation with the sofware FilmWizard. Results of the simulation are presented in Fig. 4.15. They show an oxidation of the silicon sub-layer and therefore an increase in the thickness of the SiO$_2$-layer formed between the Si- and the RuO$_2$-layers from 1.7 nm (as-deposited state) to 2.2 nm (after irradiation).

The corresponding reduction of the thickness of the Si-layer, from 1.2 to 0.8 nm, is in agreement with the ratio previously calculated (Eq. 4.1).

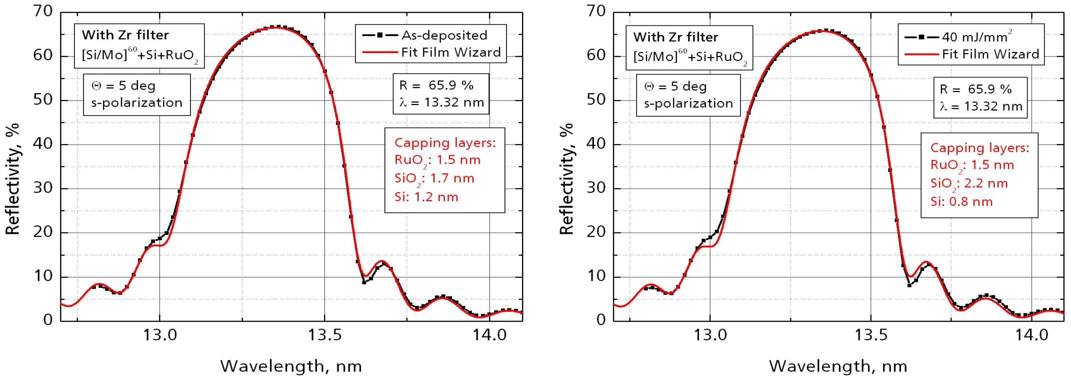

Figure 4.15: Measured and fitting EUV reflectivity curves of RuO_2-capped Mo/Si multilayer mirrors in as-deposited state (left) and irradiated with D = 40 mJ/mm^2 (right)

Although RuO_2-capped Mo/Si multilayer mirror present an enhancement of the radiation stability in comparison with Si-capped ones, they are not stable under EUV radiation and therefore do not meet the stringent requirements for EUVL. To further enhance the stability of the imaging optics, TiO_2-capped Mo/Si multilayer mirrors have also been investigated. Optimized as-deposited TiO_2-capped Mo/Si multilayers present a peak reflectivity R = 66.4 % at the wavelength $\lambda = 13.39$ nm. After irradiation with an EUV-dose D = 40 mJ/mm^2 no drop of reflectivity was found (R = 66.4 % at $\lambda = 13.39$ nm). The evolution of the EUV properties of TiO_2-capped Mo/Si multilayer mirrors is introduced in Fig. 4.16. Irradiations performed on such TiO_2-capped multilayer mirrors with synchrotron radiation [110] show a degradation of the optical performances with different irradiation doses. Bajt et al. [109] demonstrated a drop of reflectivity of -0.3 % with D = 720 J/mm^2, whereas mirrors deposited by Yulin et al. [110] exhibited a loss of -0.6 % with D = 760 J/mm^2.

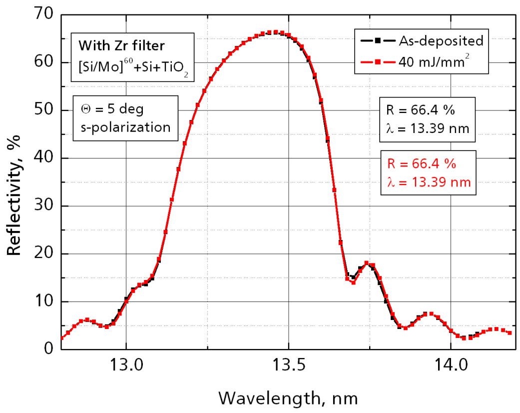

Figure 4.16: Evolution of the EUV properties of TiO_2-capped Mo/Si multilayer mirrors irradiated with $D = 40$ mJ/mm^2

4.3 Thermal stability of Mo/Si multilayer mirrors

The stability of Si-based multilayer mirrors under heat loads has been investigated up to 650°C and potential solutions for the improvement of the thermal stability have been developed. Two different approaches (part 2.4) are presented here for the enhancement of the thermal stability of Si-based multilayer mirrors. One method in order to enhance the thermal stability of Mo/Si multilayer mirrors is based on a phase and structure equilibrium of the layers, a minimal specific energy of interfaces, high melting temperatures and a similar thermal expandability of the multilayer materials at all investigated temperatures: The thermodynamic equilibrium of two phases at their interfaces can be only achieved if they are neighbors divided by a region of their own eutectic in the phase diagram of a binary alloy system. Therefore, $MoSi_2$/Si systems were selected for the study as a potential solution for high-thermal multilayer coatings. The second method consists in a maximal increase of the activation energy of the diffusion process: The higher the activation energy is, the lower the interdiffusion between the layers is. Multilayer mirrors with enhanced thermal stability can be obtained by the insertion of very thin diffusion barriers between the molybdenum and the silicon layers. Therefore, Mo/C/Si/C multilayer mirrors were also investigated as enhanced multilayer mirrors. Calculations of the normal incidence reflectivity for both multilayer systems, performed with the software FilmWizard and with material optical constants derived from the scattering factors of Henke [10, 11] ($\rho_{Si} = 2.33$ g/cm^3, $\rho_{Mo} = 10.22$ g/cm^3, $\rho_{MoSi_2} = 6.31$ g/cm^3, $\rho_C = 2.27$ g/cm^3 and $\rho_{SiO_2} = 2.55$ g/cm^3), are introduced in Fig. 4.17.

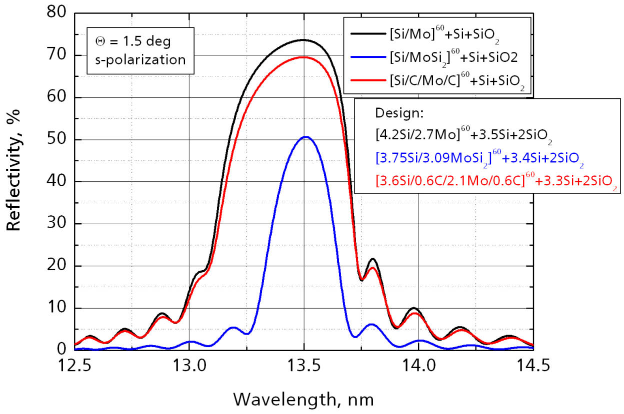

Figure 4.17: Calculated optical performances of $MoSi_2$/Si and Mo/C/Si/C multilayer mirrors designed for $\lambda = 13.5$ nm

All calculations have been performed assuming ideal multilayer structures with 60 bilayers (no interface-roughness and no imperfection at the interfaces). A carbon thickness of 0.6 nm was used in the design of Mo/C/Si/C multilayer mirrors. A top-layer of two nanometers of silicon oxide SiO_2 has also been included into the design in order to represent the natural oxidation of the silicon in air. According to the previous calculations, Mo/C/Si/C multilayer mirrors have a considerably higher theoretical reflectivity at the wavelength $\lambda = 13.5$ nm (R = 69.6 %) than $MoSi_2$/Si ones (R = 50.7 %). The reflectivity of $MoSi_2$/Si multilayer mirrors can be increased with a larger number of periods. Although mirrors with 80 periods have a theoretical reflectivity of 53.5 %, it has been decided to deposit samples with only 60 periods because of their larger FWHM (the theoretical FWHM of classical Mo/Si multilayer mirrors is 0.57 nm). The design optimization of Mo/C/Si/C multilayers is complexer compared to the optimization of $MoSi_2$/Si multilayer systems, since there are four layers to optimize in terms of maximum thermal stability and maximum reflectivity. The peak reflectivity of Mo/C/Si/C multilayer mirrors decreases with increasing the thickness of the diffusion barriers at the interfaces. To achieve a maximum reflectivity, a minimal thickness of carbon has to be used. However, the kinetic approach to more stable multilayers implies a maximum increase in the activation energy of the diffusion processes, that can only be realized with an increased thickness of carbon. Based on first annealing tests and EUV reflectivity measurements, Mo/C/Si/C multilayer with the following design were deposited: Mo/C(0.6 nm)/Si/C(0.8 nm). The experimental peak reflectivity more than 60 % was chosen as the main criteria of that design. The calculated and design parameters of Mo/Si, $MoSi_2$/Si and Mo/C/Si/C multilayer mirrors are summarized in Tab. 4.4.

Table 4.4: Calculated and design parameters of Mo/Si, $MoSi_2$/Si and Mo/C/Si/C multilayer mirrors

System	**N**	**R, %**	**FWHM, nm**
Mo/Si	60	73.7	0.57
$MoSi_2$/Si	60	50.7	0.30
$MoSi_2$/Si	80	53.5	0.27
Mo/C/Si/C	60	69.6	0.56

4.3.1 $MoSi_2$/Si multilayer mirrors

Characterization of as-deposited $MoSi_2$/Si multilayer mirrors

According to the previous calculations, optimal $MoSi_2$/Si multilayer mirrors have the following design: $[3.75 \text{ nm Si} / 3.09 \text{ nm MoSi}_2]^{60} + 3.40$ nm Si. The main characteristics of $MoSi_2$/Si multilayer mirrors (such as the period H, the layer ticknesses and the interface-roughnesses) can be extracted from the simulation of the X-ray reflectivity measurement curves. In the case of $MoSi_2$/Si multilayer mirrors, all simulations were performed using a two-layer model, since they are based on a system that does not interdiffuse (Fig. 2.7). A SAXR curve and the corresponding fitting curve of an as-deposited $MoSi_2$/Si multilayer mirror is introduced in Fig. 4.18. According to the simulation results, the actual thickness ratio Γ ($\Gamma = t_{MoSi_2}/H$) is 0.45 and the period H of this sample 6.85 nm. An additional interface-roughness in the range of 0.2–0.3 nm has been found between each layer and mirrors have a top-roughness of 0.22 nm. Finally, Si-layers have a density of 2.33 g/cm^3, that is equal to the density of the bulk material, and MoSi$_2$-layers a density of 5.80 g/cm^3. As-deposited MoSi$_2$/Si multilayers consisted of amorphous Si- and highly dispersed (almost amorphous) MoSi$_2$-layers as shown by the LAXD measurement (Fig. 4.18). Bragg reflection peaks can be detected up to a grazing angle of 20 degrees (as shown on the LAXD pattern), that is an obvious sign of the excellent geometrical quality of the deposited multilayer structures. The two broad peaks at 13.3 deg (lattice spacing a = 0.337 nm) and 20.8 deg (a = 0.217 nm) respectively result from the reflection of the [101] and [111] planes of the hexagonal MoSi$_2$ stucture modification (h-MoSi$_2$).

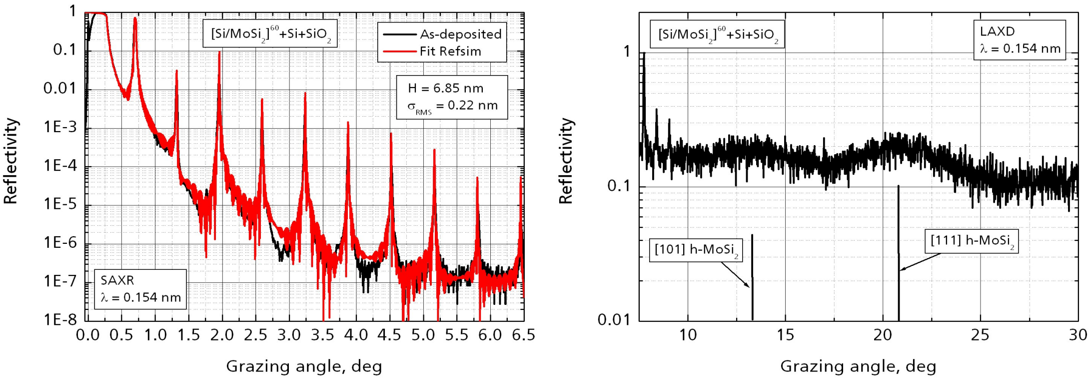

Figure 4.18: Measured and fitting SAXR curves (left) and LAXD curve (right) of an as-deposited MoSi$_2$/Si multilayer mirror

The TEM image (Fig. 4.19) of as-deposited MoSi$_2$/Si multilayer mirrors presents bright and dark bands respectively corresponding to the Si- and MoSi$_2$-layers. The structure is continuous and smooth and there is no evidence of increasing roughness or columnar growth through the multilayer stack. One period of the multilayer consists of two amorphous regions of different contrast. The rms-roughness has been found to be $\sigma = 0.16$ nm (Fig. 4.19) after AFM investigations. This value is close to the one extracted from the SAXR simulation ($\sigma = 0.22$ nm).

The optimization of the multilayer design and deposition process resulted in a MoSi$_2$/Si multilayer peak reflectivity of R = 41.2 % and a FWHM = 0.26 nm at the wavelength $\lambda = 13.5$ nm. The fit of that curve, achieved with the software IMD, gives a multilayer period of 6.855 nm, a thickness ratio of 0.42, an interface roughness of 0.4–0.5 nm. The formation of 1.8 nm of SiO$_2$ on top has also been found. The fit was performed with the following material densities: $\rho_{Si} = 2.33$ g/cm^3, $\rho_{MoSi_2} = 5.70$ g/cm^3 and $\rho_{SiO_2} = 2.55$ g/cm^3. The fitting parameters show therefore a good agreement with the results of the SAXR simulation. Both measured and fitting curves are introduced in Fig. 4.20.

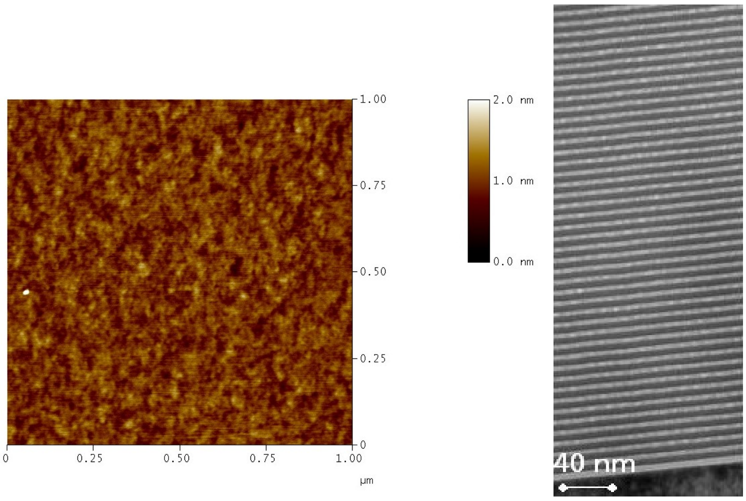

Figure 4.19: Surface morphology (σ = 0.16 nm, left) and TEM image (right) of an as-deposited $MoSi_2/Si$ multilayer mirror

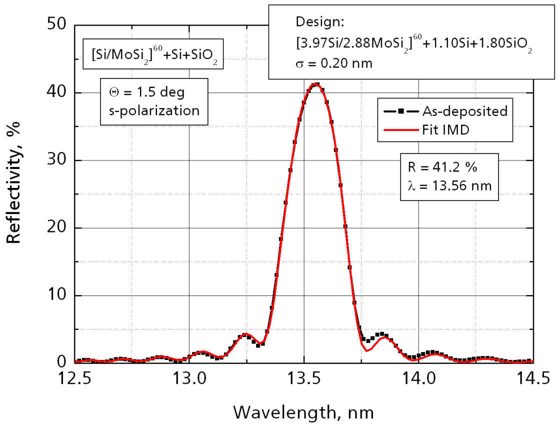

Figure 4.20: Measured and fitting EUV reflectivity curves of an as-deposited $MoSi_2/Si$ multilayer mirror

Annealed $MoSi_2/Si$ multilayer mirrors

After annealing of the samples at 250°C for 1, 10 and 100 hours, no considerable changes in the multilayer structure were found. The comparison of two SAXR measurements for a $MoSi_2/Si$ multilayer mirror as-deposited and after annealing (T = 250°C, τ = 100 h) and the evolution of the EUV properties of $MoSi_2/Si$ multilayer mirrors annealed 1, 10 and 100 hours at 250°C are presented in Fig. 4.21. According to Eq. 2.9, changes in the position of the reflection peaks (Θ_m), for both the SAXR and the EUV reflectivity measurements, are linked to an increase or a decrease in the multilayer period. A little increase in the multilayer period thickness (about 0.015 nm) has been found after 100 hours annealing at 250°C. This phenomenon can unfortunately not be explained by the formation of any silicide (the formation of silicides typically causes a reduction of the multilayer period). No crystalline structure transformations in $MoSi_2$- and Si-layers were found by LAXD investigations. A small shift of the resonance wavelength (+0.01–0.03 nm) predicted by the SAXR measurements and an insignificant increase of the FWHM were found after annealing at 250°C. The reflectivity of $MoSi_2$/Si multilayer mirrors is invariant with increasing the annealing time up to 100 hours.

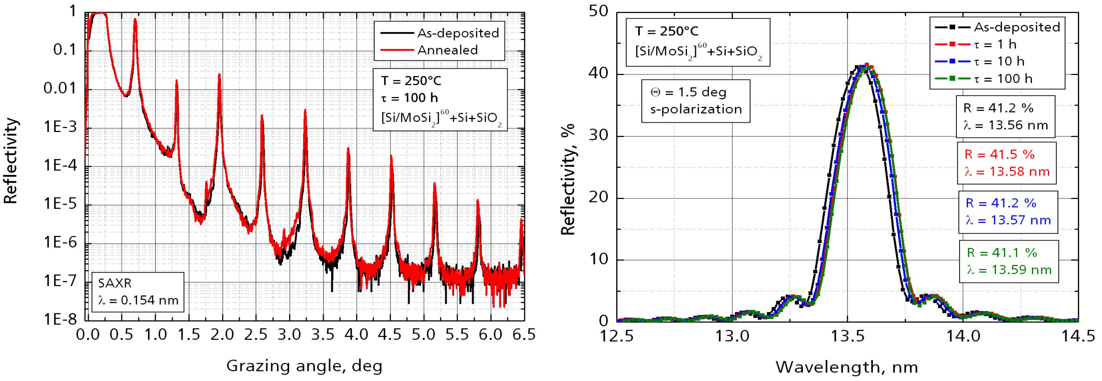

Figure 4.21: Evolution of the SAXR curves (left) and of the EUV properties (right) of $MoSi_2$/Si multilayer mirrors annealed at 250°C up to 100 hours

A decrease of the multilayer period thickness of -0.12 nm compared to the as-deposited state has been observed after 100 hours of annealing at 400°C (Fig. 4.22). That period contraction can be explained by a phase transformation from an amorphous to a polycrystalline $MoSi_2$-layer structure. A polycrystalline hexagonal $MoSi_2$ (h-$MoSi_2$) was found using LAXD (Fig. 4.22). The peak at 20.8 deg (lattice spacing a = 0.217 nm) comes from the reflection of the [111] plane of the h-$MoSi_2$ structure modification.

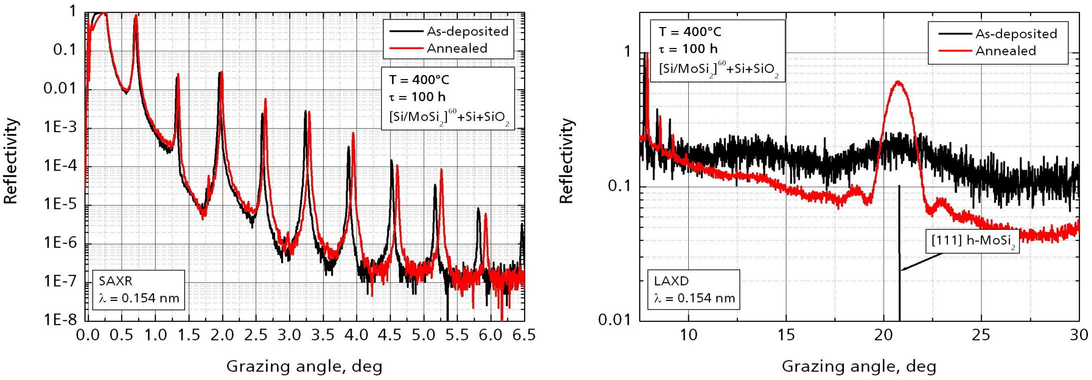

Figure 4.22: Comparison of the SAXR (left) and LAXD (right) curves for $MoSi_2$/Si multilayer mirrors as-deposited and after 100 hours annealing at 400°C

The evolution of the EUV properties of $MoSi_2$/Si multilayers annealed at 400°C for 1, 10 and 100 hours is presented in Fig. 4.23. A shift of the center wavelength of -0.23 nm, predicted by the SAXR measurements (Fig. 4.22), and a reflectivity drop of -1.0 % were found after annealing at 400°C. The reflectivity drop can be explained by the crystallization process of the $MoSi_2$-layers (Fig. 4.22), that induces a tiny development of the interface roughness. The reflectivity of $MoSi_2$/Si multilayer mirrors is nevertheless invariant with the increase of the annealing time up to 100 hours.

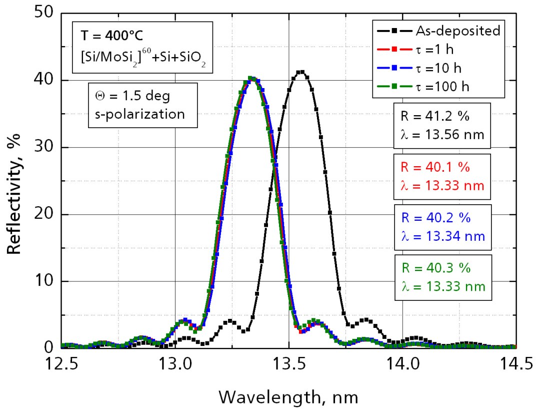

Figure 4.23: Evolution of the EUV properties of $MoSi_2$/Si multilayer mirrors annealed at 400°C for 1, 10 and 100 hours

The increase of the annealing temperature from 400°C to 500°C (annealing for 1, 10 and 100 hours) was not accompanied with any recrystallization process of the $MoSi_2$-layers. A similar period change was found in $MoSi_2$/Si multilayers annealed at 500°C and 400°C (decrease of the multilayer period by -0.12 nm compared to the as-deposited state). The TEM cross-section image of the $MoSi_2$/Si multilayer mirror annealed at 500°C for 100 hours shows that the $MoSi_2$-layers (dark lines) are polycrystalline and the Si-layers (bright lines) have a typical amorphous structure (Fig. 4.24). The multilayer structure is continuous and smooth and there is no evidence of increasing roughness or columnar growth through the multilayer stack. The formation of interlayer transition zones (interdiffusion layers) in $MoSi_2$/Si structures has not been found, that is the principal structural difference between $MoSi_2$/Si and Mo/Si multilayer systems. The prevention the of interdiffusion process at the interfaces in the $MoSi_2$/Si multilayer mirrors is the result of a phase equilibrium between the selected materials. The rms-roughness of $MoSi_2$/Si multilayer mirrors annealed at 500°C during 100 hours is $\sigma = 0.15$ nm (Fig. 4.26). The surface morphology of $MoSi_2$/Si mirrors does not change after annealing at 500°C ($\sigma = 0.16$ nm for the as-deposited state). The evolution of the EUV properties of $MoSi_2$/Si multilayer mirrors annealed at 500°C for 1, 10 and 100 hours is presented in Fig. 4.23. A shift of the center wavelength of -0.23 nm, predicted by the SAXR measurements and comparable to the one found after annealing at 400°C, and a reflectivity drop of -1.1 %

were found after annealing at 500°C and can be explained by the crystallization of the $MoSi_2$-layers, that occurs at 400°C (Fig. 4.22). The reflectivity of $MoSi_2$/Si multilayer mirrors is invariant with increasing the annealing time up to 100 hours.

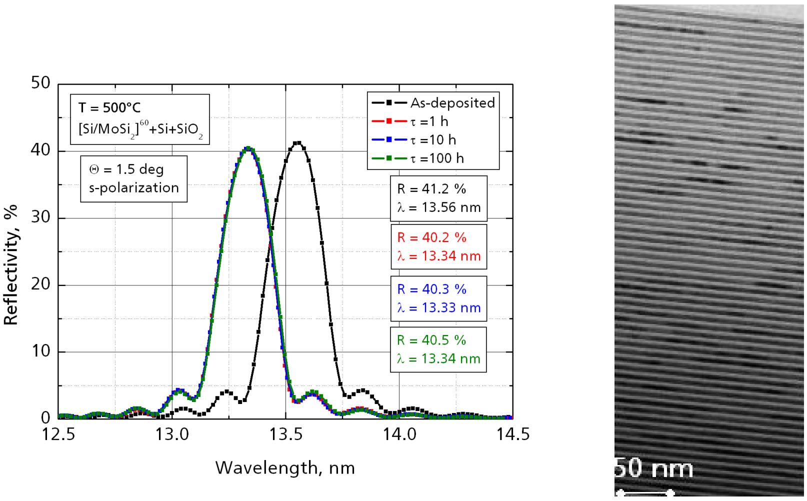

Figure 4.24: Evolution of the EUV properties of $MoSi_2$/Si multilayer mirrors annealed at 500°C for 1, 10 and 100 hours (left) and TEM image of a $MoSi_2$/Si multilayer mirror after 100 hours annealing at 500°C(right)

The optical properties of $MoSi_2$/Si multilayer mirrors do not change when the annealing time was increased from 1 hour to 100 hours at all examined temperatures up to 600°C. The total degradation of the optical properties that occurs above 650°C (Fig. 4.25), where the EUV reflectivity becomes lower than 1 %, and can be explained by a recrystallization process of the $MoSi_2$-layers. Such a phenomenon has already been found by Kondratenko et al. [130]. They nevertheless studied it with SAXR measurements and did not investigate its influence on the resulted EUV reflectivity. A polycrystalline hexagonal $MoSi_2$ (h-$MoSi_2$) has been found using LAXD measurements. The peak at 20.8 deg (lattice spacing a = 0.217 nm) comes from the reflection of the [111] plane of the h-$MoSi_2$ structure modification. The structural coherence length of the $MoSi_2$-crystallites can be calculated from the FWHM of the LAXD peak (Fig. 4.25) with the Scherrer formula [172]:

$$L = \frac{0.9\lambda}{\Delta 2\theta \cos\theta} \tag{4.3}$$

where λ is the wavelength, $\Delta 2\theta$ the FWHM and θ the Bragg angle. The coherence length L is a measure of the average crystallite size in the direction of the momentum transfer of the X-rays. As the momentum transfer direction is perpendicular to the layers, L approximately equals to the thickness of the $MoSi_2$-layer. After annealing at 650°C, the shape of the peak is narrower, that corresponds to larger grains in the structure.

The LAXD patterns were measured at the wavelength $\lambda = 0.154$ nm and the peak corresponding to the h-MoSi$_2$ appeared at $\theta = 20.8$ deg after annealing at 500°C and 20.6 deg after annealing at 650°C. The calculation of the coherence length (Eq. 4.3) after annealing at 500°C and 650°C respectively gives: $L_{500°C} = 3.15$ nm ($\Delta 2\theta = 2.68$ deg) and $L_{650°C} = 5.48$ nm ($\Delta 2\theta = 1.20$ deg). $L_{500°C}$ approximately equals to the thickness of the MoSi$_2$-layer, that was determined by SAXR, and $L_{650°C}$ approximately equals to the period thickness of the multilayer mirror, evidence of a recrystallization process of the MoSi$_2$-layers and a large increase of the interface roughness in the multilayer structure.

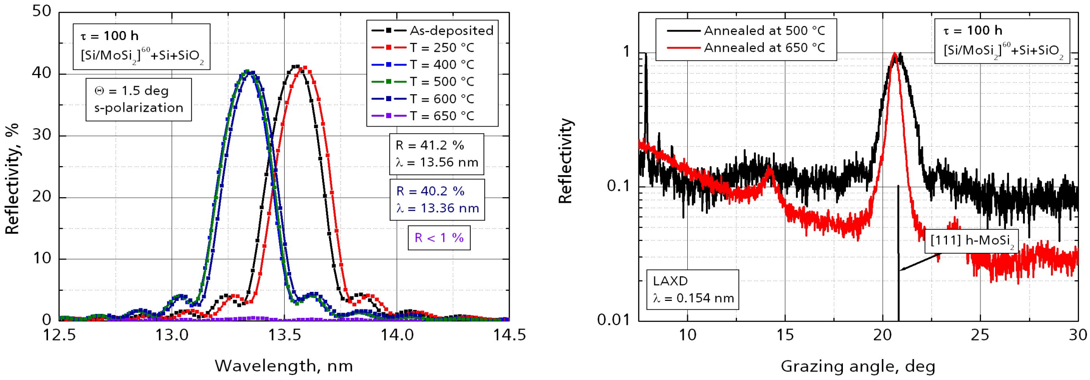

Figure 4.25: Evolution of the EUV properties of MoSi$_2$/Si multilayer mirrors after long-term annealing up to 650°C (left) and comparison of their LAXD curves (right) after annealing at 500°C and 650°C

The rms-roughness of MoSi$_2$/Si multilayer mirrors annealed at 650°C during 100 hours is $\sigma = 0.35$ nm (Fig. 4.26). It has been found that the recrystallization process of the MoSi$_2$-layers is therefore also accompanied by an increase of the surface roughness ($\sigma = 0.15$ nm after 100 hours annealing at 500°C).

According to the previous results, the following model for the degradation process of the MoSi$_2$/Si multilayer mirrors upon annealing at temperatures up to 650°C can be suggested (Fig. 4.27). The as-deposited multilayer mirrors consist of amorphous Si- and MoSi$_2$-layers. After annealing at 400°C, a crystallization of the MoSi$_2$-layers has been found. It is accompanied by a reduction of the multilayer period thickness. The annealing of the MoSi$_2$/Si multilayer mirrors at 650°C induces a recrystallization process of the MoSi$_2$-layers with a very high development of the interface roughness.

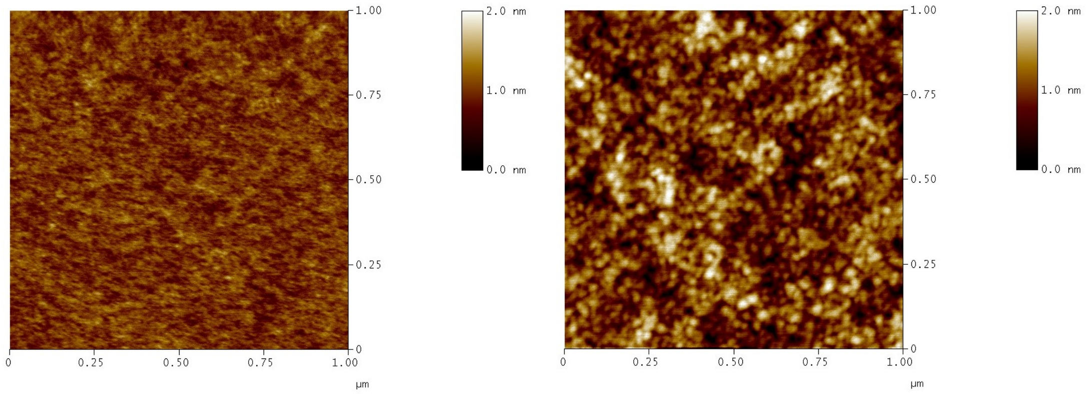

Figure 4.26: Surface morphology of a $MoSi_2/Si$ multilayer mirrors after 100 hours annealing at 500°C ($\sigma = 0.15$ nm, left) and 650°C ($\sigma = 0.35$ nm, right)

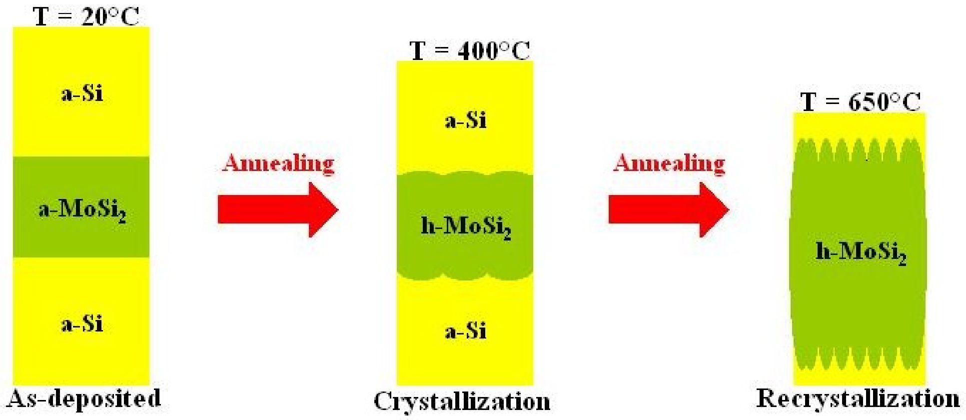

Figure 4.27: Model of degradation of the $MoSi_2/Si$ multilayer mirrors upon annealing in temperature range from 200 to 650°C

4.3.2 Mo/C/Si/C multilayer mirrors

Characterization of as-deposited Mo/C/Si/C multilayer mirrors

In order to achieve both a high reflectivity (R $\geq$ 60 %) and a high thermal stability, Mo/C/Si/C multilayer mirrors were deposited with the following design: [2.89 nm Si / 0.8 nm C / 2.71 nm Mo / 0.6 nm C]^{60} + 3.40 nm Si. A SAXR curve of an as-deposited Mo/C/Si/C/Si multilayer mirror is introduced in Fig. 4.28. A four-layer model (Mo/C/Si/C) was used for the simulation, since the carbon diffusion barriers have to block the interdifusion process between the Mo- and Si-layers. According to the simulation results, the actual multilayer period H was 6.99 nm. An additional interface-roughness in the range of 0.2–0.3 nm has been found between each layer and mirrors had a top-roughness of around 0.2 nm. As-deposited Mo/C/Si/C multilayers consisted of amorphous Si-layers. The determination of one broad diffraction peak gives insufficient information for the exact interpretation of the crystalline phase: Formation of hexagonal Mo_2C (h-Mo_2C) or body-centered cubic Mo (bcc-Mo). The reflection of the [101] plane of the body-centered cubic Mo stucture modification (bcc-Mo) induces for instance a broad peak at 20.35 deg (lattice spacing a = 0.315 nm). The Bragg reflection peaks of the Mo/C/Si/C multilayer mirrors can be determined up to 20 degrees, that is an obvious sign of the excellent geometrical quality of the deposited multilayer structures (Fig. 4.28). Finally, Si-layers had a density of 2.33 g/cm^3, that is equal to the density of the bulk material, and Mo-layers a density of 10.10 g/cm^3.

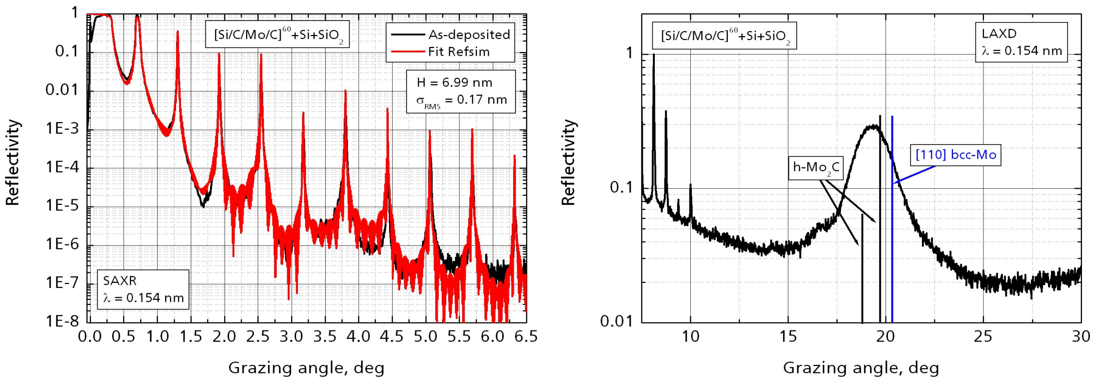

Figure 4.28: Measured and fitting SAXR curves (left) and LAXD curve (right) of an as-deposited Mo/C/Si/C multilayer mirror

The TEM image (Fig. 4.29) of an as-deposited Mo/C/Si/C multilayer mirror presents bright and dark bands respectively corresponding to the Si- and Mo-layers. The structure is continuous and smooth and there is no evidence of increasing roughness or columnar growth through the multilayer stack. One period of the multilayer consists of amorphous Si- (and C-) and polycrystalline Mo-layers. The interfaces are abrupt without any sign of interdiffusion process. The difference between the silicon and the carbon layers cannot be found because of the small divergence in electron densities. The rms-roughness, σ = 0.16 nm (Fig. 4.29), is close to the one extracted from the SAXR simulation (Fig. 4.28).

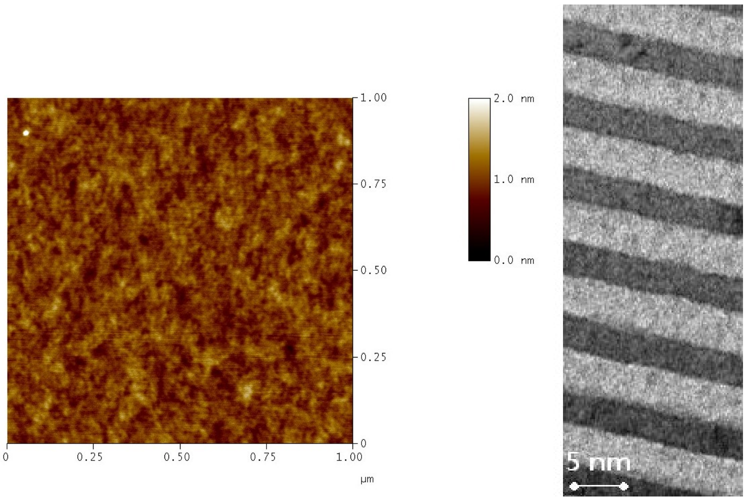

Figure 4.29: Surface morphology (σ = 0.16 nm, left) and TEM image (right) of an as-deposited Mo/C/Si/C multilayer mirror

The optimization of the Mo/C/Si/C multilayer design and the multilayer deposition process resulted in a peak reflectivity of R = 59.6 % and a FWHM = 0.54 nm at the wavelength $\lambda = 13.54$ nm. The fit of that curve, achieved with the software IMD, gives a multilayer period of 6.97 nm and an interface roughness of 0.4–0.5 nm. The formation of 2.1 nm of SiO_2 on top has also been found, corresponding to the native oxidation of the silicon top-layer. The fit was performed with the following material densities: $\rho_{Si} = 2.33$ g/cm^3, $\rho_{Mo} = 9.60$ g/cm^3, $\rho_C = 2.26$ g/cm^3 and $\rho_{SiO_2} = 2.55$ g/cm^3. The fitting parameters show a good agreement with the results of the SAXR simulation (Fig. 4.28) and of the AFM investigations (Fig. 4.29). Both measured and fitting curves are introduced in Fig. 4.30.

Annealed Mo/C/Si/C multilayer mirrors

After annealing of the samples at 250°C for 1, 10 and 100 hours, no considerable changes in the multilayer structure were found. The comparison of two SAXR measurements for a Mo/C/Si/C multilayer mirror as-deposited and after annealing (T = 250°C, τ = 100 h) and the evolution of the EUV properties of Mo/C/Si/C multilayer mirrors annealed at 250°C for 1, 10 and 100 hours are introduced in Fig. 4.31. The position of the resonance wavelength and the reflectivity peak of Mo/C/Si/C multilayer mirrors are invariant with increasing the annealing time up to 100 hours.

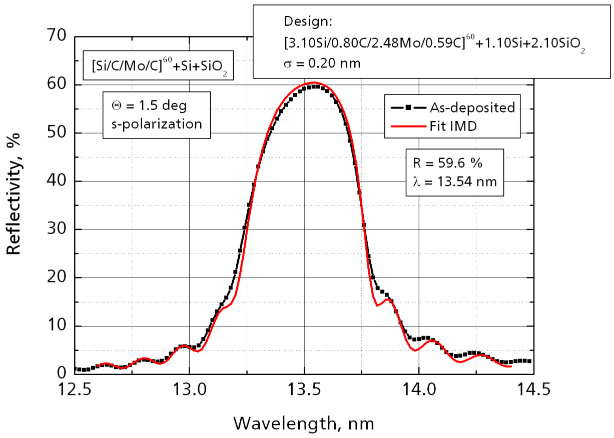

Figure 4.30: Measured and fitting EUV reflectivity curves of an as-deposited Mo/C/Si/C multilayer mirror

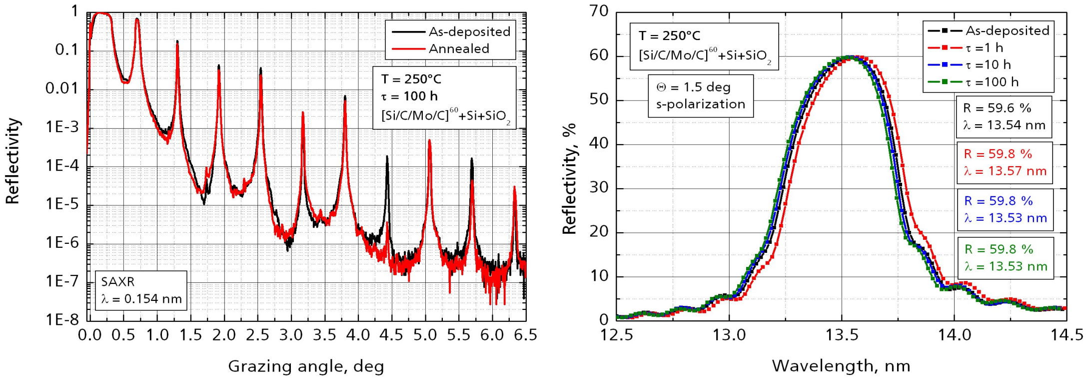

Figure 4.31: Comparison of the SAXR curves (left) and evolution of the EUV properties (right) of Mo/C/Si/C multilayer mirrors annealed at 250°C up to 100 hours

After annealing of the samples at 400°C for 1, 10 and 100 hours, a decrease of the multilayer period, depending on the annealing time, compared to the as-deposited state has been observed. It achieves a maximal contraction of -0.08 after 100 hours of annealing. This period contraction can be explained by a diffusion/intermixing process that occurs at the interfaces. A new compound (SiC) was formed after 1 hour annealing at 400°C and characterized using LAXD (Fig. 4.32). The evolution of the EUV properties of Mo/C/Si/C multilayer mirrors annealed at 400°C for 1, 10 and 100 hours is presented in Fig. 4.32. A continous slow degradation of the reflective properties and a shift of the resonance wavelength with increasing annealing time (1–100 hours) have been found. A decrease of the center wavelength from 13.45 to 13.38 nm and a reflectivity drop from 59.3 to 58.8 % result after annealing at 400°C for 1 and 100 hours respectively. The change of the resonance wavelength versus the annealing time is a piece of evidence of low interdiffusion processes at the interfaces.

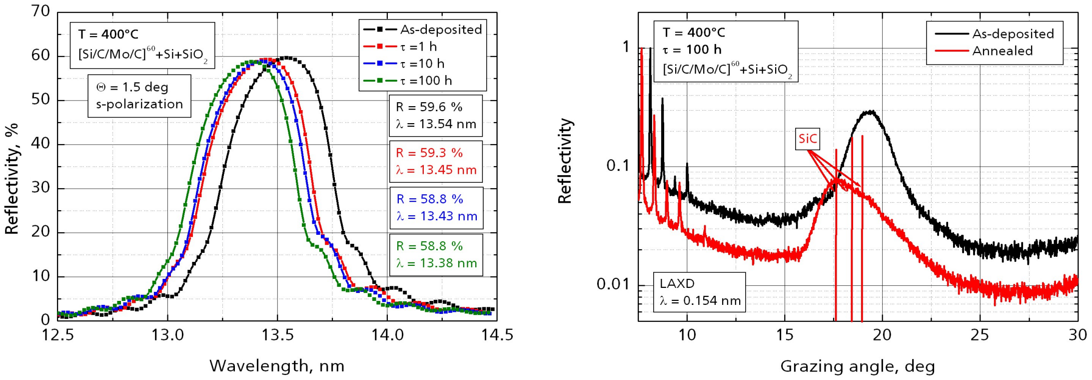

Figure 4.32: Evolution of the EUV properties of Mo/C/Si/C multilayer mirrors annealed at 400°C for 1, 10 and 100 hours (left) and comparison of the LAXD curves in as-deposited state and after 100 hours annealing at 400°C (right)

On the samples annealed at 500°C, a maximum decrease of the multilayer period by -0.14 nm compared to the as-deposited state has been observed after 100 hours of annealing. The period contraction can be explained by the diffusion/intermixing process and the formation of SiC at the interfaces found at 400°C(Fig. 4.32). The evolution of the EUV properties of Mo/C/Si/C multilayer mirrors annealed at 500°C for 1, 10 and 100 hours is presented in Fig. 4.33. Thermally induced changes of the optical properties depend on both the annealing time and temperature. A decrease of the center wavelength from 13.35 to 13.26 nm and a reflectivity drop from 58.8 to 58.1 % have been found after annealing at 500°C for 1 and 100 hours respectively. The TEM cross-section image of the Mo/C/Si/C multilayer mirror annealed at 500°C for 100 hours shows that the silicon layers (bright lines) have a typical amorphous structure (Fig. 4.33). The formation of interlayer transition zones (SiC) has been found at the interaces. The carbon diffusion barriers, deposited in order to block the diffusion between the silicon and the molybdenum layers, interdiffuse with the multilayer materials and induce a degradation of the optical properties of the Mo/C/Si/C multilayer mirrors. The rms-roughness of Mo/C/Si/C multilayer mirrors increases from 0.16 to 0.20 nm after 100 hours annealing at 500°C (Fig. 4.35). The formation of SiC at the interfaces is therefore accompanied by a development of roughness, that results in the loss of reflectivity of -1.5 % measured between the as-deposited state and after the annealing at 500°C fot 100 hours.

The change of the resonance wavelength versus the annealing time is a piece of evidence of low interdiffusion processes at the interfaces. In order to characterize that diffusion process between the layers upon annealing, the interdiffusion coefficients in Mo/C/Si/C systems can be calculated from the decay rate of the peak reflectivity after an isothermal annealing (Eq. 2.16). Assuming H $\approx$ 6.95 nm and if α is the slope of the linear dependence (ln(R(τ)/R(0)) vs the annealing time τ), the effective interdiffusion coefficient D$_e$ is:

$$D_e = \frac{-\alpha H^2}{8\pi^2} \tag{4.4}$$

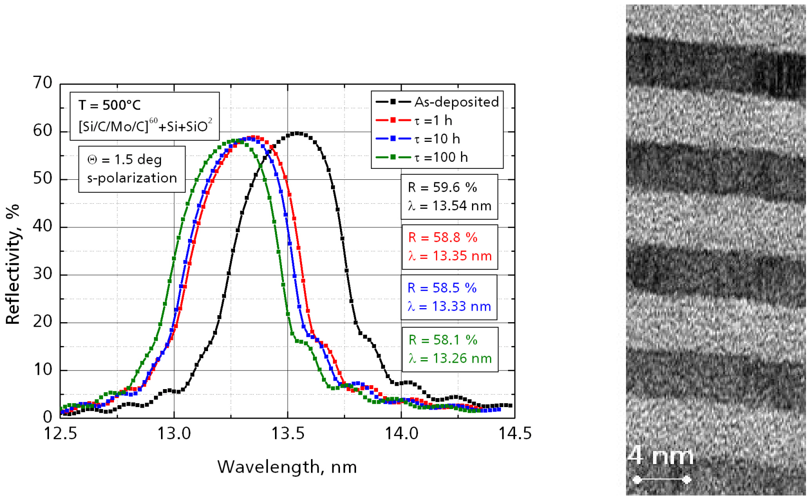

Figure 4.33: Evolution of the EUV properties of Mo/C/Si/C multilayer mirrors annealed at 500°C for 1, 10 and 100 hours (left) and TEM image of a Mo/C/Si/C multilayer mirror after 100 hours annealing at 500°C (right)

For each annealing temperature (250, 400 and 500°C), the effective interdiffusion coefficient D_e is presented in Tab. 4.5:

Table 4.5: Effective interdiffusion coefficients of Mo/C/Si/C at 250, 400 and 500°C

250°C	$D_e = 5.73\times10^{-27}$ m^2/s
400°C	$D_e = 1.75\times10^{-26}$ m^2/s
500°C	$D_e = 7.56\times10^{-26}$ m^2/s

For Mo/C/Si/C multilayer mirrors, the interdiffusion coefficient at 400°C was found to be $D_e = 1.75\times10^{-26}$ m^2/s. In comparison with the interdiffusion coefficient calculated for classical Mo/Si multilayer mirrors from the decay rate of the EUV peak reflectivity ($D_e = 3\times10^{-22}$ m^2/s, Tab. 2.4), the diffusion has been reduced by four orders of magnitude. The introduction of ultra-thin barrier layers into the multilayer design is therefore a successful way to reduce the diffusion processes taking place in such structures.

A continuous slow degradation of the reflective properties and a shift of the center wavelength with increasing annealing time (1–100 hours) was found after annealing at all investigated temperatures up to 650°C (Fig. 4.34). The comparison of surface morphology of Mo/C/Si/C multilayer mirrors in as-deposited state and after 100 hours annealing at 500 and 650°C shows an increase in the rms-roughness upon the annealing temperature from 0.16 to 0.29 nm (Fig. 4.35). That development of roughness is responsible for the loss of EUV reflectivity measured after annealing of Mo/C/Si/C multilayer mirrors.

The change of the center-wavelength with annealing time is a clear evidence of slow interdiffusion processes at the Mo/C/Si/C interfaces. As a result of interdiffusion, the

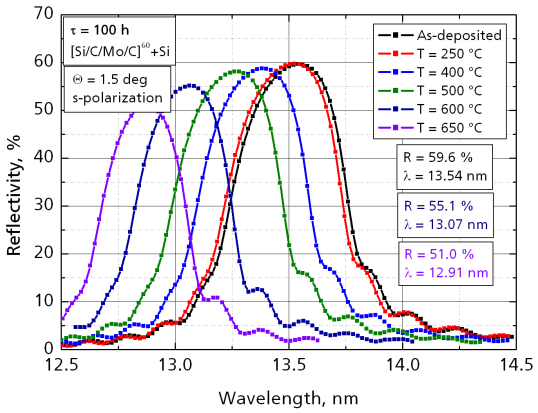

Figure 4.34: Evolution of the EUV properties of Mo/C/Si/C multilayer mirrors after long-term annealing up to 650°C

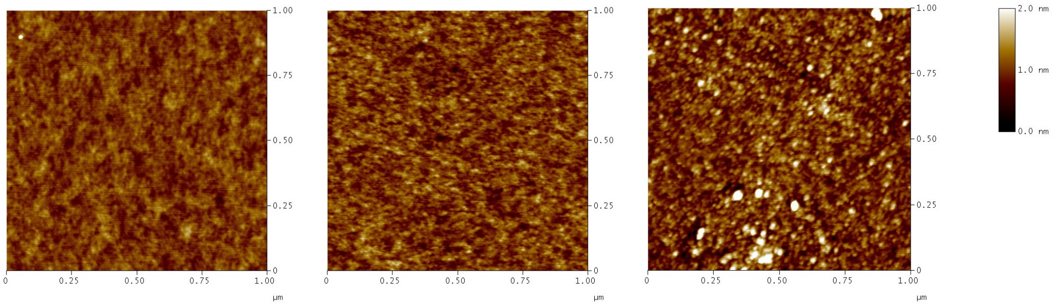

Figure 4.35: Evolution of the surface morphology of Mo/C/Si/C multilayer mirrors: as-deposited (σ = 0.16 nm, left), after annealing at 500°C (σ = 0.20 nm, middle) and after annealing at 650°C (σ = 0.29 nm, right)

formation of a new compound, SiC, was confirmed by LAXD studies (Fig. 4.32) after sample annealing at 400°C for 100 hours. Thermally induced changes of the optical and structural properties are dependent on both annealing times and temperatures. A decrease of the center wavelength from 13.07 to 12.91 nm and a reflectivity drop from 55.1 to 51.0 % resulted after long term annealing at 600°C and 650°C respectively (Fig. 4.34). The shift of the center wavelength to the shorter wavelengths can be explained by the formation of a SiC layer at the interfaces (Fig. 4.32), resulting of the following reaction between the carbon and the silicon atoms:

$$Si + C \overset{annealing}{\rightarrow} SiC \tag{4.5}$$

Considering one-dimensional volume changes in the Mo/C/Si/C multilayer mirrors upon annealing [173] and assuming that the molar volumes of Si, C and SiC are respectively V$_{Si}$

= 12.1 cm^3/mol, V$_C$ = 4.4 cm^3/mol and V$_{SiC}$ = 12.5 cm^3/mol, the total thickness of the two SiC-layers (one at the Si-on-Mo interface and one at the Mo-on-Si interface) obtained after the full transformation of both C layers (t$_C$ = 0.8 + 0.6 = 1.4 nm) contained in one period is:

$$t_{SiC} = \frac{V_{SiC}}{V_C}\ t_C \approx 2.84\ t_C \approx 3.98\ nm \tag{4.6}$$

$$t_{Si} = \frac{V_{Si}}{V_{SiC}}\ t_{SiC} = \frac{V_{Si}}{V_C}\ t_C \approx 2.75\ t_C \approx 3.85\ nm \tag{4.7}$$

The full transformation of the carbon layers (t$_C$ = 1.4 nm) induces a silicon carbide layer with a thickness of t$_{SiC}$ = 3.98 nm. This reaction also consumes a quantity of silicon equivalent to a layer of t$_{Si}$ = 3.85 nm. Since (t$_C$ + t$_{Si}$) $\geq$ t$_{SiC}$, the formation of that silicon carbide layer causes a contraction of the multilayer period and therefore a shift of the center wavelength to the shorter wavelengths (Eq. 2.8). The maximal period contraction, corresponding to the full consommation of the carbon layers, is ΔH = t$_{SiC}$ - (t$_C$ + t$_{Si}$) = -1.27 nm. According to the Eq. 2.8, this maximal period contraction is accompanied by a maximal wavelength shift of $\Delta\lambda$ = -2.54 nm. The combination of the Eq. 2.8, Eq. 4.6 and Eq. 4.7 gives a relationship between the wavelength shift $\Delta\lambda$ and the corresponding thickness of carbon t$_C$ involved in the formation of the silicon carbide layer:

$$\Delta\lambda = 2(t_{SiC} - (t_C + t_{Si})) = 2(\frac{V_{SiC}}{V_C}\ t_C - (1 + \frac{V_{Si}}{V_C})\ t_C) \approx -1.82\ t_C \tag{4.8}$$

The formation of a SiC-layer at the interfaces in Mo/C/Si/C multilayer mirrors upon annealing at temperature up to 650°C is therefore responsible for the shift of the peak wavelength to the shorter wavelengths: It induces a contraction of the multilayer period thickness, as shown by the Eq. 4.8. According to the previous results, the following model for the degradation process of the Mo/C/Si/C multilayer mirrors upon annealing at temperatures up to 650°C can be developed (Fig. 4.36). The as-deposited multilayer mirrors consist of amorphous Si- and crystalline bcc-MoSi$_2$-layers. After annealing at temperatures above 250°C, an interdiffusion/intermixing process at the interfaces has been found. It is accompanied by the formation of a new compound (SiC) at the interfaces. Thermally induced changes of the structural properties are dependent on both annealing times and temperatures. The formation of the SiC layer induces both a contraction of the multilayer period and a development of the interface roughness in the Mo/C/Si/C multilayer structure.

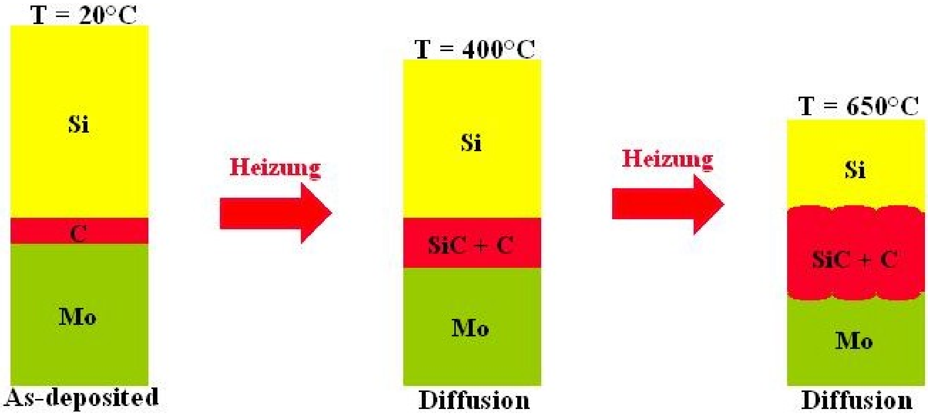

Figure 4.36: Model of degradation of the Mo/C/Si/C multilayer mirrors upon annealing in temperature range from 200 to 650°C

5 Conclusions

The demand to enhance the optical resolution and to structure ever smaller details, has pushed the optics development in recent years. Mainly induced by the production of more powerful electronic circuits with the aid of projection lithography, an increasing interest is directed towards optical components for the EUV spectral region. Such mirrors will be used for applications in EUVL steppers. It requires not only the highest possible normal-incidence reflectivity but also a long-term thermal and radiation stability at operating temperatures. The radiation and thermal stability of Si-based multilayer mirrors designed fot the wavelength $\lambda = 13.5$ nm has been therefore investigated.

The lifetime of Mo/Si multilayer-coated projection optics under EUV radiation is one of the outstanding issues on the road of the commercialization of EUVL. In order to investigate the radiation stability of classical Mo/Si multilayer mirrors as collector mirrors (without Zr-filter), high-reflective Mo/Si multilayer mirrors were successfully deposited by dc-magnetron sputtering. The optimization of the multilayer design and deposition process for Mo/Si multilayers results in a peak reflectivity of 68.2 % and a FWHM = 0.50 nm at the wavelength of 13.44 nm. As-deposited multilayer mirrors consist of amorphous Si- and polycrystalline Mo-layers, separated by amorphous $MoSi_2$ intermixing zones. Si-capped Mo/Si multilayer mirrors irradiated with a Xe-gas discharge source with an EUV-dose D = 40 mJ/mm^2 present a loss of reflectivity of -18.4 %. The oxidation of the silicon and molybdenum top layers (full oxidation of the silicon top layer and partial oxidation of the molybdenum layer) leads to the degradation of the optical properties of Mo/Si multilayer mirrors. That oxidation process therefore induces a larger absorption, an increase of the thickness of the top layers and is accompanied by a development of the top-roughness from 0.24 to 0.49 nm after irradiation.

The introduction of a Zr-filter, that mitigates the impact of the out-of-band radiation and partially protects the optics from the debris coming from the source, allows the study of the radiation stability of imaging optics. Si-capped Mo/Si multilayer mirrors irradiated with an EUV-dose D = 40 mJ/mm^2 present a loss of reflectivity of -1 % in presence of the Zr-filter. It is explained by the oxidation of the silicon top layer. Ru-capped Mo/Si multilayer mirrors demonstrate a drop of reflectivity of -3.0 % after irradiation with D = 40 mJ/mm^2. That loss of reflectivity is caused by the oxidation of the silicon and ruthenium top layers. New perspective capping layer materials as TiO_2 and RuO_2 can considerably enhance the radiation stability of Si-based multilayer mirrors. RuO_2-capped Mo/Si multilayer mirrors present a drop of reflectivity of -0.8 % at the wavelength $\lambda = 13.5$ nm after irradiation with D = 40 mJ/mm^2, because of the oxidation of the silicon sub-layer. TiO_2-capped Mo/Si multilayer mirrors showed no degradation of their optical properties after irradiation with D = 40 mJ/mm^2.

Another serious problem of Mo/Si multilayers is the instability of reflectivity and peak wavelength under high heat load, because of interdiffusion processes occurring between the Si- and Mo-layers. The development of high-temperature multilayers was focused on two alternative Si-based systems: $MoSi_2/Si$ and Mo/C/Si/C multilayer mirrors. High reflective $MoSi_2/Si$ multilayer mirrors with enhanced thermal stability were successfully deposited by dc magnetron sputtering. The optimization of the multilayer design and deposition process for $MoSi_2/Si$ multilayers results in a peak reflectivity of 41.2 % and a FWHM = 0.26 nm at the wavelength of 13.50 nm. The optical properties of pre-annealed $MoSi_2/Si$ multilayer mirrors (T = 400°C, $\tau = 1$ h) are constant in a temperature range up to 600°C. As-deposited multilayer mirrors consist of amorphous Si- and $MoSi_2$-layers. A wavelength shift of - 1.7 % and a reflectivity drop of -1.0 % are found after annealing at 400°C for 100 hours. The degradation of the optical properties is explained by the crystallization of the $MoSi_2$-layers. A simple pre-annealing at the temperature T = 400°C for 1 hour can therefore stabilize the internal structure of $MoSi_2/Si$ multilayer mirrors. The total degradation of the optical properties above 650°C ($R \leq 1$ %) is due to the recrystallization process in the $MoSi_2$-layers, accompanied by a high development of the interface roughness in the multilayer structure. The replacement of Mo by one of its neighbors in the Mo/Si binary phase diagram is then a successful way to enhance the thermal stability of Si-based multilayer mirrors.

Mo/C/Si/C multilayer mirrors with enhanced thermal stability were successfully deposited by dc magnetron sputtering. The optimization of the multilayer design and deposition process for Mo/C/Si/C multilayers results in a peak reflectivity of 59.6 % and a FWHM = 0.54 nm at the wavelength of 13.54 nm. The optical properties of Mo/C/Si/C multilayer mirrors remain stable in the temperature range 20–250°C during long term annealing (100 hours). The interdiffusion/intermixing process at the interfaces and the formation of a new compound (SiC) are responsible for the slow-current degradation of Mo/C/Si/C optical properties after annealing at temperatures above 250°C. Thermally induced changes of the optical and structural properties are dependent on both annealing times and temperatures and are due to the formation of the SiC layer at the multilayer interfaces (contraction of the multilayer period) and to a development of the interface roughness in the Mo/C/Si/C multilayer structure. The interdiffusion coefficients in Mo/C/Si/C systems, calculated from the decay rate of the peak reflectivity during isothermal annealing at different temperatures (250, 400 and 500°C), gives an interdiffusion coefficient at 400°C of 10^{-26} m^2/s. That value represents a reduction of the diffusion processes by four orders of magnitude in comparison with interdiffusion coefficients calculated for classical Mo/Si multilayer mirrors. The introduction of ultra-thin barrier layers into the multilayer design is therefore a successful way to reduce the diffusion processes taking place in such structures.

The combination of high reflective properties and enhanced thermal and radiation stability and of Mo/Si multilayer mirrors provides good prospects for their industrial application as coating for EUV collector and imaging optics.

Bibliography

[1] D. Attwood. Soft X-rays and extreme ultraviolet radiation: principles and applications. *Cambridge University Press, Cambridge*, ISBN 0–521–65214–6:1–23, 2000.

[2] R. van den Berg. Extreme UV lithography preserves moore's law. *Opto and Laser Europe*, **129**:29–31, 2005.

[3] P.J. Silverman. Extreme ultraviolet lithography: overview and development status. *Journal of Microlithography, Microfabrication and Microsystems*, **4**:1–5, 2005.

[4] D.G. Stearns, R.S. Rosen, and S.P. Vernon. Multilayer mirror technology for soft-X-ray projection lithography. *Applied Optics*, **32**:6952–6960, 1993.

[5] K. Fujii, T. Hagiwara, S. Matsuura, T. Ishimaru, Y. Matsubara, and W. Wakamiya. Status of 157 nm lithography and prospects for immersion. *Proc. SPIE*, **5754**:226–236, 2005.

[6] V. Paret, P. Boher, R. Geyl, B. Vidal, M. Putero-Vuaroqueaux, E. Quesnel, and J.Y. Robic. Characterization of optics and masks for the EUV lithography. *Microelectronic Engineering*, **61–62**:145–155, 2002.

[7] C. Gwyn. EUV lithography update. *SPIE OE Magazine*, **2**:22–24, 2002.

[8] H.J. Levinson. Principles of lithography. *Second Edition, SPIE Press, Bellingham*, ISBN 0–8194–5660–8:382–392, 2005.

[9] E. Spiller. Soft X-ray optics. *SPIE Optical Engineering Press, Bellingham*, ISBN 0–8194–1655–X:5–22, 1994.

[10] B.L. Henke, P. Lee, T.J. Tanaka, and R.L. Shimabukuroand B.K. Fujikawa. Low-energy X-ray interaction coefficients: Photoabsorption, scattering, and reflection: E=100–2000 eV Z=1–94. *Atomic Data and Nuclear Tables*, **27**:1–144, 1982.

[11] B.L. Henke, E.M. Gullikson, and J.C. Davis. X-ray interactions: Photoabsorption, scattering, transmission, and reflection at e=50–30 000 eV, Z=1–92. *Atomic Data and Nuclear Tables*, **54**:181–342, 1993.

[12] A.M. Hawryluk and L.G. Seppala. Soft X-ray projection lithography using an X-ray reduction camera. *Journal of Vacuum Science and Technology B*, **6**:2162–2166, 1988.

[13] W.T. Silfvast and O.R. Wood. Tenth micron lithography with a 10 hz 37.2 nm sodium laser. *Microelectronic Engineering*, **8**:3–11, 1988.

[14] G. Marsh. Moore's law at the extremes. *Materials Today*, **6**:28–33, 2003.

[15] A. Parker. Extreme ultraviolet lithography: Imaging the future. *Imaging the future of microcomputer chips, Science and Technology Review*, pages 4–9, 1999.

[16] G. Schriever, U. Stamm, K. Gabel, M. Darscht, V. Borisov, O. Khristoforov, and A. Vinokhodov. High power EUV sources based on gas discharge plasmas and laser produced plasmas. *Microelectronic Engineering*, **61–62**:83–88, 2002.

[17] U. Stamm. Extreme ultraviolet light sources - state of the art, future developments and potential applications. *RIKEN Review*, **50**:63–70, 2003.

[18] V. Bakshi. Technology status and workshop summary. *SEMATECH EUV Source Workshop*, San Jose, United States, 2005.

[19] P.B. Mirkarimi, S. Bajt, and M.A. Wall. Mo/Si and Mo/Be multilayer thin films on zerodur substrates for extreme-ultraviolet lithography. *Applied Optics*, **39**:1617–1625, 2000.

[20] V.Y. Banine, J.P.H. Benschop, and H.G.C. Werij. Comparison of extreme ultraviolet sources for lithography applications. *Microelectronic Engineering*, **53**:681–684, 2000.

[21] R.H. Hughes, T.A. Heumier, and P.M. Griffin. Vacuum UV and soft X-ray optical emissions from electron impact on metals. *Applied Optics*, **20**:1350–1354, 1981.

[22] G. Dattoli, A. Doria, G.P. Gallerano, L. Giannessi, K. Hesch, H.O. Moser, P.L. Ottaviani, E. Pellegrin, R. Rossmanith, R. Steininger, V. Saile, and J. Wüst. Extreme ultraviolet (EUV) sources for lithography based on synchrotron radiation. *Nuclear Instruments and Methods in Physics Research Section A: Accelerators, Spectrometers, Detectors and Associated Equipment*, **474**:259–272, 2001.

[23] R.L. Kauffman, D.W. Phillion, and R.C. Spitzer. X-ray production 13 nm from laser-produced plasmas for projection X-ray lithography applications. *Applied Optics*, **32**:6897–6900, 1993.

[24] M. McGeoch. Radio-frequency-preionized xenon Z-pinch source for extreme ultraviolet lithography. *Applied Optics*, **37**:1651–1658, 1998.

[25] F. Bijkerk, L.A. Shmaenok, A.P. Shevelko, R.K.F.J. Bastiaensen, C. Bruineman, and A.G.J.R. van Honk. A high-power, low-contamination laser plasma source for extreme UV lithography. *Microelectronic Engineering*, **27**:299–301, 1995.

[26] D.C. Ockwell, N.C.E. Crosland, and V.C. Kempson. Synchrotron light as a source for extreme ultraviolet lithography. *Journal of Vacuum Science and Technology B: Microelectronics and Nanometer Structures*, **17**:3043–3046, 1999.

[27] R. Lebert, L. Aschke, K. Bergmann, S. Düsterer, K. Gäbel, D. Hoffmann, P. Loosen, W. Neff, P. Nickles, O. Rosier, R. Poprawe, D. Rudolph, W. Sandner, R. Sauerbrey, G. Schmahl, H. Schwoerer, H. Stiehl, I. Will, and C. Ziener. Preliminary results from key experiments on sources for EUV lithography. *Microelectronic Engineering*, **57–58**:87–92, 2001.

[28] R. Lebert, K. Bergmann, G. Schriever, and W. Neff. A gas discharged based radiation source for EUV-lithography. *Microelectronic Engineering*, **46**:449–452, 1999.

[29] R. Lebert, K. Bergmann, G. Schriever, and W. Neff. Comparison of laser produced and gas discharge based EUV sources for different applications. *Microelectronic Engineering*, **46**:465–468, 1999.

[30] P.A.C. Jansson, B.A.M. Hansson, O. Hemberg, M. Otendal, A. Holmberg, J. de Groot, and H.M. Hertz. Liquid-tin-jet laser-plasma extreme ultraviolet generation. *Applied Physics Letters*, **84**:2256–2258, 2004.

[31] D.W. Myers, I.V. Fomenkov, B.A.M. Hansson, B.C. Klene, and D.C. Brandt. EUV source system development update: advancing along the path to HVM. *Proc. SPIE*, **5751**:248–259, 2005.

[32] U. Stamm, J. Kleinschmidt, K. Gabel, G. Hergenhan, C. Ziener, G. Schriever, I. Ahmad, D. Bolshukhin, J. Brudermann, R. de Bruijn, T.D. Chin, A. Geier, S. Gotze, A. Keller, V. Korobotchko, B. Mader, J. Ringling, and T. Brauner. EUV sources for EUV lithography in alpha-, beta- and high volume chip manufacturing: An update on GDPP and LPP technology. *Proc. SPIE*, **5751**:236–247, 2005.

[33] C.S. Koay, S. George, K. Takenoshita, R. Bernath, E. Fujiwara, M. Richardson, and V. Bakshi. High conversion efficiency microscopic tin-doped droplet target laser-plasma source for EUVL. *Proc. SPIE*, **5751**:279–292, 2005.

[34] B.A.M. Hansson, O. Hemberg, H.M. Hertz, M. Berglund, H.J. Choi, B. Jacobsson, E. Janin, S. Mosesson, L. Rymell, J. Thoresen, and M. Wilner. Characterization of a liquid-xenon-jet laser-plasma extreme-ultraviolet source. *Review of Scientific Instruments*, **75**:2122–2129, 2004.

[35] L.A. Shmaenok, C.C. de Bruijn, H.F. Fledderus, R. Stuik, A.A. Schmidt, D.M. Simanovski, A.V. Sorokin, T.A. Andreeva, and F. Bijkerk. Demonstration of a foil trap technique to eliminate laser plasma atomic debris and small particulates. *Proc. SPIE*, **3331**:90–94, 1998.

[36] G. Niimi, Y. Ueno, K. Nishigori, T. Aota, H. Yashiro, and T. Tomie. Experimental evaluation of stopping power of high-energy ions from a laser-produced plasma by a magnetic field. *Proc. SPIE*, **5037**:370–377, 2003.

[37] J. Hue, E. Quesnel, V. Muffato, C. Pellé, D. Granier, S. Favier, and P. Besson. Reduction of defect density on blanks: application to the extreme ultraviolet lithography. *Microelectronic Engineering*, **61–62**:203–211, 2002.

[38] E. Quesnel, C. Teyssier, V. Muffato, and J. Thibault. Study of ion beam sputtered Mo/Si mirrors for EUV lithography mask: influence of sputtering gas. *Proc. SPIE*, **5250**:88–98, 2004.

[39] C. Teyssier, E. Quesnel, V. Muffato, and P. Schiavone. Stress characteristics in EUV mask Mo/Si multilayers deposited by ion beam sputtering. *Microelectronic Engineering*, **61–62**:241–250, 2002.

[40] P. Seidel. EUV mask blank readiness for 45 nm HP 2009 manufacturing. *Proc. SPIE*, **5751**:178–179, 2005.

[41] J. Hue, E. Quesnel, V. Muffato, M. Vabre, and S. Favier. EUV mask blank activities at LETI: defect detection at 80 nm. *Proc. SPIE*, **5751**:423–434, 2005.

[42] T. Hashimoto and I. Nishiyama. Simulation analysis of defect repair methods for EUVL Mo/Si multilayer mask blanks manufacturing. *Proc. SPIE*, **5751**:466–476, 2005.

[43] R.L. Brainard, G.G. Barclay, E.H. Anderson, and L.E. Ocola. Resists for next generation lithography. *Microelectronic Engineering*, **61–62**:707–715, 2002.

[44] W. Yueh, H.B. Cao, V. Thirumala, and H. Choi. Quantification of EUV resist outgassing. *Proc. SPIE*, **5753**:765–770, 2005.

[45] S. Yulin, T. Feigl, N. Benoit, and N. Kaiser. EUV/soft X-ray multilayer optics. *Proc. SPIE*, **5645**:289–298, 2004.

[46] B.A.M. Hansson. Laser-plasma sources for extreme-ultraviolet lithography. *Ph.D. Thesis, Royal Institute of Technology*, Stockholm, Sweden, 2003.

[47] H. Meiling, V. Banine, P. Kuerz, B.D. Blum, G.J. Heerens, and N. Harned. The EUV program at ASML: an update. *Proc. SPIE*, **5037**:24–35, 2003.

[48] S. Yulin, N. Benoit, T. Feigl, and N. Kaiser. Interface-engineered multilayer mirrors. *Proc. SPIE*, **5963**:253–260, 2005.

[49] D.W. Myers, I.V. Fomenkov, W. Partlo, D.C. Brandt, and B.C. Klene. High-volume manufacturing requirements drive EUV source development. *Solid State Technology*, **14**:67–73, 2005.

[50] T. Koide, S. Sato, T. Shidara, M. Niwano, M. Yanagihara, A. Yamada, A. Fujimori, A. Mikuni, H. Kato, and T. Miyahara. Investigation of carbon contamination of mirror surfaces exposed to synchrotron radiation. *Nuclear Instruments and Methods in Physics Research Section A: Accelerators, Spectrometers, Detectors and Associated Equipment*, **246**:215–218, 1986.

[51] S.S. Andreev, N.N. Salashchenko, L.A. Suslov, A.N. Yablonsky, and S.Yu. Zuev. Stress reduction of Mo/Si multilayer structures. *Nuclear Instruments and Methods in Physics Research Section A: Accelerators, Spectrometers, Detectors and Associated Equipment*, **470**:162–167, 2001.

[52] M. Born and E. Wolf. Principles of optics. *Seventh Edition, Cambridge University Press, Cambridge*, ISBN 0–5216–4222–1:38–53, 1999.

[53] T. Feigl, J. Heber, A. Gatto, and N. Kaiser. Optics developments in the VUV-soft X-ray spectral region. *Nuclear Instruments and Methods in Physics Research Section A: Accelerators, Spectrometers, Detectors and Associated Equipment*, **483**:351–356, 2002.

[54] K.D. Joensen, P. Voutov, A. Szentgyorgyi, J. Roll, P. Gorenstein, P. Høghøj, and F.E. Christensen. Design of grazing-incidence multilayer supermirrors for hard-X-ray reflectors. *Applied Optics*, **34**:7935–7944, 1995.

[55] E. Ziegler. Multilayer optics for synchrotron X-ray applications. *Proc. SPIE*, **2253**:248–254, 1994.

[56] E. Spiller. Low-loss reflection coatings using absorbing materials. *Applied Physics Letters*, **20**:365–367, 1972.

[57] F. Schäfers. Multilayers for the EUV/soft X-ray range. *Physica B: Condensed Matter*, **283**:119–124, 2000.

[58] S. Yulin. Multilayer coatings for EUV/soft X-ray mirrors. *Kaiser and Pulker (Eds.), Optical Interference Coatings, Springer Series in Optical Sciences, Berlin*, ISBN 3–540–00364–9:281–307, 2003.

[59] T.W. Barbee Jr., S. Mrowka, and M.C. Hettrick. Molybdenum-silicon multilayer mirrors for the extreme ultraviolet. *Applied Optics*, **24**:883–886, 1985.

[60] J.H. Underwood and T.W. Barbee Jr. Layered synthetic microstructures as bragg diffractors for X-rays and extreme ultraviolet: theory and predicted performance. *Applied Optics*, **20**:3027–3034, 1981.

[61] W.H. Bragg. The intensity of reflection of X-rays by crystals. *Philosophical Magazine*, **27**:881–896, 1914.

[62] P. Rouard. Etudes des propriétés optiques des lames métalliques très minces. *Annales de Physique*, **7**:291–384, 1937.

[63] F. Abeles. Recherches sur la propagation des ondes électromagnétiques sinusoïdales dans les milieux stratifiés. application aux couches minces. *Annales de Physique*, **5**:596–639, 1950.

[64] E. Spiller. Soft X-ray optics. *SPIE Optical Engineering Press, Bellingham*, ISBN 0–8194–1655–X:101–138, 1994.

[65] A.E.Rosenbluth and P. Lee. Bragg condition in absorbing X-ray multilayers. *Applied Physics Letters*, **40**:466–468, 1982.

[66] E. Spiller. Soft x-ray optics. *SPIE Optical Engineering Press, Bellingham*, ISBN 0–8194–1655–X:139–168, 1994.

[67] K.M. Skulina, C.S. Alford, R.M. Bionta, D.M. Makowiecki, E.M. Gullikson, R. Soufli, J.B. Kortright, and J.H. Underwood. Molybdenum/beryllium multilayer mirrors for normal incidence in the extreme ultraviolet. *Applied Optics*, **34**:3727–3730, 1995.

[68] N. Kaiser, S. Yulin, T. Feigl, H. Bernitzki, and H. Lauth. EUV and soft X-ray multilayer optics. *Proc. SPIE*, **5250**:109–118, 2003.

[69] M. Singh and J.J.M. Braat. Improved theoretical reflectivities of extreme ultraviolet mirrors. *Proc. SPIE*, **3997**:412–419, 2000.

[70] http://cindy.lbl.gov/multilayer/survey.html.

[71] A.E.Rosenbluth. Computer search for layer materials that maximize the reflectivity of X-ray multilayers. *Revue de Physique Appliquée*, **23**:1599–1621, 1988.

[72] S. Braun, H. Mai, M. Moss, R. Scholz, and A. Leson. Mo/Si multilayers with different barrier layers for applications as extreme ultraviolet mirrors. *Japanese Journal of Applied Physics*, **41**:4074–4081, 2002.

[73] T.W. Barbee Jr. Multilayer for X-ray optics. *Optical Engineering*, **25**:893–915, 1986.

[74] D.G. Stearns and E.M. Gullikson. Nonspecular scattering from extreme ultraviolet multilayer coatings. *Physica B: Condensed Matter*, **283**:84–91, 2000.

[75] P. Debye. Über die Intensitätsverteilung in den mit Röntgenstrahlung erzeugten Interferenzbildern. *Verlag der Deutschen Physikalischen Gesellschaft*, **15**:738, 1913.

[76] I. Waller. Zur Frage der Einwirkung der Wärmebewegung auf die Interferenz von Röntgenstrahlen. *Zeitschrift für Physik*, **17**:398–408, 1923.

[77] P. Croce and L. Névot. Etude des couches minces et des surfaces par réflexion rasante, spéculaire ou diffuse, de rayons X. *Revue de Physique Appliquée*, **11**:113–125, 1976.

[78] L. Névot and P. Croce. Caractérisation des surfaces par réflexion rasante de rayon x. application à l´étude du polissage de quelques verres silicates. *Revue de Physique Appliquée*, **15**:761–779, 1980.

[79] S.P. Vernon, D.G. Stearns, and R.S. Rosen. Ion-assisted sputter deposition of molybdenum-silicon multilayers. *Applied Optics*, **32**:6969–6974, 1993.

[80] D.L. Windt, R. Hull, and W.K. Waskiewicz. Interface imperfections in metal/Si multilayers. *Journal of Applied Physics*, **71**:2675–2678, 1992.

[81] S. Yulin, T. Feigl, T. Kuhlmann, N. Kaiser, A.I. Fedorenko, V.V. Kondratenko, O.V. Poltseva, V.A. Sevryukova, A.Y. Zolotaryov, and E.N. Zubarev. Interlayer transition zones in Mo/Si superlattices. *Journal of Applied Physics*, **92**:1216–1220, 2002.

[82] D.G. Stearns and R.S. Rosen. High-performance multilayer mirrors for soft X-ray projection lithography. *Proc. SPIE*, **1547**:2–13, 1991.

[83] P. van Loevezijn, R. Schlatmann, J. Verhoeven, B.A. van Tiggelen, and E.M. Gullikson. Numerical and experimental study of disordered multilayers for broadband X-ray reflection. *Applied Optics*, **35**:3614–3619, 1996.

[84] E. Spiller. Evaporated multilayer dispersion elements for soft X-rays. *AIP Conference Proc.*, **75**:124–130, 1981.

[85] M. Singh and J.J.M. Braat. Design of multilayer extreme-ultraviolet mirrors for enhanced reflectivity. *Applied Optics*, **39**:2189–2197, 2000.

[86] S. Bajt, J. Alameda, T. Barbee Jr., W.M. Clift, J.A. Folta, B. Kaufmann, and E. Spiller. Improved reflectance and stability of Mo/Si multilayers. *Proc. SPIE*, **4506**:65–75, 2001.

[87] S. Yulin, N. Benoit, T. Feigl, and N. Kaiser. Interface-engineered EUV multilayer mirrors. *Microelectronic Engineering*, **83**:692–694, 2006.

[88] P.B. Mirkarimi. Stress, reflectance and temporal stability of sputter-deposited Mo/Si and Mo/Be multilayer films for extreme ultraviolet lithography. *Optical Engineering*, **38**:1246–1259, 1999.

[89] N. Benoit, S. Yulin, T. Feigl, and N. Kaiser. Radiation stability of EUV Mo/Si multilayer mirrors. *Physica B: Condensed Matter*, **357**:222–226, 1999.

[90] R.J. Anderson, D.A. Buchenauer, L. Klebanoff, O.R. Wood II, and N.V. Edwards. The erosion of materials exposed to a laser-pulsed plasma (LPP) extreme ultraviolet (EUV) illumination source. *Proc. SPIE*, **5374**:710–719, 2004.

[91] D.A. Tichenor, G.D. Kubiak, W.C. Replogle, L.E. Klebanoff, J.B. Wronosky, L.C. Hale, H.N. Chapman, J.S. Taylor, J.A. Folta, C. Montcalm, and R.M. Hudyma. EUV Engineering Test Stand. *Proc. SPIE*, **3997**:48–69, 2000.

[92] W.P. Ballard, L.J. Bernardez II, R.E. Lafon, R.J.M. Anderson, Y.E. Perras, A.H. Leung, H. Shields, M.B. Petach, R.J. St. Pierre, and R.L. Bristol. High-power Laser-Produced-Plasma EUV source. *Proc. SPIE*, **4688**:302–309, 2002.

[93] P.A. Grunow, L.E. Klebanoff, S. Graham Jr., S.J. Haney, and W.M. Clift. Rates and mechanisms of optic contamination in the EUV engineering test stand. *Proc. SPIE*, **5037**:418–428, 2003.

[94] R.J. Anderson, D.A. Buchenauer, K.A. Williams, W.M. Clift, L.E. Klebanoff, N.V. Edwards, O.R. Wood II, and S. Wurm. Investigation of plasma-induced erosion of multilayer condenser optics. *Proc. SPIE*, **5751**:128–139, 2005.

[95] M.E. Malinowski, C.A. Steinhaus, D.E. Meeker, W.M. Clift, L.E. Klebanoff, and S. Bajt. Relation between electron- and photon-caused oxidation in EUVL optics. *Proc. SPIE*, **5037**:429–438, 2003.

[96] R.A. Rosenberg and D.C. Mancini. Deposition of carbon on gold using synchrotron radiation. *Nuclear Instruments and Methods in Physics Research Section A: Accelerators, Spectrometers, Detectors and Associated Equipment*, **291**:101–106, 1990.

[97] K. Boller, R.P. Haelbich, H. Hogrefe, W. Jark, and C. Kunz. Investigation of carbon contamination of mirror surfaces exposed to synchrotron radiation. *Nuclear Instruments and Methods in Physics Research*, **208**:273–279, 1983.

[98] N. Koster, B. Mertens, R. Jansen, A. van de Runstraat, F. Stietz, M. Wedowski, H. Meiling, R. Klein, A. Gottwald, F. Scholze, M. Visser, R. Kurt, P. Zalm, E. Louis, and A. Yakshin. Molecular contamination mitigation in EUVL by environmental control. *Microelectronic Engineering*, **61–62**:65–76, 2002.

[99] R. Kurt, M. van Beek, C. Crombeen, P. Zalm, and Y. Tamminga. Radiation induced carbon contamination of optics. *Proc. SPIE*, **4688**:702–709, 2002.

[100] A. Barty and K.A. Goldberg. The effects of radiation induced carbon contamination on the performance of an EUV lithographic optic. *Proc. SPIE*, **5037**:450–459, 2003.

[101] S. Bajt, H.N. Chapman, N. Nuygen, J. Alameda, J.C. Robinson, M. Malinowski, E. Gullikson, A. Aquila, C. Tarrio, and S. Grantham. Design and performance of capping layers for EUV multilayer mirrors. *Proc. SPIE*, **5037**:236–248, 2003.

[102] Y. Kakutani, M. Niibe, H. Takase, S. Terashima, H. Kondo, S. Matsunari, T. Aoki, Y. Gomei, and Y. Fukuda. Reflectance change of Si- and Ru-capped Mo/Si multilayer mirrors caused by intense EUV irradiation. *Proc. SPIE*, **5751**:1077–1083, 2005.

[103] H. Takase, Y. Gomei, S. Terashima, H. Kondo, T. Aoki, S. Matsunari, M. Niibe, and Y. Kakutani. Characterization of capped multilayer mirrors using XPS, AES and SIMS. *Proc. SPIE*, **5751**:1084–1091, 2005.

[104] S. Bajt, Z. Dai, E.J. Nelson, M.A. Wall, J. Alameda, N. Nguyen, S. Baker, J.C. Robinson, J.S. Taylor, M. Clift, A. Aquila, E.M. Gullikson, and N.V.G. Edwards. Oxidation resistance of Ru-capped EUV multilayers. *Proc. SPIE*, **5751**:118–127, 2005.

[105] S. Bajt, H.N. Chapman, N. Nguyen, J. Alameda, J.C. Robinson, M. Malinowski, E. Gullikson, A. Aquila, C. Tarrio, and S. Grantham. Design and performance of capping layers for extreme-ultraviolet multilayer mirrors. *Applied Optics*, **42**:5750–5758, 2003.

[106] A.E. Yakshin, E. Louis, E.L.G. Maas, F. Bijkerk, R. Klein, F. Scholze, G. Ulm, P. Zalm, F. Stietz, M. Wedowski, S. Müllender, B. Mertens, and H. Meiling. Protection of Mo/Si multilayers with a carbon capping layer. *ASET/SEMATECH Workshop on EUV Lithography*, Matsue, Japan, 2001.

[107] L.E. Klebanoff, W.M. Clift, M.E. Malinowski, C. Steinhaus, P. Grunow, and S. Bajt. Radiation-induced protective carbon coating for extreme ultraviolet optics. *Journal of Vacuum Science and Technology B: Microelectronics and Nanometer Structures*, **20**:696–703, 2002.

[108] L.E. Klebanoff, M.E. Malinowski, W.M. Clift, C. Steinhaus, and P. Grunow. Use of gas-phase ethanol to mitigate extreme UV/water oxidation of extreme UV optics. *Journal of Vacuum Science and Technology A: Vacuum, Surfaces and Films*, **22**:425–432, 2004.

[109] S. Bajt, S. Hau-Riege, Z.R. Dai, J. Alameda, E. Nelson, C. Evans, J.S. Taylor, F. Dollar, E. Gullikson, S. Hill, M. Chandhok, and M. Fang. Protective capping layer for EUVL optics using TiO_2. *4th EUVL Symposium*, San Diego, USA, 2005.

[110] S. Yulin, N. Benoit, T. Feigl, N. Kaiser, F. Dollar, E. Gullikson, S. Hill, T. Lucatorto, M. Chandhok, M. Fang, and M. Shell. Mo/Si multilayers capped by TiO_2. *5th EUVL Symposium*, Barcelona, Spain, 2006.

[111] S. Graham Jr., M.E. Malinowski, C. Steinhaus, P.A. Grunow, and L.E. Klebanoff. Studies of EUV contamination mitigation. *Proc. SPIE*, **4688**:431–441, 2002.

[112] S. Graham, C. Steinhaus, M. Clift, and L. Klebanoff. Radio-frequency discharge cleaning of silicon-capped Mo/Si multilayer extreme ultraviolet optics. *Journal of Vacuum Science and Technology B: Microelectronics and Nanometer Structures*, **20**:2393–2400, 2002.

[113] S. Graham Jr., C.A. Steinhaus, W.M. Clift, L.E. Klebanoff, and S. Bajt. Atomic hydrogen cleaning of EUV multilayer optics. *Proc. SPIE*, **5037**:460–469, 2003.

[114] M.E. Malinowski, P.A. Grunow, C. Steinhaus, W.M. Clift, and L.E. Klebanoff. Use of molecular oxygen to reduce EUV-induced carbon contamination of optics. *Proc. SPIE*, **4343**:347–356, 2001.

[115] R.S. Rosen, D.G. Stearns, M.A. Viliardos, M.E. Kassner, S.P. Vernon, and Y. Cheng. Silicide layer growth rates in Mo/Si multilayers. *Applied Optics*, **32**:6975–6980, 1993.

[116] O.B. Loopstra, W.G. Sloof, T.H. de Keijser, E.J. Mittemeijer, S. Radelaar, A.E.T. Kuiper, and R.A.M. Wolters. Composition, microstructure and properties of crystalline molybdenum silicide thin films produced by annealing of amorphous Mo/Si multilayers. *Journal of Applied Physics*, **63**:4960–4969, 1988.

[117] A.K. Srivastava, P. Tripathi, M. Nayak, G.S. Lodha, and R.V. Nandedkar. Formation of Mo5Si3 phase in Mo/Si multilayers. *Journal of Applied Physics*, **92**:5119–5126, 2002.

[118] M. Paulson and J.E. Hilliard. Interdiffusion in composition-modulated copper-gold thin films. *Journal of Applied Physics*, **48**:2117–2123, 1977.

[119] J. Kucera, K. Cíha, and K. Stránský. Interdeffusion in the Co-Ni system-III. Intrinsic diffusion coefficients. *Czechoslovak Journal of Physics*, **27**:1049–1058, 1977.

[120] A. Dudás, G.A. Langer, D.L. Beke, M. Kis-Varga, L. Daróczi, and Z. Erdélyi. Thermal stability of Mo-V epitaxial multilayers. *Journal of Applied Physics*, **86**:2008–2013, 1999.

[121] W.H. Wang, H.Y. Bai, M. Zhang, J.H. Zhao, X.Y. Zhang, and W.K. Wang. Interdiffusion in nanometer-scale multilayers investigated by in situ low-angle X-ray diffraction. *Physical Review B*, **59**:10811–10822, 1999.

[122] D.G. Stearns, M.B. Stearns, Y. Cheng, J.H. Stith, and N.M. Ceglio. Thermally induced structural modification of Mo-Si multilayers. *Journal of Applied Physics*, **67**:2415–2426, 1990.

[123] J.Y. Cheng, H.C. Cheng, and L.J. Chen. Cross-sectional transmission electron microscope study of the growth kinetics of hexagonal MoSi2 on (001) Si. *Journal of Applied Physics*, **61**:2218–2223, 1987.

[124] K. Holloway, K. Ba Do, and R. Sinclair. Interfacial reactions on annealing molybdenum-silicon multilayers. *Journal of Applied Physics*, **65**:474–480, 1989.

[125] H. Nakajima, H. Fujimori, and M. Koiwa. Interdiffusion and structural relaxation in Mo/Si multilayer films. *Journal of Applied Physics*, **63**:1046–1051, 1988.

[126] W.G. Sloof, O.B. Loopstra, T.H. de Keijser, and E.J. Mittemeijer. Diffusion and structural relaxation in amorphous Mo/Si multilayers. *Scripta Metallurgica*, **20**:1683–1687, 1986.

[127] B. Heidemann, T. Tappe, B. Schmiedeskamp, and U. Heinzmann. Thermal stability and diffusion processes in MoxSiy/Si multilayers studied with high-resolution RBS. *Zeitschrift für Physik B*, **99**:37–42, 1995.

[128] S. Rines. Diagrams of phase equilibrium in metallurgy. *Metallurgizdat, Moscow*, 1960.

[129] M. Hansen and K. Anderko. Structure of binary alloys. *Metallurgizdat, Moscow*, **2**, 1962.

[130] V.V. Kondratenko, I.P. Pershin, O.V. Poltseva, A.I. Fedorenko, E.N. Zubarev, S.A. Yulin, I.V. Kozhevnikov, S.I. Sagitov, V.A. Chirkov, and V.E. Levashov. Thermal stability of soft X-ray Mo-Si and MoSi2-Si multilayer mirrors. *Applied Optics*, **32**:1811–1816, 1993.

[131] N. Suresh, M.H. Modi, P. Tripathi, G.S. Lodha, S.M. Chaudhari, A. Gupta, and R.V. Nandedkar. Heat resistance of electron beam deposited Mo/C X-ray multilayer. *Thin Solid Films*, **368**:80–85, 2000.

[132] T. Feigl, H. Lauth, S. Yulin, and N. Kaiser. Heat resistance of EUV multilayer mirrors for long-time applications. *Microelectronic Engineering*, **57–58**:3–8, 2001.

[133] M. Ishino and O. Yoda. Optimization of the silicon oxide layer thicknesses inserted in the Mo/Si multilayer interfaces for high heat stability and high reflectivity. *Journal of Applied Physics*, **92**:4952–4958, 2002.

[134] T. Feigl, S. Yulin, T. Kuhlmann, and N. Kaiser. Damage resistant and low stress euv multilayer mirrors. *Japanese Journal of Applied Physics*, **41**:4082–4085, 2002.

[135] H. Takenaka and T. Kawamura. Thermal stability of Mo/C/Si/C multilayer soft x-ray mirrors. *Journal of Electron Spectroscopy and Related Phenomena*, **80**:381–384, 1996.

[136] F.P. Wang. Thermal stability of Mo/SiO2 multilayers. *Thin Solid Films*, **379**:308–312, 2000.

[137] J.A. Dobrowolski J.R. Pekelsky, R. Pelletier, M. Ranger, B.T. Sullivan, and A.J. Waldorf. Practical magnetron sputtering system for the deposition of optical multilayer coatings. *Applied Optics*, **31**:3784–3789, 1992.

[138] G. Bräuer. Large area deposition. *Kaiser and Pulker (Eds.), Optical Interference Coatings, Springer Series in Optical Sciences, Berlin*, ISBN 3–540–00364–9:155–180, 2003.

[139] P. Mohan Babu, B. Radhakrishna, G. Venkata Rao, P. Sreedhara Reddy, and S. Uthanna. Bias voltage dependence properties of dc reactive magnetron sputtered indium oxide films. *Journal of Optoelectronics and Advanced Materials*, **6**:205–210, 2004.

[140] A.E. Yakshin, E. Louis, P.C. Görts, E.L.G. Maas, and F. Bijkerk. Determination of the layered structure in Mo/Si multilayers by grazing incidence X-ray reflectometry. *Physica B: Condensed Matter*, **283**:143–148, 2000.

[141] T. Feigl. Struktur und Eigenschaften von Schichtsystemen für den EUV-Spektralbereich. *Ph.D. Thesis, Friedrich-Schiller-Universität*, Jena, Germany, 2000.

[142] E. Spiller. Characterization of multilayer coatings by X-ray reflection. *Revue de Physique Appliquée*, **23**:1687–1700, 1988.

[143] V. Holý, U. Pietsch, and T. Baumbach. High resolution X-ray scattering from thin films and multilayers. *Springer-Verlag Berlin Heidelberg New York*, ISBN 3–540–62029–X, 1999.

[144] W.E. Wallace and W.L. Wu. A novel method for determining thin film density by energy-dispersive x-ray reflectivity. *Applied Physics Letters*, **67**:1203–1205, 1995.

[145] S. Grassel and D. Fuchs. WIN-REFSIM, Vers. 1.1i. *Siemens AG*, 1992–1995.

[146] D. Fuchs, M. Krumrey, P. Müller, F. Scholze, and G. Ulm. High precision soft x-ray reflectometer. *Review of Scientific Instruments*, **66**:2248–2250, 1995.

[147] F. Scholze, B. Beckhoff, G. Brandt, R. Fliegauf, R. Klein, B. Meyer, D. Rost, D. Schmitz, M. Veldkamp, J. Weser, G. Ulm, E. Louis, A.E. Yakshin, S. Oestreich, and F. Bijkerk. The new PTB beamlines for high-accuracy EUV reflectometry at BESSY II. *Proc. SPIE*, **4146**:72–82, 2000.

[148] F. Scholze, M. Krumrey, P. Müller, and D. Fuchs. Plane grating monochromator beamline for vuv radiometry. *Review of Scientific Instruments*, **65**:3229–3232, 1994.

[149] F. Scholze, C. Laubis, C. Buchholz, A. Fischer, S. Plöger, F. Scholz, H. Wagner, and G. Ulm. Status of EUV reflectometry at PTB. *Proc. SPIE*, **5751**:749–758, 2005.

[150] G. Binnig, C.F. Quate, and C. Gerber. Atomic force microscope. *Physical Review Letters*, **56**:930–933, 1986.

[151] N.J. DiNardo. Nanoscale characterization of surfaces and interfaces. *Weinheim: VCH*, ISBN 3–527–29247–0:118–137, 1994.

[152] Q. Zhong, D. Inniss, K. Kjoller, and V.B. Elings. Fractured polymer/silica fiber surface studied by tapping mode atomic force microscopy. *Surface Sciences Letters*, **290**:L688–L692, 1993.

[153] L. Manning, B. Rogers, M. Jones, J.D. Adams, J.L. Fuste, and S.C. Minne. Self-oscillating tapping mode atomic force microscopy. *Review of Scientific Instruments*, **74**:4220–4222, 2003.

[154] R. Garcia and R. Perez. Dynamic atomic force microscopy methods. *Surface Science Reports*, **47**:197–301, 2002.

[155] J.M. Bennett and L. Mattsson. Introduction to surface roughness and scattering. *Second Edition, Optical Society of America, Washington D.C.*, ISBN 1–55752–609–5:20–26, 1999.

[156] A. Duparré, J. Ferre-Borrull, S. Gliech, G. Notni, J. Steinert, and J.M. Bennett. Surface characterization techniques for determining the root-mean-square roughness and power spectral densities of optical components. *Applied Optics*, **41**:154–169, 2002.

[157] P.D. Nellist and S.J. Pennycook. Subangstrom resolution by underfocused incoherent transmission electron microscopy. *Physical Review Letters*, **81**:4156–4159, 1998.

[158] D.B. Williams and C.B. Carter. Transmission electron microscopy: A textbook for materials science. *Plenum Press, New York and London*, ISBN 0–306–45247–2:3–16, 1996.

[159] A.K. Petford-Long, M.B. Stearns, C.H. Chang, S.R. Nutt, D.G. Stearns, N.M. Ceglio, and A.M. Hawryluk. High-resolution electron microscopy study of x-ray multilayer structures. *Journal of Applied Physics*, **61**:1422–1428, 1987.

[160] T. Ishitani and T. Yaguchi. Cross-sectional sample preparation by focused ion beam: A review of ion-sample interaction. *Microscopy Research and Technique*, **35**:320–333, 1996.

[161] G. Radnóczi and Á. Barna. Transmission electron microscopy characterization of hard coatings and films: sample preparation aspects and results. *Surface and Coatings Technology*, **80**:89–95, 1996.

[162] P. Weissbrodt, L. Raupach, and E. Hacker. Improved method for contamination control during fabrication of space equipment. *Proc. SPIE*, **2210**:672–680, 1994.

[163] A. Einstein. Über einen die erzeugung und verwandlung des lichtes betreffenden heuristischen gesichtspunkt. *Annalen der Physik*, **322**:132–148, 1905.

[164] S. Hofmann. Practical surface analysis: state of the art and recent developments in AES, XPS, ISS and SIMS. *Surface and Interface Analysis*, **9**:3–20, 1986.

[165] J.F. Moulder, W.F. Stickle, P.E. Sobol, and K.D. Bomben. Handbook of X-ray photoelectron spectroscopy: A reference book of standard spectra for identification and interpretation of XPS data. *Physical Electronics Inc., Eden Prairie, Minnesota*, ISBN 0–964–81241–X, 1995.

[166] R. Lebert, C. Wies, B. Jägle, L. Juschkin, U. Bieberle, M. Meisen, W. Neff, K. Bergmann, K. Walter, O. Rosier, M.C. Schuermann, and T. Missalla. Status of the EUV-lamp development and demonstration of applications. *Proc. SPIE*, **5374**:943–953, 2004.

[167] http://www.aixuv.de/index.php?item=1.

[168] F.R. Powell and T.A. Johnson. Filter windows for euv lithography. *Proc. SPIE*, **4343**:585–589, 2001.

[169] http://www.sci-soft.com/.

[170] M.H. Modi, G.S. Lodha, M. Nayak, A.K. Sinha, and R.V. Nandedkar. Determination of layer structure in Mo/si multilayers using soft X-ray reflectivity. *Physica B: Condensed Matter*, **325**:272–280, 2003.

[171] D.L. Windt. IMD–Software for modeling the optical properties of multilayer. *Computers in Physics*, **12**:360–370, 1998.

[172] J.M. Slaughter, D.W. Schulze, C.R. Hills, A. Mirone, R. Stalio, R.N. Watts, C. Tarrio, T.B. Lucatorto, M. Krumrey, P. Mueller, and C.M. Falco. Structure and performance of Si/Mo multilayer mirrors for the extreme ultraviolet. *Journal of Applied Physics*, **76**:2144–2156, 1994.

[173] O.B. Loopstra, E.R. van Snek, T.H. de Keijser, and E.J. Mittemeijer. Model for stress and volume changes of a thin film on a substrate upon annealing: Application to amorphous Mo/Si multilayers. *Physical Review B*, **44**:13519–13533, 1991.

Acknowledgements

I would like first to thank Prof. Andreas Tünnermann, for the supervising of my thesis at the Fraunhofer Institut für Angewandte Optik und Feinmechanik (IOF), Jena.

Furthermore I want to thank Prof. Norbert Kaiser, who offered me the chance to work on this interesting and challenging topic of EUV optics in his department "Optical Coatings" at the IOF Jena. His interest in my work was a source of motivation for me.

I would also like to thank Dr. Sergiy Yulin very much for his time, his support of my work and all the fruitful discussions we had over the last four years. His great experience in EUV multilayer coatings was very helpful during my PhD. Many thanks to Dr. Torsten Feigl who is leading the EUV activity at the IOF. He got me the possibility to discover a new fascinating world.

I gratefully acknowledge the fruitful collaborations with Cymer Inc. on high-temperature multilayer mirrors and Intel. Corp. about the environmental stability of different capping layers.

Many thanks to the rest of my colleagues at the department A1 for the join work, the interesting discussions and making the department a nice workplace. I would like to thank Tino Benkenstein for his help about the EUV source at the IOF. Special thanks also to Marcel Flemming and Sven Schröder for the AFM measurements and for answering many of my questions about the German language.

Thanks to the team of Dr. Christian Laubis at the PTB Berlin for the EUV reflectivity measurements, to the group of Prof. Ute Kaiser at the University of Ulm for providing the TEM images and to Lutz Raupach (Jenoptik L.O.S.) for the XPS investigations.

Finally I would like to thank my parents and my family, who encouraged my decision to pursue my PhD in Germany. Last but not least, I deeply appreciate the patience and the emotional support of Kati.

Ehrenwörtliche Erklärung

Ich erkläre hiermit ehrenwörtlich, dass ich die vorliegende Arbeit selbständig, ohne unzulässige Hilfe Dritter und ohne Benutzung anderer als der angegebenen Hilfsmittel und Literatur angefertigt habe. Die aus anderen Quellen direkt oder indirekt übernommenen Daten und Konzepte sind unter Angabe der Quelle gekennzeichnet.

Bei der Auswahl und Auswertung folgenden Materials haben mir die nachstehend aufgeführten Personen in der jeweils beschriebenen Weise entgeltlich/unentgeltlich geholfen:

1.	Dr. Sergiy Yulin	Sputtertechnik und wissenschaftliche Diskussion
2.	Prof. Dr. Ute Kaiser	Transmissions-Elektromikroscopie
3.	Dr. Andrey Chuvilin	Transmissions-Elektromikroscopie
4.	Dr. Christian Laubis	EUV-Reflektometrie
5.	Lutz Raupach	XPS-Untersuchungen
6.	Marcel Flemming	Rasterkraftmikroscopie
7.	Tino Benkenstein	EUV-Quelle

Weitere Personen waren an der inhaltlich-materiellen Erstellung der vorliegenden Arbeit nicht beteiligt. Insbesondere habe ich hierfür nicht die entgeltliche Hilfe von Vermittlungs- bzw. Beratungsdiensten (Promotionsberater oder andere Personen) in Anspruch genommen. Niemand hat von mir unmittelbar oder mittelbar geldwerte Leistungen für die Arbeiten erhalten, die im Zusammenhang mit dem Inhalt der vorgelegten Dissertation stehen.

Die Arbeit wurde bisher weder im In- noch im Ausland in gleicher oder ähnlicher Form einer anderen Prüfungsbehörde vorgelegt.

Die geltende Promotionsordnung der Physikalisch-Astronomischen Fakultät ist mir bekannt.

Ich versichere ehrenwörtlich, dass ich nach bestem Wissen die reine Wahrheit gesagt und nichts verschwiegen habe.

Jena, den 15. Februar 2007 Nicolas Benoit

Lebenslauf

Persönliche Daten

Name: Nicolas Benoit
Geburtsdatum: 21. Januar 1979
Geburtsort: Paris (Frankreich)

Ausbildung

1985 - 1990	Ecole élémentaire André Marsault, La Garenne Colombes (Frankreich)
1990 - 1994	Collège Les Vallées, La Garenne Colombes (Frankreich) Abschluss: Brevet des Collèges
1994 - 1997	Lycée Paul Lapie, Courbevoie (Frankreich) Abschluss: Baccalauréat S
1997 - 2000	Lycée Jacques Decour, Paris (Frankreich)
2000 - 2003	Ecole Nationale Supérieure de Physique, Marseille (Frankreich) Abschluss: Diplomphysiker
seit 2003	Doktorand am Fraunhofer-Institut Angewandte Optik und Feinmechanik, Jena

Jena, den 15. Februar 2007 Nicolas Benoit